Development of a Low Cost Secondary Slave Manipulator for a Minimally Invasive Robotic Surgical System

by
Siebert Christo Worst

Thesis presented in fulfilment of the requirements for the degree of Master of Science in the Faculty of Mechanical & Mechatronic Engineering at Stellenbosch University

Supervisor: Prof Cornie Scheffer
Co-Supervisor: Prof Kristiaan Schreve

December 2012

Declaration

I, the undersigned, hereby declare that the work contained in this thesis is my own original work and that I have not previously in its entity or in part submitted it at any university for a degree.

Signature: ……

Siebert Christo Worst

Date: ……

Abstract

Minimally Invasive Surgery (MIS) in human beings is performed by making small incisions in the abdominal region of the patient and inflating the abdominal cavity with CO_2. This procedure enables the surgeon to manipulate long rigid surgical instruments inside the patient in order to perform the surgery. Unfortunately the current methods of insertion and assembly of MIS instruments limit the surgeon to only five (of a possible seven) Degrees of Freedom (DOF). Along with this, the surgeon's movements are mirrored (called the Fulcrum effect) and scaled around the point of incision.

Minimally invasive surgical robots attempt to alleviate these drawbacks by eliminating the Fulcrum effect, as well as improving dexterity and accuracy. These robots' abilities to improve the surgeon's hand-eye coordination, enables the surgeon to perform surgeries using their natural movements with reduced fatigue. As a result of this, the risk to both patient and surgeon is reduced.

Existing MIS robotic systems are extremely expensive and large, and as a result they are not widely used. In this thesis a new, lower cost, seven DOF robotic manipulator is further developed. The thesis focuses on the external three DOF Secondary Slave Manipulator (SSM) and combines it with the Primary Slave Manipulator (PSM) that was developed by a previous Masters student. Tests done on the SSM showed that the manipulator has a minimum resolution of 0.7 ± 0.2 mm (mean ± standard deviation) on the shoulder joint's yaw rotation and 0.5 ± 0.2 mm in pitch rotation. The linear actuator used for insertion has a minimum resolution of 0.2 ± 0.2 mm. A strength test was also conducted and showed that the manipulator is easily capable of producing a 10 N actuation force as required during Minimally Invasive Robotic Surgery (MIRS) procedures. In conclusion the complete system has potential as a viable alternative to the existing systems due to its accuracy and lower cost.

Future work will include the development of a user interface and control system for the complete robot.

Opsomming

Minimaal Indringende Chirurgie (MIC) op mense word uitgevoer deur klein insnydings in die pasiënt se buik te maak en dan die abdominale holte met CO_2 te vul. Dit stel die chirurg in staat om lang, onbuigbare instrumente binne die pasiënt te manipuleer om sodoende die operasie uit te voer. Die manier waarop die MIC instrument ontwerp is en die pasiënt binnegaan, laat egter slegs vyf vryheidsgrade toe, terwyl die chirurg self sewe vryheidsgrade in sy handbewegings het. Verder veroorsaak hierdie instrumente ook dat die chirurg se aksies in spieëlbeeld vertolk word (Fulcrum effek) en geskaleer is.

Chirurgiese robotika poog om hierdie nadele teen te werk deur die Fulcrum effek te verwyder, en ook om handvaardigheid en akkuraatheid te bevorder. Die robot se potensiaal om die chirurg se hand-oog koördinasie te verbeter, maak dit moontlik vir die chirurg om op ’n meer natuurlike en gemaklike manier te werk te gaan en bring minder vermoeienis mee. Dit verminder die risiko’s vir beide die pasiënt en die chirurg.

Bestaande robotiese stelsels is egter baie duur en groot, en word dus nie meer algemeen gebruik nie. In hierdie tesis word ‘n nuwe sewe-vryheidsgraad robotiese manipuleerder ontwikkel. Die tesis fokus op die eksterne drie-vryheidsgraad Sekondêre Slaaf Manipuleerder (SSM) en kombineer dit met die Primêre Slaaf Manipuleerder (PSM) wat deur ’n vorige Meestersstudent ontwikkel is. Toetse wat uitgevoer is op die SSM het getoon dat dit ’n minimum resolusie van 0.7 ± 0.2 mm (gemiddeld ± standaard afwyking) op die skouer se afwyking en 0.5 ± 0.2 mm om die onderskeie skouer aslyne toon. Die linieêre aktueerder wat vir inlassing gebruik word het ’n minimum resolusie van 0.2 ± 0.2 mm. ’n Sterktetoets is uitgevoer en het getoon dat die manipuleerder maklik die nodige 10 N krag soos benodig in Minimaal Indringende Robotiese Chirurgie (MIRC) prosedures kan lewer. Ter afsluiting, die volledige stelsel het die potensiaal as lewensvatbare alternatief tot die bestaande stelsels vanweë die akkuraatheid en laer koste verbonde.

Toekomstige navorsing kan moontlik die ontwikkeling van ’n gebruikerkoppelvlak en beheerstelsel vir die volledige robot insluit.

Acknowledgments

The author would like to thank the supervisors, Professor C. Scheffer and Professor K. Schreve for their guidance and support throughout the thesis, along with the countless hours spent reading and correcting the attempts at a final thesis report.

Thank you very much to the Mechanical & Mechatronic workshop, especially Graeme Harmse, for the machining of the manipulator.

To my fellow BERG members, for their continued support over the last two years.

Lastly, my family and friends that supported me through the good times and the bad times, it means a lot and I will never forget it.

Contents

Nomenclature

Abbreviations

AESOP	Automated Endoscopic System for Optimal Positioning
CCD	Charge Coupled Device
CT	Computerised Tomography
DC	Direct Current
DOF	Degree of Freedom
EEPROM	Electrically Erasable Programmable Read-Only Memory
FDA	Food and Drug Association
GUI	Graphical User Interface
LCD	Liquid Crystal Display
LVDT	Linear Variable Differential Transformer
MIRS	Minimally Invasive Robotic Surgery
MIS	Minimally Invasive Surgery
MOSFET	Metal Oxide Silicon Field Effect Transistor
NURC	National Undersea Research Centre
OR	Operating Room
PCB	Printed Circuit Board
PSM	Primary Slave Manipulator
PWM	Pulse Width Modulation
RIO	Robotic arm Interactive Orthopaedic system

SCARA	Selective Compliant Assembly Robot Arm
SOFIE	Surgeon's Operating Force-feedback Interface Eindhoven
SSM	Secondary Slave Manipulator
TTL	Transistor-Transistor Logic
UART	Universal Asynchronous Receiver/Transmitter
USB	Universal Serial Bus
VPR	Virtual Point of Rotation

Glossary

Anterior Cruciate Ligament	Cruciate ligament which is one of the four major ligaments of the human knee.
Arthroplasty	Surgery to relieve pain and restore range of motion by realigning or reconstructing a joint.
Biopsy	Medical test involving the removal of cells or tissues for examination.
Cholecystectomy	Surgical removal of the gallbladder.
Charge Pump	DC to DC converter that uses capacitors as energy storage elements to create a higher voltage power source.
Electrocautery	Process of destroying tissue using heat conduction from a metal probe heated by electric current.
Endoscope	A thin, fibre optic tube with a light and lens, used to view the internal operating cavity while doing a surgical procedure.
Fallopian tube	Two very fine tubes, leading from the ovaries of female mammals into the uterus.
Fulcrum Effect	The tool tip moves in the opposite direction to the surgeon's movements due to the pivoting of the tool around the entry point.
Inferior	Below, as opposed to superior.
Lateral	Toward left or right, as opposed to medial.
Lymphadenectomy	Surgical removal of one or more groups of lymph nodes.
Medial	In the middle or inside, as opposed to lateral.
Myomectomy	Surgical removal of uterine leiomyomas, also known as fibroids.
Superior	Above, as opposed to inferior.
Transurethral	Performed through or by way of the urethra.
Trocar	Portal for the subsequent placement of other devices
Tubal Reversal	Surgical procedure that attempts to restore fertility to women by rejoining the separated segments of the fallopian tube.

List of Figures

List of Tables

Chapter 1: Introduction

This chapter gives a broad discussion of Minimally Invasive Surgery (MIS). It explains how these surgeries are performed and why they are beneficial to patients. It will continue to explain the drawbacks to the surgeon and how surgical robotics attempt to alleviate these drawbacks. The problems associated with the costs of the surgical robotics will be discussed and this will lead to the objectives set out for this thesis.

1.1 Minimally Invasive Surgery

MIS is a modern surgical technique whereby the size of the surgical incisions are reduced, in comparison with open surgery. This type of surgery has found many applications and can be performed on the abdomen (Wilson, 2009), knee (Tria, 2003), hip (Waldman, 2003), spine (McAfee *et al*, 2010) and even the heart (Svensson *et al*, 2010). This thesis is primarily concerned with abdominal MIS. MIS started out in 1985, with the first laparoscopic cholecystectomy performed by Prof Dr Med Erich Mühe (Reynolds, 2001). MIS is performed by making small incisions in the abdomen and inserting a trocar through it. Once the trocar is in position the abdominal cavity is inflated with CO_2. A Charged Coupled Device (CCD) camera is inserted through the trocar in order to give a view of the abdominal cavity. Two to four additional incisions are made for the insertion of surgical tools for grasping, dissecting and electrocautery (Lee *et al*, 2003). The inflated abdominal cavity enables the surgeon to manipulate the surgical instruments inside the patient by sliding them in and out of the trocar, rotating them about their own axis and pivoting them around the point of incision. Figure 1 shows a MIS procedure being performed. Figure 2 shows the general shape of a MIS tool.

Figure 1: MIS procedure with surgeon and assistant (Image: PJ Christiane)

During surgery, the primary surgeon manipulates the surgical instruments, whilst the assistant surgeon manoeuvres the laparoscope by means of voice commands received from the primary surgeon. Should the laparoscope lens become dirty during the procedure, it is removed from the patient and washed off with water before being reinserted.

Figure 2: MIS instruments (Image: SC Worst)

MIS has several advantages for the patient over regular open surgery. The smaller incisions cause less scarring, they heal quicker (thus less hospital time) and cause less pain than regular open surgery. Some disadvantages of MIS are that it is not suitable for all patients, especially when patients are obese, and it requires special training that is quite time-consuming (American Soviety for Reproductive Medicine, 2008). The most prolific problems of MIS for the surgeon are the loss of force and tactile feedback, loss of natural hand-eye coordination, loss of dexterity and also loss of freedom of movement. The loss of dexterity is caused by the fact that if the surgeon moves his/her hand in one direction, the instrument tip will move in the opposite direction. This phenomenon is known as the Fulcrum effect (Anthony, 2004). Also, due to the nature of the procedures, the surgeon's movements are scaled during procedures. Figure 3 shows a sectioned view of the abdomen and illustrates the Fulcrum effect along with the scaling of movement around the point of incision.

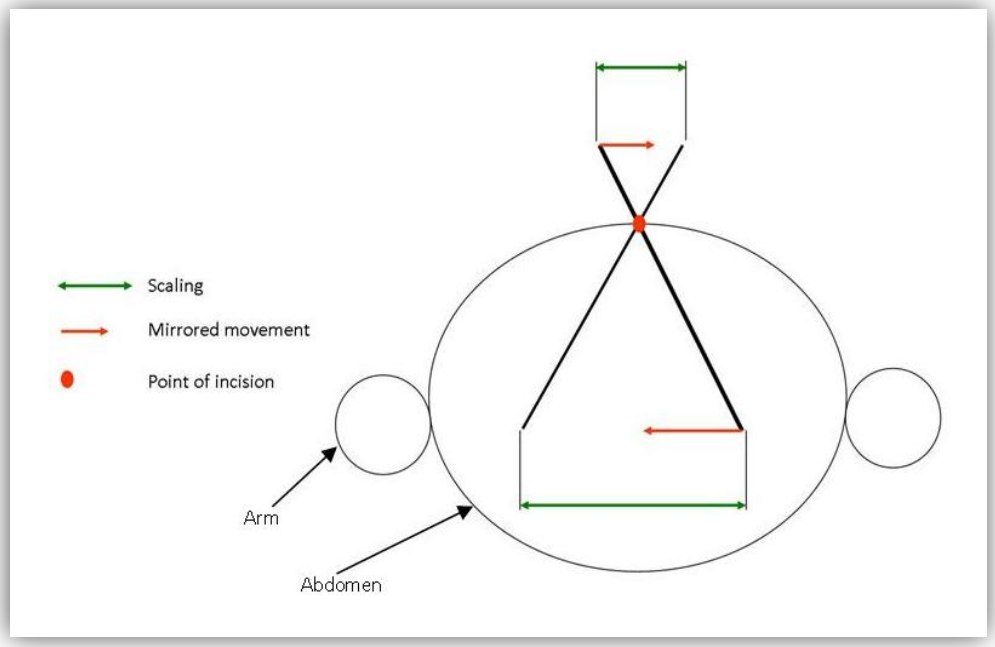

Figure 3: Disadvantages of MIS, Fulcrum effect and scaled movement

The human arm has seven Degrees Of Freedom (DOF), so in open surgery the full mobility of the hand and arm is utilized. The way the MIS instrument is inserted and assembled limits the surgeon to only four degrees of freedom, excluding gripping (Schur *et al*, 2000). This severely restricts the surgeon's movement and adds complexity to the surgery. Usually simple tasks, such as suturing and tying a knot, becomes extremely difficult due to the limitations of access and instrument motion. The ergonomics of MIS contribute significantly to surgeon fatigue and discomfort, especially with time consuming surgeries (Oehler, 2009).

1.2 Minimally Invasive Robotic Surgery

Minimally Invasive Robotic Surgery (MIRS) makes use of robotic manipulators to alleviate the drawbacks associated with MIS. Improvements offered by MIRS systems include increased precision, better manoeuvrability and enhanced dexterity. A summary of MIRS versus conventional MIS is given in Table 1. The two methods can now easily be compared to give a better indication of which type of surgery would be beneficial to a medical centre.

Table 1: MIS and MIRS advantages and disadvantages (adapted from Lanfranco et al, 2006)

	MIS	MIRS
Advantages	Well-developed technology Affordable and ubiquitous Proven efficacy	3-D visualization Improved dexterity Seven degrees of freedom Elimination of Fulcrum effect Ability to scale motion Tele-surgery is possible Ergonomic position
Disadvantages	Loss of touch sensation Loss of 3-D visualization Compromised dexterity Limited degrees of motion Fulcrum effect Physiological tremors	Absence of touch sensation Very expensive High start-up costs May require extra staff to operate New technology (acceptance)

One benefit of robotic surgery is the ability to perform tele-surgery. This implies that the surgery is done where the patient and the surgeon are located at different geographical locations. This application was first demonstrated in 2001 when a patient in Strasbourg, France, received a robotic cholecystectomy from the ZEUS robotic system (Section 2.2) whilst the surgeon was located in New York (Satava, 2006). Additionally, MIRS offer many other advantages over normal MIS. The most significant are the elimination of the Fulcrum effect, improved dexterity and removal of the surgeon's hand tremors. The robot's ability to restore proper hand-eye coordination makes it possible for the surgeon to use more natural movements with reduced fatigue. This increases the safety of the patient and also protects the surgeon against unintended mistakes. Most robotic systems achieve these advantages by having a separate surgeon and patient console. The surgeon is able to take up a seated position when performing surgeries while the patient side console can be moved and adjusted to be in the correct position for the required surgery. Even though robotic surgery has all these benefits, the existing systems are extremely expensive. The cost is usually the prohibiting factor when a hospital has to make a decision on whether a MIRS system would be beneficial to them (Lanfranco *et al*, 2004). The only available commercial system (da Vinci), costs between $ 1-2.3 million in the USA. The large difference in cost is associated with the different da Vinci models in the market. Together with this, the hospital must have a service agreement of about $ 100-180 thousand per annum. Additionally around $ 1.3-2.2 thousand is required for instruments and accessories for each procedure (Gomez, 2011). In some cases larger operating rooms are required to accommodate these systems since they take up a lot of space (Sim *et al*, 2006). Another potential problem is the upgrading of a system. Hospitals are concerned about how much it would cost to upgrade and how

often they would need to do it. Many also believe that the purchase of a robotic system would be adopted more easily if the system had a more widespread multidisciplinary usability (Satava *et al*, 2001).

Consequently, an inexpensive MIRS system can offer a competitive edge. Such a system can be used to perform the procedures that are less complex and done more frequently. Complex procedures can then be referred to the more sophisticated robotic systems or can be done manually. The less expensive system will be more accessible to most medical centres, which can improve the delivery of healthcare to all patients.

1.3 Objectives

The objective of the thesis is to design and test a low cost Secondary Slave Manipulator (SSM) for a MIRS system. This manipulator must be able to combine with a Primary Slave Manipulator (PSM) developed by PJ Christiane (2008). The SSM must have three DOF, which will bring the total movement capability of the complete manipulator to seven DOF.

The design presented in this thesis includes all the mechanical and electronic requirements, and the system must be able to actuate both the SSM and the PSM as desired. Although the four DOF of the PSM will be controlled, they will not be retested, as all testing was completed by Christiane (2008). Testing for the SSM must prove that the manipulator is capable of providing the required working range, resolution and strength, as would be required by a surgeon for a typical laparoscopic procedure.

Chapter 2: Robotics in Surgery

This section will focus on how robotics has aided surgeons during surgical procedures. It starts out with a brief overview of robotics used in procedures other than abdominal MIS in order to show the potential that robotics have in surgery. It will then continue to give detailed descriptions of MIRS systems used commercially, as well as those that were developed at other academic institutes.

2.1 History of Robotics in Surgery

The use of robots in surgeries has been around since 1985 and is gaining in popularity. Surgical robotics was started because of potential advantages, such as faster surgeries and higher accuracies, much the same way in how industrial robots were adopted (Gomes, 2011). Figure 4 shows a timeline of major robotic advances in surgery.

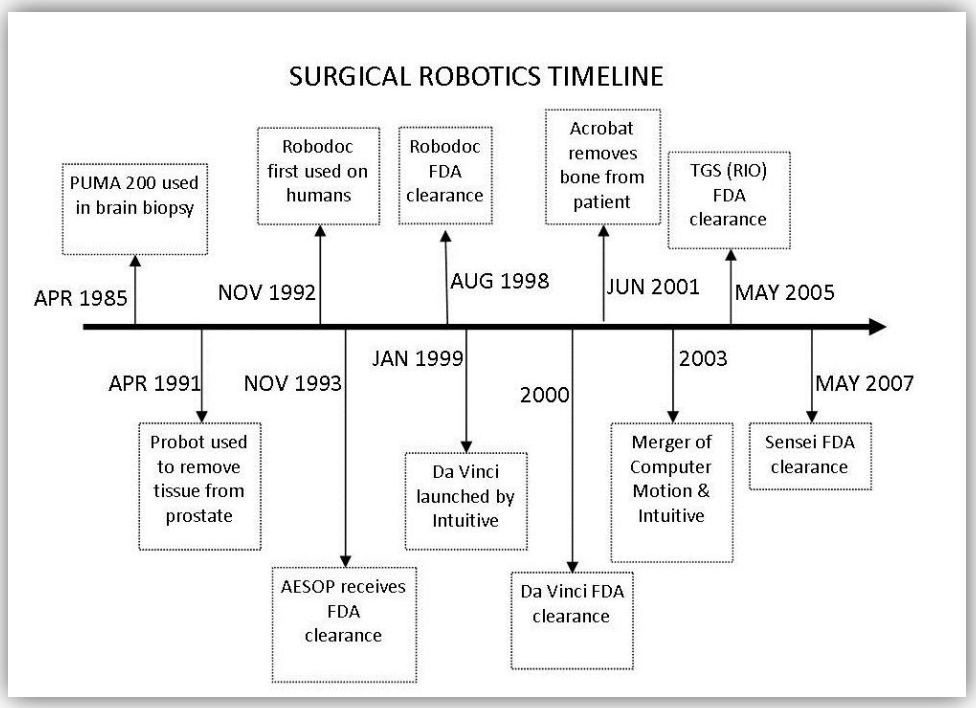

Figure 4: Timeline of robotics in surgery (adapted from Bogue, 2011)

On 11 April 1985, the first recorded use of a robotic surgical procedure was performed at the Memorial Medical Centre in Long Beach, California (Kwon *et al*, 1988). An industrial robot, the PUMA 200 was used during a CT-guided brain biopsy. During surgery, the robot was used to place the biopsy probe. Once the guide was in position,

the robot was locked and power to the robot was removed (Kwon *et al*, 1988) allowing the surgeon to insert a probe that was capable of reaching the surgical target.

From 1991 to 2006 several robotic systems were used to aid surgeons during procedures. The Probot was a custom built robot used to autonomously remove a large amount of tissue from a patient's prostate (Davies *et al*, 1991). In 1992 the Robodoc system, another robot adopted from industrial use, was used during total hip arthroplasty procedures (Taylor *et al*, 1989). The Acrobot was used for milling in total knee arthroplasty procedures in 2001 (Jakopec *et al*, 2003). Bogue (2011) provides a brief history of surgical robotics from 2005 onward: The Robotic arm Interactive Orthopaedic system (RIO) was another device used for orthopaedic joint replacement. The original version of the device was called the Tactile Guidance System (TGS). The TGS device obtained FDA clearance in May 2005. The first orthopaedic procedure done with the RIO was performed in 2006. Hansen Medical Inc. from Mountain View in California designed a master/slave robotic catheter system called Sensei. The company was founded in 2002 to develop robotics for accurate and stable control of catheter technologies. The robotic system received FDA approval in May 2007. The system allows the surgeon to remain seated whilst positioning a steerable catheter tip into the required point in the heart. Robotics has also found application in spinal surgery procedures. The SpineAssist is a highly accurate six DOF robot with a hexapod design. The robot is a bone mounted system that is responsible for accurate guidance of an implant in order to stabilize spinal fusions.

All of the aforementioned robotic systems showcase the potential that robotics have in aiding surgical procedures. The discussion of robots in MIS will be divided between the commercial systems, shown on the timeline in Figure 4, and the systems developed at research/academic institutes. The systems developed at research institutes are not used commercially, but still contain valuable information regarding the design and implementation of MIRS systems.

2.2 Commercial MIRS Systems

In 1994 the first commercially available unit called AESOP (Automated Endoscopic System for Optimal Positioning), was used to manipulate the position of an endoscope (Lanfranco *et al*, 2004). The first version, named AESOP 1000, was controlled by the surgeon using foot pedals. The next version, AESOP 2000, relied on voice commands from the surgeon. This made the system more user friendly, especially to new users. The AESOP 3000 combined the voice command with the ability to move the endoscope with seven DOF. The latest version, AESOP HR, is made by Intuitive Surgeries Inc., after their merger with Computer Motion Inc. in 2003 (Sim *et al*, 2006). Figure 5 shows AESOP being used in a MIS procedure.

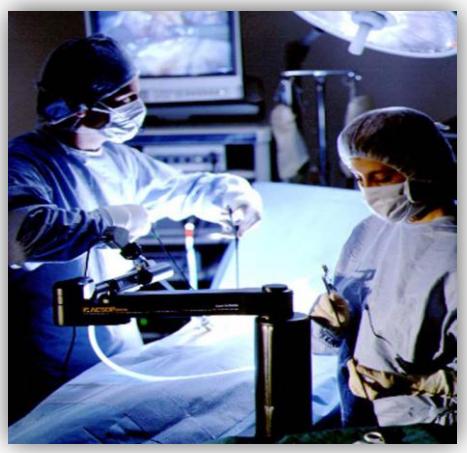

Figure 5: AESOP being used in MIS procedure (Sim *et al*, 2006)

In 1996 the Zeus system was introduced by Computer Motion Inc. It combined the AESOP's endoscope manipulator with two robotic manipulators, which were connected to the operating bed, and a surgical console (Ruurda *et al*, 2002). The surgeon was able to view the operating site in 3D on the surgical console with the help of polarized glasses. New MIS instruments were attached to the robotic manipulators which had a six DOF tip, called the MicroWrist. The instruments were 3.5 mm to 5 mm in diameter and were reusable. The surgeon was able to control the manipulators, MicroWrist and endoscope all from the surgical console. The Zeus system received FDA approval in 2002 (Marescaux & Rubino, 2003). The surgeon's console as well as the robotic manipulators can be seen in Figure 6.

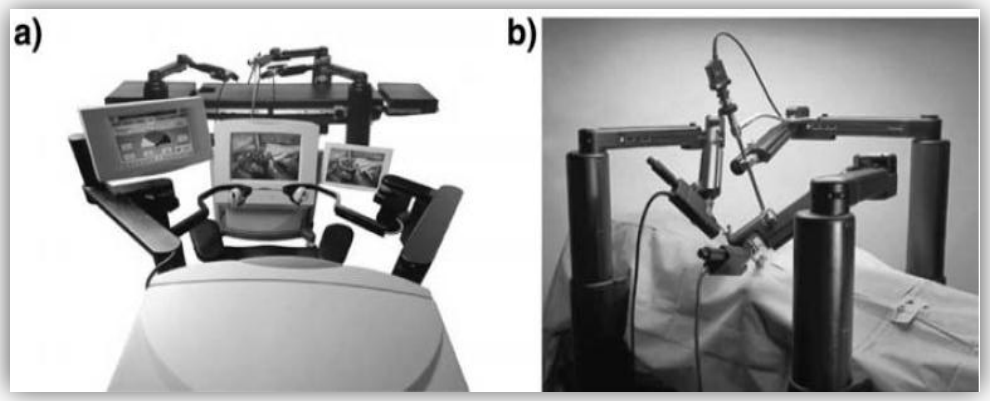

Figure 6: ZEUS robot with (a) surgeon console and (b) robotic manipulators (Eto & Naito [S.a.])

After the merger between Computer Motion Inc. and Intuitive Surgical Inc. in 2003, the Zeus system was dropped and replaced by the da Vinci surgical system which received

FDA approval in 2001. The system is made up of a master surgical console that is connected to a manipulator console, much the same as the Zeus system.

The da Vinci robotic system is the first robotic surgical system to incorporate 3D High Definition (HD) vision. This is achieved with either an 8 or 12 mm stereo endoscope. Both the aforementioned endoscopes are available in either 0° or 30° viewing angles (Lobontiu & Loisance, 2007), indicating that the lens of the endoscope is tilted at either a 0° or a 30° angle. The viewing system also utilises digital zoom, which reduces the interference between the endoscope and the surgical instruments (Hockstein *et al*, 2007).

The surgical instruments shown in Figure 7 are known as EndoWrist® and are made up of a robotic wrist and gripper which can closely represent the movements of the human hand. The instruments are controlled by fingertip on the surgeon's console (Sung & Gill, 2001). In addition the movement of the instruments are enhanced by removing tremors and scaling the surgeon's hand movement. This allows for much safer and controlled operations (Wilson, 2009). The instruments are available in both 5 and 8 mm diameters and are offered in extended lengths to allow the surgeon to easily reach difficult areas within the patient.

Figure 7: da Vinci EndoWrist (Intuitive Surgicals Inc., 2011)

The surgical console aligns the surgeon's eyes and hands over the area of interest. The surgeon places his/her eyes directly over the viewing terminal to obtain the stereo vision created by the endoscope. The surgeon can assume a comfortable seated position, thus ensuring surgeon fatigue is minimized (Jaspers, 2006).

The patient side cart in Figure 8 consists of one robotic arm to hold the endoscope and three robotic arms to hold the surgical instruments (Advincula, 2006). At the end of each robotic arm is a quick click cannula which clicks onto the trocar that is inserted into the patient's abdomen (Hubens *et al*, 2008). This simplifies the docking of the robotic arms above the patient. The patient side cart is also motorised to ensure easy and quick movement inside the operating room.

Figure 8: da Vinci robotic manipulator (Intuitive Surgicals Inc., 2011)

2.3 Academic MIRS Systems

The RAVEN surgical robot was developed by the collaboration of the BioRobotics lab at the University of California and the Department of Surgery at the University of Washington. The robot was designed from results obtained from experiments using a system called Blue Dragon, which was developed by Brown *et al*, (2002), which analyzed the surgeon's movement, force and torque requirements during test procedures. Figure 9 below shows the layout of the Blue Dragon system. Circled in blue are positional sensors, whilst the torque and force sensors are circled in red.

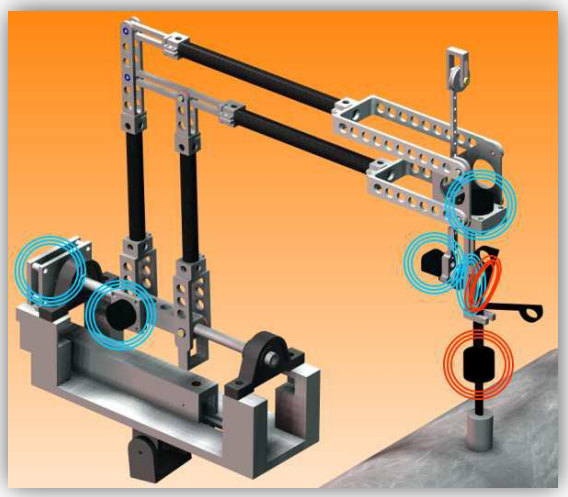

Figure 9: Blue Dragon MIS force and torque analysis robot (Mitchell & Lum, 2004)

Further experiments also evaluated whether a parallel or spherical mechanism, as seen in Figure 10, would be best suited for the manipulation of the surgical end affecter. The spherical mechanism consists of two arms that can freely and independently rotate perpendicular to each other. The parallel mechanism consists of two spherical mechanisms connected at the tip. The experiments were done by positioning the two systems at various angles to find the optimum working position for each. From these experiments it was found that the parallel mechanism suffered from collisions with itself and the patient. It was concluded that two serial mechanisms have the smallest footprint and would be able to reach a larger workspace within the abdomen of a patient (Mitchell & Lum, 2004).

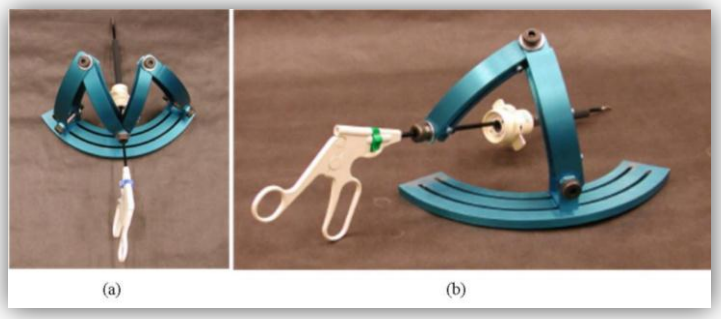

Figure 10: Parallel (a) and spherical (b) mechanisms (Mitchell & Lum, 2004)

From the experimental results, a seven DOF robot was designed. The robot uses an assembly resembling the spherical mechanism in order to realize the pivoting movement required in MIS procedures. The robot uses cables to realize all the required movement. All cables are actuated with the use of brushless DC motors. The motors that need to

provide the most torque (shoulder, elbow and insertion) are coupled with 12:1 planetary gearboxes and power off brakes should a power failure occur (Mitchell *et al*, 2006).

The RAVEN in Figure 11 has since been successful in several teleoperated scenarios. One scenario was performed at the National Undersea Research Centre (NURC) in Key Largo, Florida at the Aquarius Undersea Habitat. The Habitat is located 3.5 miles offshore at a depth of 60 ft (18.3 m). The surgeon site was set-up in a conference room in Seattle, Washington while the patient site was set-up and supported by two surgeons inside the Habitat. The goal of the experiment was to gather information on TeleRobtics over a long communication network and found that all tasks had a mean latency period over the network of 75 ms. Another teleoperation experiment was the High Altitude Platform/Mobile Robotic Telesurgery (HAPs/MRT) project. The goal of this experiment was to test the RAVEN in a field condition, which is drastically different from a clinical environment. The RAVEN was set-up in the desert of Simi Valley in California. The robot was set-up under tents and powered by gas generators during the experiment. The surgeon and patient sites were separated by a mere 100 m, but the communication link between the two sites was established by digital data link on-board an AeroVironment PUMA unmanned aerial vehicle. This experiment showed mean latency periods over the network of 16 ms (Mitchell *et al*, 2009).

Figure 11: RAVEN I robot (Raven - Mini Robot Design for Military Telesurgery in the Battlefield. [S.a.])

The surgical system has since been modified and is known as the RAVEN IV. The system now utilises the collaboration between two surgeons, with the use of two cameras and four surgical arms (Raven IV - Colaborative Surgery. [S.a]). At present there is no information regarding the cost of the RAVEN IV surgical system. The system can be seen in Figure 12.

Figure 12: RAVEN IV robot (Raven IV - Colaborative Surgery. [S.a.])

The Surgeon's Operating Force-feedback Interface Eindhoven (SOFIE) surgical robot was developed at the Eindhoven University of Technology. It was developed as part of a PhD thesis by Dr. Linda van den Bedem (Bogue, 2011). The design is based on two main parts, (a) pre-surgical set-up and (b) manipulator adjustment as seen in Figure 13. The pre-surgical set-up consists of a base and platform.

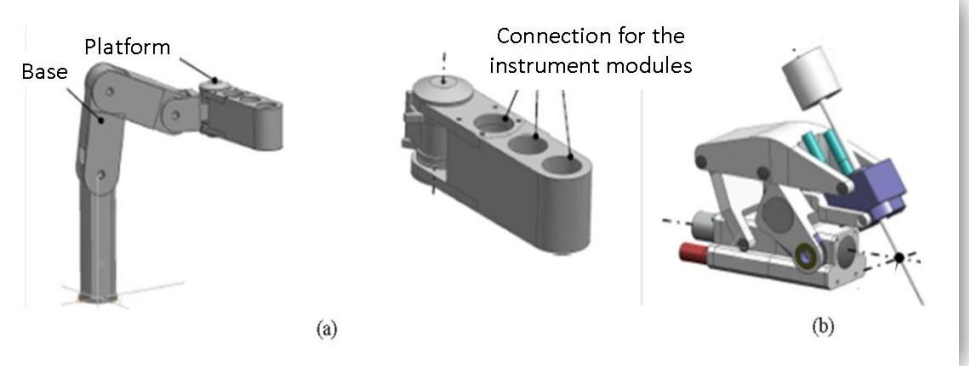

Figure 13: SOFIE robot with base and platform (a) and manipulator (b) (adapted from van den Bedem *et al*, 2009)

The base section can be mounted directly to the operating table. This eliminates the need to readjust the robot if the bed is moved. The platform that connects to the base is designed to hold three surgical manipulators. In most cases this will include two surgical instruments and an endoscope. The surgical instrument manipulator will be mounted to the platform with the use of a course adjustment arm. This will allow the surgical staff to adjust the robot into position for the procedure. The surgical instrument manipulator itself consists of a parallel arm assembly to realize the pivoting movement required. Linear movement for insertion actuation is done with a friction wheel. The housing of the friction wheel drive is then rotated to achieve instrument arm rotation.

The SOFIE robot has the additional benefit of incorporating haptic (force) feedback into its design. Torque sensors are placed after the transmission of each joint thus ensuring that friction forces are not measured. These torque measurements are then sent back to the control electronics which amplify and send them to the master controller. The master controller is thus made up of the mechanical structure, encoders to send signals to actuating motors and the motors to realise haptic feedback (van den Bedem *et al*, 2009).

Since October 2010, Dr. Van den Bedem has been investigating the possibilities for commercial application of the basic design. Due to the need for clinical trials and certification, it is expected that a market ready version will only be available from 2016. At present the researcher is exploring SOFIE's commercial potential, but no information regarding the cost of the system is available (Bogue, 2011). Figure 14 shows the robot over an OR bed.

Figure 14: SOFIE robot (Bogue, 2011)

2.4 Chapter Summary

The literature survey shows how surgeons would perform MIS procedures and the relative drawbacks associated with these techniques. It was further shown how robotics have been successfully implemented in several different types of surgical procedures, therefore showing that when designed correctly, robotics have the potential to aid and improve surgeries for both patient and surgeon.

The different MIRS systems gave insight into some design aspects that should be considered for the development of the SSM. During MIRS procedures, the placement of the robot in the Operating Room (OR) depends greatly on the reach of the robotic arms. The da Vinci robot is capable of being placed almost anywhere alongside the patient due to its large workspace. The SOFIE, RAVEN I and RAVEN IV need to mounted over the patient as the layout of their arms doesn't allow placement elsewhere in the OR.

The literature survey also showed that if a robotic manipulator is to be designed and implemented successfully in MIRS procedures, it must provide movement that is pivoted around the point of incision. Motors that are responsible for heavy loads should be supported by safety brakes in case of power failures or emergencies. In order for a manipulator to do successful surgeries, the latency of all communication lines, signal processing and mechanical functions should be minimised. The longer a surgeon has to wait for the manipulator to react to the inputs given, the more chance there is of a complication becoming life threatening. As with open surgery and MIS procedures, the use of two hands is essential. In this thesis only one manipulator was built, with the aim that the second one can be an exact duplicate.

Chapter 3: Mechanical Design

This chapter is concerned with the methodology followed in order to design the SSM. It will explain how different concepts compared against the developed criteria and why the final design was chosen. From there it will explain the systematic design of the manipulator and the analysis of its movement.

3.1 Robotic Manipulators

The challenges in designing a manipulator for MIRS is that the entry point into the abdomen must serve as a pivot point for all external movements. Therefore two DOF's need to pivot around the entry point, whilst the third DOF will be used for insertion into the abdominal cavity. There should be no forces exerted on the abdomen wall by any of the DOF's regardless of independent orientation of each DOF. The manipulator must further be able to recreate the speeds and range of movement a surgeon would require for the procedures, move from one point to another within the abdomen, as well as instrument removal.

Five types of robotic manipulators were identified as feasible for use in MIRS procedures. These manipulators will be explained and analysed according to criteria determined from the literature survey.

3.1.1. SCARA Manipulator

A Selective Compliant Assembly Robot Arm (SCARA) robot consists of three motorised joints capable of moving in an x-y-z coordinate system (Das & De Iger, 2007), as shown in Figure 15.

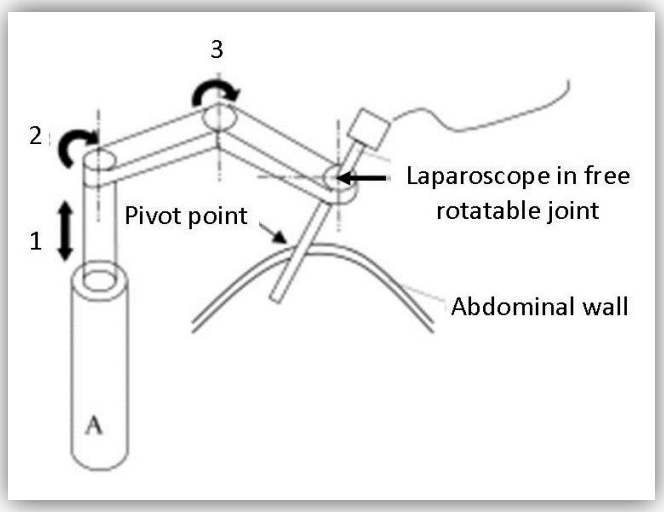

Figure 15: Working principle of SCARA robot (adapted from Jaspers, 2006)

It is called a Selective Compliance Robot as it cannot comply with all coordinates in the x-y system. Figure 16 shows the workable area of different variations of SCARA robots (Milutinov & Potkonjak, 1990).

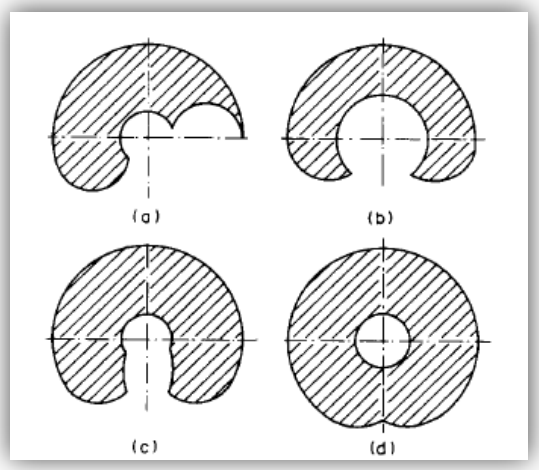

Figure 16: Limitations on SCARA robot's working range (Milutinov & Potkonjak, 1990)

Due to the configuration of the robot assembly, the links in the manipulator are cantilevered. Therefore SCARA robots must be carefully designed in order to achieve acceptable trade-offs between stiffness of the arms (this will cause increased settling times after fast motions) and minimising the weight of the arms, which allows for faster acceleration as well as smaller actuators (Quaid & Hollis, 1996).

The ZEUS robot is based on the SCARA principle. Since the manipulator simply moves the surgical instrument in the x-y coordinate system, the incision point in the abdomen serves as a passive joint. This means that the surgical tool effectively pushes against the abdomen wall to create a ball joint. Therefore this manipulator will have about the same scarring effects on the patient as conventional MIS.

3.1.2. Stewart Platform

The Stewart platform (shown in Figure 17) was invented in 1965 by D. Stewart. Stewart platforms work with the aid of linear actuators moving concurrently to create motion. Since more than one actuator is responsible for any of the required movements, the loads on the actuators are small. With serial manipulators, the first motor has to support the weight of all motors on succeeding joints. Therefore the Stewart platform is capable of higher accuracy and uses smaller actuators when compared to some serial manipulators (Lazarevic, [S.a.]). This type of manipulator was used for the SpineAssist robot that was mentioned in Section 2.1.

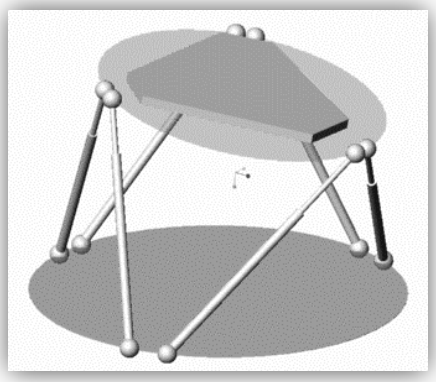

Figure 17: Stewart platform (Markine [S.a.])

A disadvantage of this concept is the smaller workspace in comparison with serial manipulators (Fichter, 1986). Concurrent movement is required to create the three DOF pivoting movement required for the purposes of this thesis, resulting in a complex control algorithm to realize such a movement. The platform needs to move through an arc to enable the surgical instrument to pivot around the point of incision. The pivot radius of the platform will also need to change every time the length of insertion changes. This is because the radius that the platform needs to pivot around will become smaller as the platform moves closer to the point of incision.

3.1.3. Seven Axis Robotic System

Several manufacturers supply industrial robotic systems that are capable of part handling, welding and painting. Figure 18 shows a Motoman robot that can work with a payload of 5 kg. These robots are supplied in a series of sizes, depending on the weight they are required to handle. Seven axis robots are extremely complex and offer several different movement capabilities, such as pivoting around a tool tip, translation and independent axis movement.

Figure 18: Motoman 7-axis robotic manipulator (Motoman, 2011)

The robot can be programmed to have its movement pivot around a pre-determined tool tip, which can act as the pivoting point required in MIRS. However, this will require that an additional actuator be mounted in the last axis of the robot for insertion of the surgical manipulator. This is due to the pivot point which will remain the same regardless of the height. The robot can be adjusted to the specific patient via the robot controls with the aid of all of the other programmable robot movements, before it is switched to pivoting movement.

The robot can also be used in translation mode. This means the programmed tool tip will translate in a perfectly straight line in the x-y-z coordinate system. This will enable the robot to function as a SCARA manipulator.

These robots are also extremely expensive and their load bearing capacity typically far exceeds that required for surgical procedures. Additionally, the software of these systems will have to be updated since they are not designed to operate with a remote input. These reasons possibly contribute to why there has not been a documented use of this type of robot in a surgical procedure.

3.1.4. Parallel Arms Manipulator

When combining two sets of parallel arms as in the configuration presented in Figure 19, a double parallelogram is formed. These combined parallelograms would cause movement around a Virtual Point of Rotation (VPR). If the parallel arm assembly is mounted on a shaft that is directly in line with the VPR, it is possible to have two DOFs moving through the required pivoting point without the need for any control algorithms (van den Bedem *et al*, 2009). It should be kept in mind that when using this type of configuration, proper alignment is critical. All centres of rotation must be aligned to ensure the correct VPR.

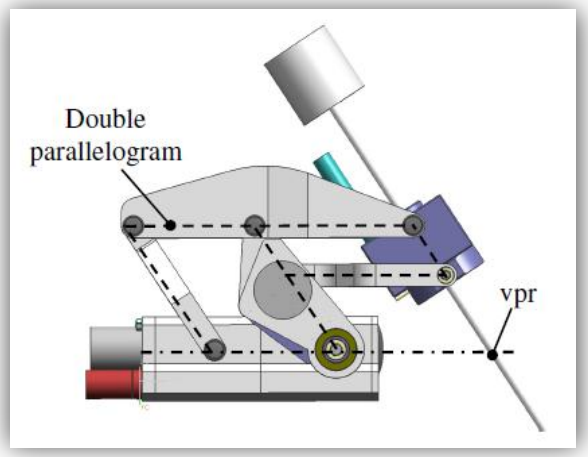

Figure 19: Working principle of parallel arms configuration (van den Bedem *et al*, 2009)

This manipulator gives the added benefit of having a large range of motion. The length of the arms as well as the distance between them contributes to the total reachable range. The shaft which houses the arms can usually rotate 360° around its own axis. Therefore the movement of the shaft is mostly limited by the workspace inside the abdominal cavity.

3.1.5. Spherical Mechanism

The spherical mechanism mentioned in Section 2.3 is another manipulator concept that can generate a VPR. A single pivoting arm attached perpendicular to a base arm is capable of generating the VPR without the need for a complicated control algorithm. As long as the base arm and attached arm's pivoting axes are in line, a single VPR will be generated that can be aligned with the surgical entry point. Figure 20 shows the concept of the manipulator. The base arm rotates around axis Z1. The pivoting arm will pivot around axis Z3. Rotation around axis Z2 is achieved by the PSM. As with the parallel arm concept, alignment is critical with this manipulator.

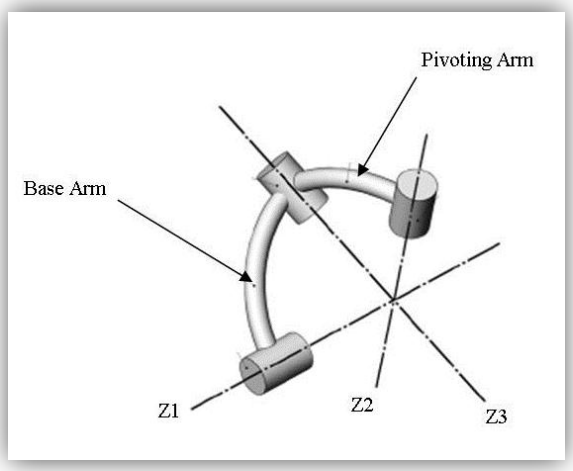

Figure 20: Working principle of spherical mechanism (adapted from Mitchell & Lum, 2004)

The layout of this concept requires it to be mounted above the patient. Thus interference with the patient is a concern. The manipulator must therefore be designed so that the required range of motion is achieved by moving the base arm away from the patient.

3.2 Concept Evaluation

At this stage, an evaluation of the different layouts can be made against the criteria generated by means of the literature survey. In order for the manipulator to be successful, it must generate a pivoting movement around the point of incision and not have the possibility of singularities within the abdominal region. Since the aim of the thesis is to design a cost effective manipulator, the cost of the manipulator must be kept to a minimum. Also, it was important to keep the design simple, as to keep the cost of the manipulator down and allow future work to be easily integrated into the design. Table 2 shows how well each of the concepts satisfies the criteria. The quantative data is given in Appendix C. Each manipulator is rated on how well it fulfils the given criteria with a mark out of three. The colour bar at the bottom of the table indicates the mark given.

Table 2: Concept evaluation

	No force exerted on abdomen	Movement complexity	Range of movement	Low cost
SCARA				
Stewart Platform				
7Axis Robotic System				
Parallel Arms				
Spherical Mechanism				

1	2	3

The SCARA manipulator exerts forces on the abdomen wall to create the required pivoting movement. This could cause unwanted discomfort to the patient, and thus this manipulator will not be considered further. The Stewart platform's complex control seems an unnecessary and time consuming feature when there are other manipulators capable of creating the required pivoting movement automatically. Along with the possibility of a time consuming design, its movement is limited and may prove problematic during MIRS procedures. Another requirement of the thesis is to keep costs to a minimum. This means the seven axis robotic system would not be suitable.

Since there is currently only one surgical manipulator in development, there is no clear indication of how the robot will be positioned in the OR. Therefore, when choosing from the remaining two manipulators (parallel arm and spherical mechanism) it would be beneficial for future work to incorporate the manipulator with the widest range of positioning freedom. The single arm concept must be mounted above the patient while the parallel arm concept, if given adequate reach, can stand away from the patient and have a larger freedom of adjustment than the single arm manipulator. Thus, from this argument, the parallel arm manipulator will be designed and manufactured.

3.3 Manipulator Design

This section will discuss the methodology of the design process. It will state the design criteria and explain the steps followed in order to design the manipulator.

From the literature survey presented in Section 2 and the objectives discussed in Section 1.3, the principal design requirements for the manipulator are:

- Generate a two DOF (perpendicular to each other) pivoting movement around the point of incision along with a third insertion DOF.
- The manipulator must be able to support the weight of the PSM (5 kg) along with any additional weight of bearings, actuators etc.
- Although it is not a direct requirement of the manipulator to have tele medicine capabilities, it would be beneficial to showcase the possibility of such an application.
- The costs of the manipulator must be kept low. In order to quantify low cost, the design of the SSM will be compared to the design of the da Vinci to establish whether the design could indeed be more cost effective than the existing commercial system.
- Able to generate a 10 N force at the tip of the PSM. This force was a design requirement set out by Christiane (2008) and was achieved by the PSM.
- Ability to produce end effecter speeds required for procedures, instrument relocation and instrument removal/insertion.
- Ability to produce end effecter resolution required for procedures, instrument relocation and instrument removal/insertion.

The different speeds required for the various parts of surgery were obtained by studying video footage taken during several laparoscopic procedures. The videos showed that the speeds required from the manipulator (for the rotary two DOF movements) ranges from around 5 rev/min to 20 rev/min. The speeds required from the insertion DOF ranged from around 5 mm/sec to 70 mm/sec.

The required resolution of the manipulator was determined in the operating theatre. During laparoscopic procedures the surgeon had very little control over the precision of the tool tip. It was found that the surgeon very rarely located the tool tip within 10 mm when moving the surgical tool inside the patient's abdomen at normal procedure speeds. The surgeon explained that in these types of surgeries if the organ is grasped, dissected or sutured close by the intended location, the task can still be completed successfully. Therefore, from these observations it was decided to set the required resolution of the manipulator at 1 mm. This resolution will allow the surgeon a degree of control that cannot be realized with conventional methods.

The pivoting movement is achieved by the double parallelogram effect of the parallel arms. Reviewing the work done by Christiane (2008), it is evident that the major contributing factor to the cost of the manipulator would most likely be the actuators. The actuators perform a critical role in the manipulator's functioning, so it will be important not to compromise in their selection. To maintain a balance between good accuracy and low cost, DC electric motors would be used to actuate the manipulator, rather than more expensive pneumatics or hydraulic systems. DC motors have a high start-up torque, and since the manipulator would be required to move in a stop/start way, this torque curve would be beneficial to the system.

To ensure an adequate range of movement, it must first be established what an acceptable range of movement is. Mitchell & Lum (2004) described that in order to reach all the organs in the abdomen from the umbilicus, a single manipulator must move 90° in the medial/lateral direction (left to right) and 60° in the superior/inferior direction (head to foot) thus creating a elliptical cone with vertex angles of 60° and 90° as in Figure 21.

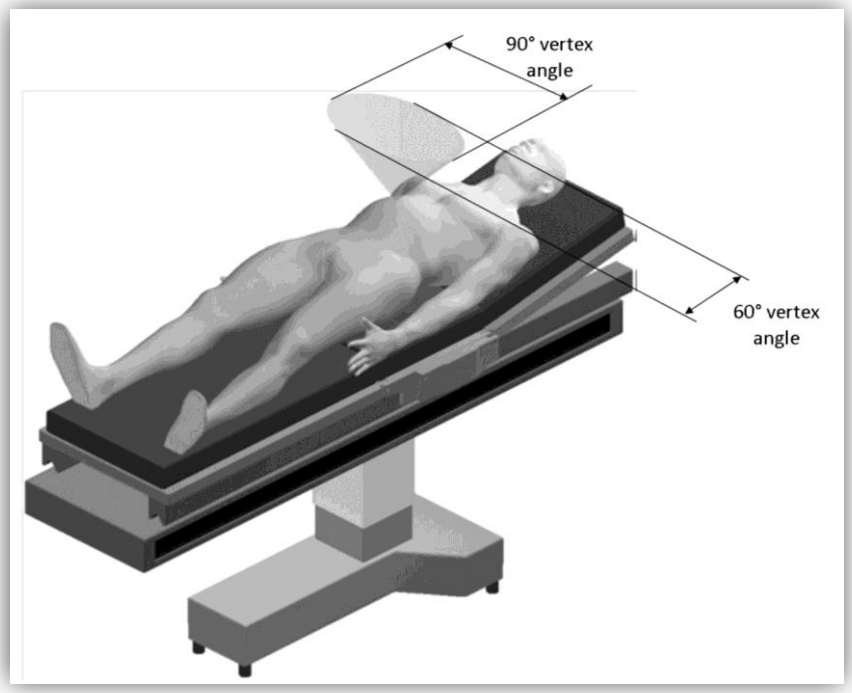

Figure 21: Elliptical cone with vertex angles of 60° and 90° (adapted from Mitchell & Lum (2004))

In MIRS procedures it would be highly unlikely that only one manipulator would be used (the da Vinci has three, the RAVEN IV has four). Therefore these parameters are quite excessive when keeping in mind that at least two manipulators would be used by a surgeon when performing procedures. Figure 22 shows the trocar placement for three

common MIRS procedures, (a) aortic lymphadenectomy, (b) tubal reversal and (c) myomectomy using the da Vinci robot. The figure shows that the endoscope is usually placed through, or just above, the umbilicus while the two robotic arms are placed toward the inferior. The robot will then operate toward either the superior or the inferior, thus leaving the organs located toward opposite direction of the incisions untouched (Holloway *et al.*, 2009). Additional incisions may be required for assistance, however a surgeon will typically operate through these ports. Figure 22 thus shows that the workspace of MIRS is limited to the section of the abdomen where the relevant organs are located. Thus two or more manipulators should require a smaller range than specified by Mitchell & Lum (2004). Considering the arguments made above and from observations made during surgical procedures, a working range of 30˚ in the superior/inferior direction (the robot only needs to reach the relevant organs located toward the superior or inferior of the incisions, thus half of the 60˚ vertex angle) and 90˚ in the lateral/medial direction (it could be possible for the manipulator on the left of the endoscope to reach over to the right of the endoscope to perform a necessary task) will be set as target values. The design will however still attempt to obtain the range of 60° in the superior/inferior direction for a single manipulator.

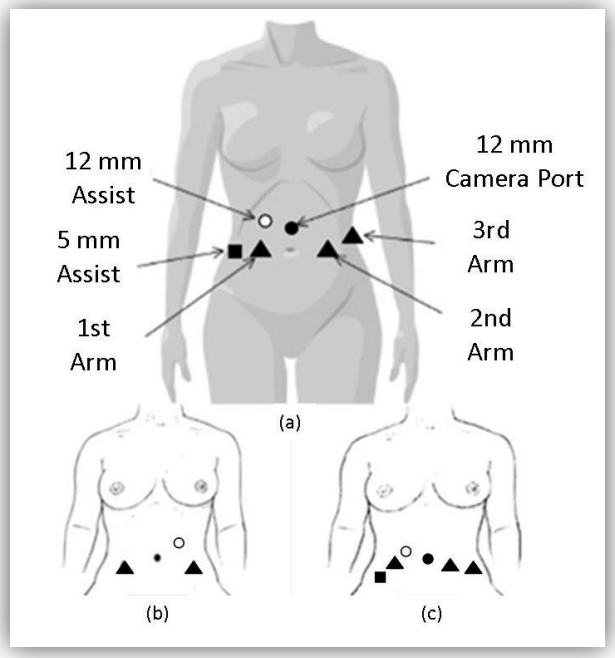

Figure 22: Incision location for MIRS lymphadenectomy (a) tubal reversal (b) and myomectomy (c) (adapted from Holloway *et al*, 2009)

Table 3 summarises the design requirements for the SSM.

Table 3: Design Requirements of the SSM

	Value
Movement	Two rotary DOF (perpendicular to each other) along with one linear DOF for insertion
Required mass that should be supported	Must hold 5 kg mass of PSM along with bearing assembly along with any additional mass of bearings, actuators etc
Rotational Speed	5-20 rpm
Insertion Speed	5-70 mm/sec
Force produced at tip of PSM	10 N
Medial/lateral Vortex Angle	90˚
Superior/inferior Vortex Angle	30˚ (attempting 60˚)

Lastly, the use of steel cables as a means of actuation will be avoided in the design. It was found by Christiane (2008) that such cables can cause hysteresis problems once stretched. Therefore all DOFs of the manipulator will be directly driven through the accompanying actuator.

3.4 Parallel Arm Concept

In this section the torque required by the two actuators responsible for the pivoting movement is calculated. Since the PSM has a mass of 5 kg, the actuators would be required to move this mass, as well as the mass of the linear actuator and the mass of its bearing assembly.

3.4.1. Torque Analysis

A linear actuator must move the PSM along with any bearing or other sliding mechanism it is attached to for insertion into the and out of the abdomen of the patient. Two rotary actuators will be responsible for moving the arms of the manipulator around the X and Z axes. In Figure 23 the general layout of the parallel arm design is given.

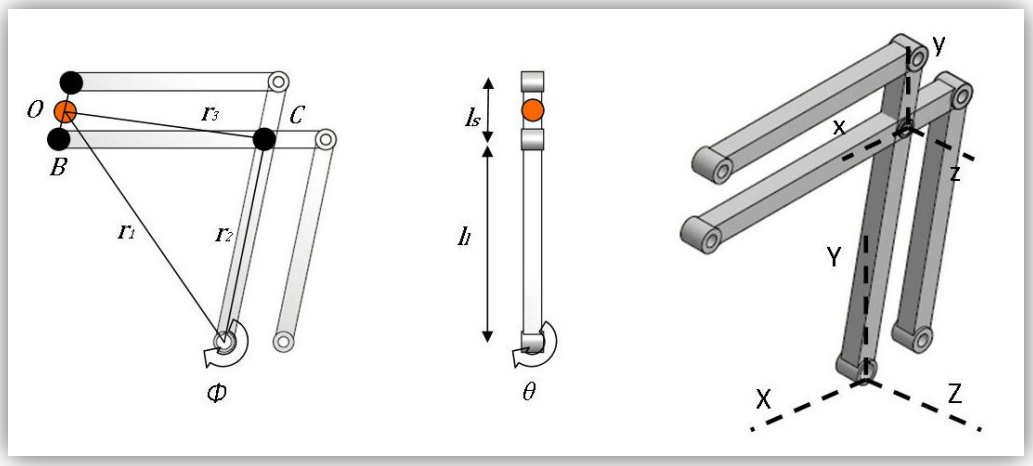

Figure 23: Layout for parallel arm concept

The vectors $\boldsymbol{r_1}$ and $\boldsymbol{r_2}$ describe the distance from the driven actuating point to the centre of the x-y-z coordinate system and the centre of mass of the combined masses of the PSM, linear motor and bearing assembly respectively. Vector $\boldsymbol{r_3}$ describes the distance from point C to the centre of mass of the combined masses of the PSM, linear motor and bearing assembly. The lengths l_l *and* l_s represent the true lengths between the pivoting joints. Angular velocity and acceleration of the driven link is represented by $\boldsymbol{\omega}$ and $\boldsymbol{\alpha}$ respectively.

Since only the mass of the PSM is known at 5 kg, an estimate has to be made concerning the combined mass of the linear motor and bearing assembly. An initial estimate of 10 kg for the mass of the linear motor and bearing assembly was used. The entire 15 kg load will be referred to as the end-effecter mass (the final mass of the assembly was 18 kg).

In order to analyse the torque requirements of the manipulator, a MATLAB simulation model was compiled. The model calculated the static torque caused by the mass of the end effecter. The vector of the contributing weight has a X-Y-Z coordinate and was evaluated over a range spanning from -45° to 45° around both the X (described by θ) and Z (described by Ø) axes. Equations 1 to 3 describe the vectors $\boldsymbol{r_1}$ to $\boldsymbol{r_3}$.

$$\boldsymbol{r_1} = [(l_l sin\theta + l_l + l_s sin\theta) \;\; (l_l + l_s)cos\theta cos\emptyset \;\; (l_l + 0.5l_s)sin\emptyset] \quad (1)$$

$$\boldsymbol{r_2} = [l_l sin\theta \quad l_l cos\theta cos\emptyset \quad l_l cos\theta sin\emptyset] \quad (2)$$

$$\boldsymbol{r_3} = [0.5l_s sin\theta + l_l \quad 0.5l_s cos\theta \quad 0] \quad (3)$$

In order to move these masses, a dynamic element would be added to the torque output, thus a dynamic component was added to the simulation. The simulation will represent the start-up torques required from each of the motors along the same span as

that of the static simulation. The reason for this approach is due to the operating principle of a DC motor. The operating current of a DC motor is described by Equation 4:

$$I = (E_s - E_o)/R \tag{4}$$

E_s is the source voltage applied to the motor. E_o is called the counter-electromotive force, and its polarity always acts against the source voltage. R is the resistance of the motor windings. E_o is induced in the armature conductors the moment they cut a magnetic field. Thus, the faster the motor rotates, the larger E_o becomes. So at standstill the current through the motor is described by Equation 5:

$$I = E_s/R \tag{5}$$

The starting current will be significantly higher than the nominal full load current. This then produces the large start-up torque of the motor and therefore rapid start-up angular acceleration (Wildi, 2006). This angular acceleration will cause an acceleration of particle A tangential to the direction of rotation, as seen in Figure 24. Angular velocity will also contribute toward an acceleration of particle A, but this acceleration is normal to the direction of rotation and will have no effect on the torque required from the source of rotation. Therefore it can be concluded that the maximum torque would be required when the particle has maximum tangential acceleration, no matter what the angular velocity is. Since the DC motor will produce a maximum tangential acceleration of a particle at start-up, the torque analysis of the manipulator will be constructed so that it simulates the start-up conditions of the manipulator on every individual angle over the same range as the static analysis.

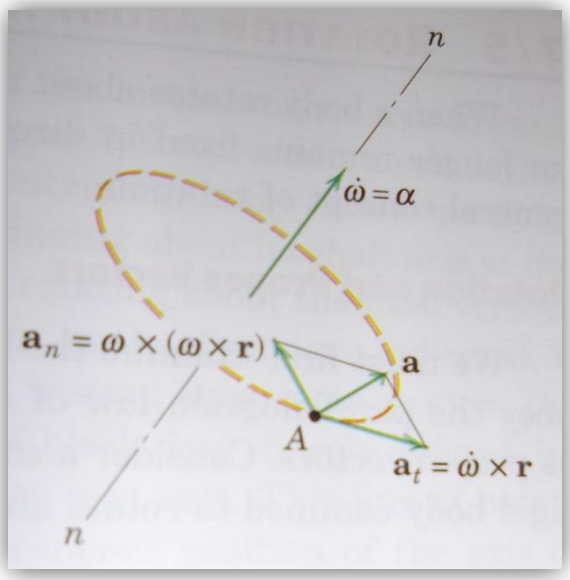

Figure 24: Effects of fixed axis velocity and acceleration

Mabie & Reinholtz (1987) describe the acceleration of a weight caused by a rotating actuation source as follows:

$$\boldsymbol{A_p} = \boldsymbol{A_o} + \boldsymbol{A} + 2\boldsymbol{\omega} \times \boldsymbol{V} + \boldsymbol{\alpha} \times \boldsymbol{R} + \boldsymbol{\omega} \times (\boldsymbol{\omega} \times \boldsymbol{R}) \quad (6)$$

With reference to the coordinate system in Figure 23, $\boldsymbol{A_p}$ is the acceleration of the weight being analysed relative to the X-Y-Z coordinate system. $\boldsymbol{A_o}$ is the acceleration of the x-y-z system origin relative to the X-Y-Z system. $\boldsymbol{A}$ is the acceleration of the point of interest as seen by an observer in the x-y-z system. $\boldsymbol{V}$ is the velocity of the point of interest as seen by an observer in the x-y-z system. $\boldsymbol{R}$ is the vector describing the distance from the x-y-z origin to the point of interest. The values of $\boldsymbol{\omega}$ and $\boldsymbol{\alpha}$ are the angular velocity and angular acceleration of the link on which the point of interest is located. As with the static torques, the dynamic torques were simulated between -45° and 45° around both the X and Z axes. During the simulation different combinations of axis rotation was implemented. The angular velocity was kept constant at 0, to simulate the movement when the manipulator starts up. This would mean that the values of $\boldsymbol{V}$ and $\boldsymbol{\omega}$ will always be zero. Therefore the simulation is not handled as a differential equation, but rather simulates the manipulator starting up from standstill at one degree intervals over both axes. The angular acceleration was selected at 0.87 rev/s^2, this is the final value used as it represents the motor chosen for the manipulator reaching its full rotational speed, 26 rpm, in half a second.

In order to determine the dynamic element of the manipulator around the Z axis, the acceleration of point O on the manipulator must be calculated. In order to do this, the

acceleration of the x-y-z coordinate system must first be determined. Since the angular acceleration of the driven link is known, the acceleration of point C can be calculated. The acceleration of point C is simply the product of the driven angular acceleration and the vector r_1. With the acceleration of point C known, the angular acceleration of link CB must be determined. However, since the configuration of the manipulator causes the link to stay horizontal, the angular velocity and acceleration of the link is zero. From here the acceleration of point O can be determined. Since the configuration of the manipulator causes link BO to stay parallel with the driven link, the angular acceleration of link BO will be the same as that of the driven link. Since the link BO accelerates relative to the link CB, the value of A in Equation 6 will not be zero. The acceleration of point O in link BO relative to link CB is the product of the angular acceleration of link BO and the vector r_3. To complete the calculation for the acceleration of point O the following values are used in Equation 6: $\mathbf{A}_o$ is the acceleration of point C, A is the acceleration of point O relative to point C, α is the angular acceleration of link BO (which is the same as that of the driven link) and R is distance vector from C to O (r_3). The acceleration of point O is then multiplied with the end effecter mass in order to find the force generated by the end effecter. The product of this generated force and the vector r_1 will give the moment generated by the dynamic element of the end effecter. The moments generated around the X axis are calculated with the product of the driven link's angular acceleration and the distance vector the end effecter centre of gravity. This is because around the X axis the manipulator behaves a single driven arm and not a four bar linkage.

Lastly, the inertial effects of the mass must also be included. The end effecter's mass moment of inertia will be modelled as a cylinder with the dimensions of the PSM and a mass of 30 kg. Also, since the mass moment of inertia is located away from the point of rotation, the parallel axis theorem is applicable. Figure 25 shows how the axis of the SSM and the simulated cylinder are orientated. For rotation around the Z axis, the parallel axis theorem is applied to axes q and Z, whilst for rotation around the X axis, the theorem is applied to axes w and X.

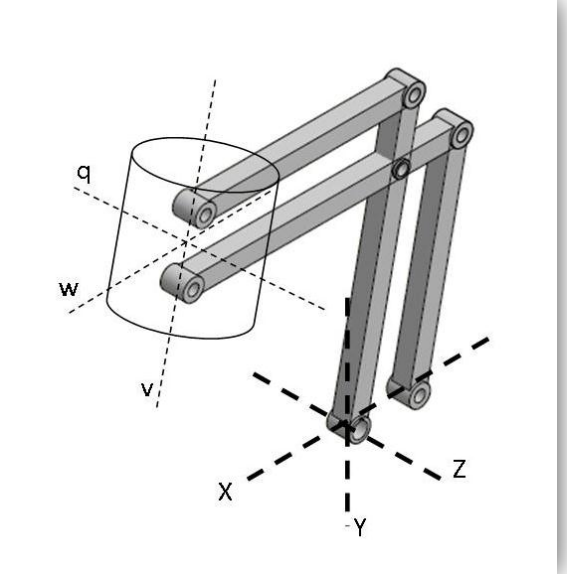

Figure 25: Parallel axis theorem for moment of inertia

Therefore for rotation about the Z and X axes the moment of inertia for the end effecter is described by Equation 7:

$$I = \bar{I} + md^2 \tag{7}$$

Where I is the moment of inertia by the parallel axis theorem, $\bar{I}$ is moment of inertia of the cylinder about its own axis, m is the 30 kg mass and d is the distance from the cylinder's parallel axis to the axis of rotation. The torque resulting from the inertia is determined with Equation 8:

$$T = I\alpha \tag{8}$$

Where T is the torque resulting from the inertia I and the angular acceleration α.

Before evaluating the combination of the static and dynamic torques, Figure 26 shows the difference in dynamic torque values of combined axis rotation versus only z-axis rotation of the pitch motor. From the figure it can be seen that with only z-axis rotation the torque demand increases gradually to a maximum required torque of just over 150 N.m. However, when combining the rotation of both axis it can be seen how the torque demand stays low up until 0° from where it increases rapidly to a maximum required torque of 200 N.m, 50 N.m more that with only z-axis rotation. Also, it can be observed that the maximum torque requirements is not constant at the extremities of the z-axis but slopes gradually with x-axis angle. From this analysis, Figure 26 (b) will be used to combine with the static torque requirements of the pitch motor.

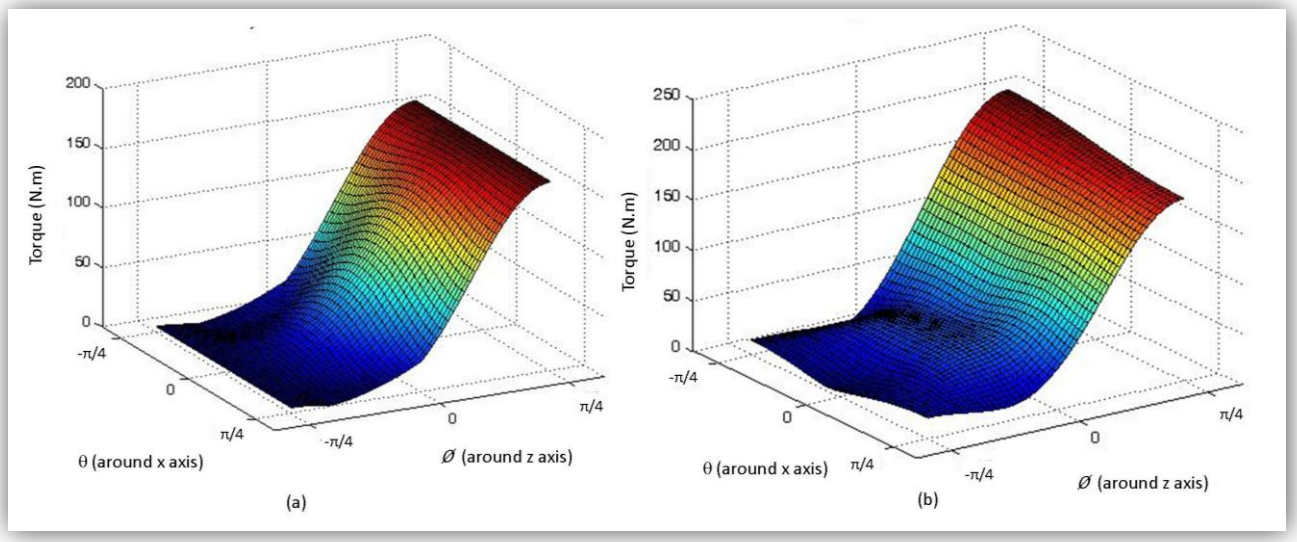

Figure 26: Pitch motor dynamic torque with (a) only z-axis rotation and (b) both z- and x-axis rotation

Figure 27 shows the difference in dynamic torque values of combined axis rotation versus only x-axis rotation of the yaw motor. From the figure it can be seen that with combined axis rotation the torque demand is not significantly more than with only x-axis rotation, but it can be seen how the maximum required torque is shifted rather than being constant at the x-axis extremities. Due to the fact that the required torques do not differ significantly, the required torque from with only x-axis rotation will be used to combine with the static torque requirements of the yaw motor.

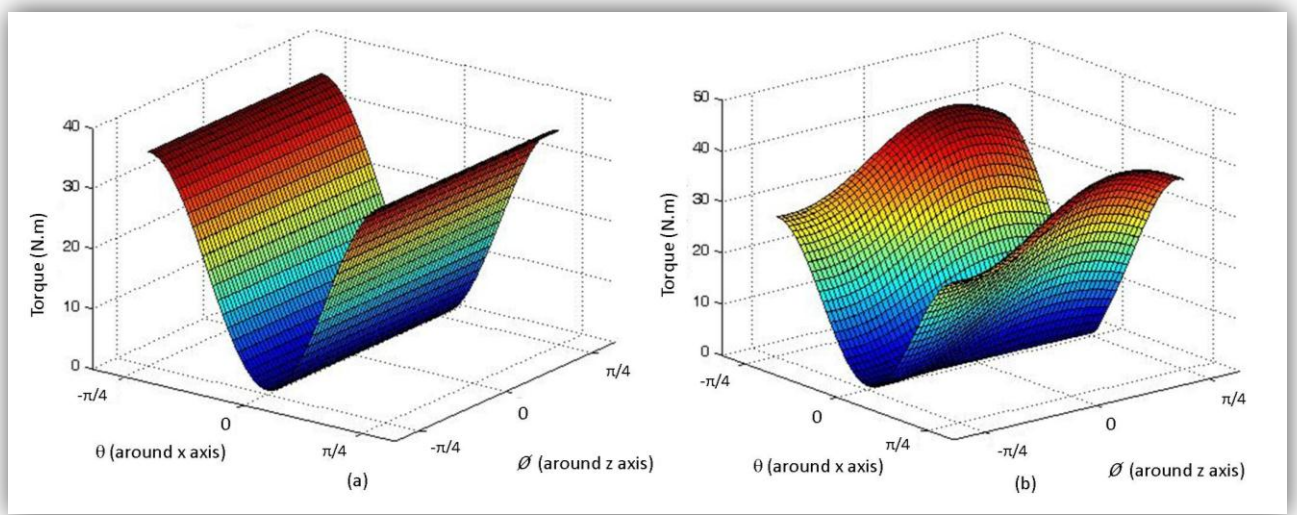

Figure 27: Yaw motor dynamic torque with (a) only x-axis rotation and (b) both x- and z-axis rotation

When combining the static and dynamic torques, the results from the simulation for the pitch motor (Z-axes rotation) can be seen in Figure 28, while the results for the yaw motor (X-axes rotation) are shown in Figure 29.

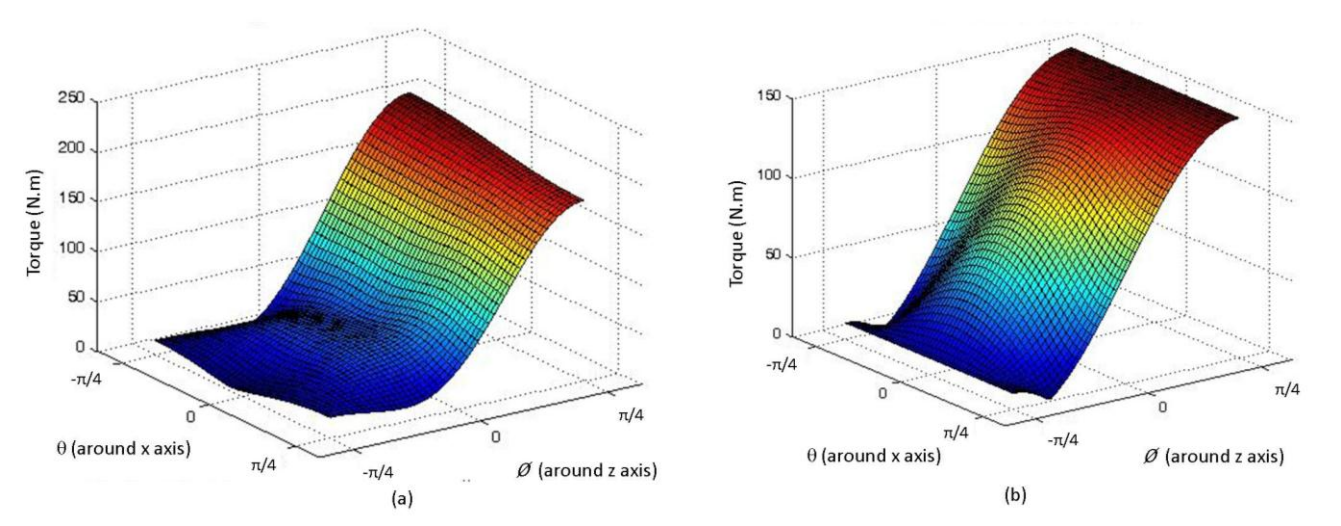

Figure 28: Dynamic torque (a) and static torque (b) requirements from parallel arm concept for the pitch motor

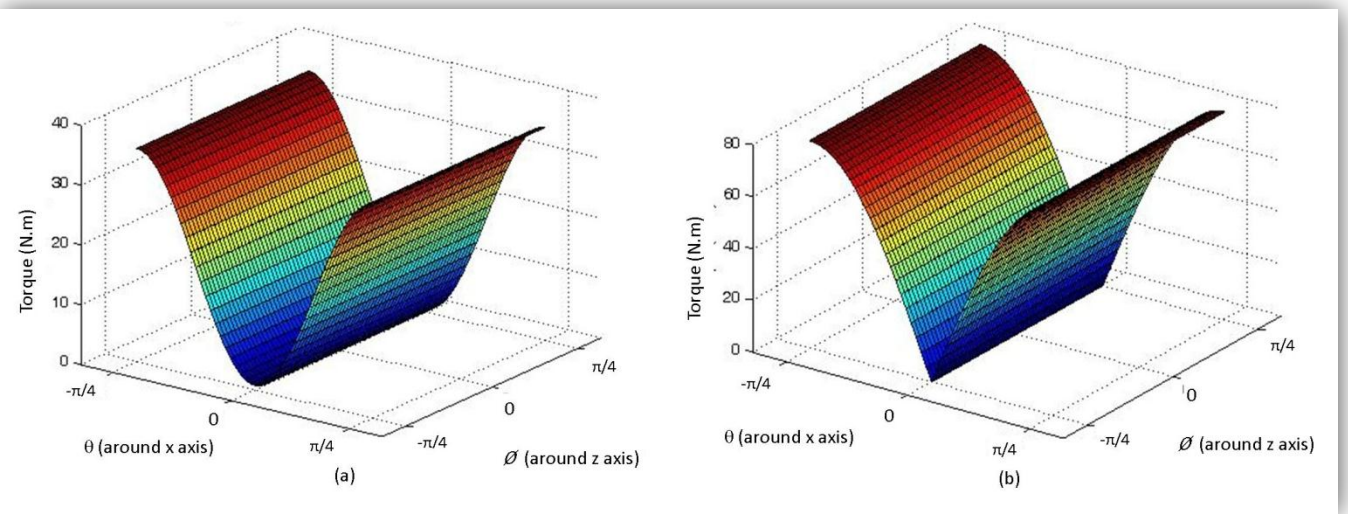

Figure 29: Dynamic torque (a) and static torque (b) requirements from parallel arm concept for the yaw motor

The analysis of the parallel arm manipulator showed that at the extremities of its movement range, the actuators would need to provide over 300 N.m of torque. Research conducted for suitable motors for this application for rotary speeds of up to

26 rpm, the maximum achievable torque of about 200 N.m. Even with the rotary speed reduced to 10 rpm, had a maximum achievable torque is 250 N.m. Not only does this not meet the design requirements for rotary speed, but it is also not enough torque to power the manipulator at its extremities. This analysis shows that the attempted range of 90˚ movement in the lateral/medial direction cannot be achieved with the parallel arm prototype. A large moment of inertia caused by rotation around the Z axis combined with a large static torque requirement from the large distance from the point of rotation were the primary reasons for failure of this prototype.

Fortunately the solution to this problem can be done in one step. By eliminating the four bar linkage, the large distance from the point of rotation is eliminated and consequently the large moment of inertia as well. Thus by pivoting the mass of the PSM by means of a spherical mechanism as shown in Figure 20, the distance from the point of rotation is limited to the length of the actuating arm.

3.5 Spherical Mechanism Concept

This section explains the torque analysis of the spherical mechanism concept. The idea in this case is to decrease the torque requirements of the motor by removing the four bar linkage system thus removing as many rotating linkages as possible along with shortening the distance the PSM is located from the point of rotation.

3.5.1. Torque Analysis of Spherical Mechanism

In this design the use of a four bar linkage is avoided and the end-effecter weight simply pivoted around the two motor axes. The torque required from the pitch motor should be less since all rotating joints have been removed therefore only one arm is being actuated. Along with this the total distance that the PSM is moved away from the Z axis lessened. The motor was simulated with a mass of 12 kg (the mass of the motor chosen for actuation) while the PSM and bearing assembly have a combined mass of 18 kg (the mass of the final bearing and PSM assembly) over a range spanning from -45˚ to 45˚ for X-axis rotation and 0˚ to 90˚ for Z-axis rotation. This is simply because rotation around the Z-axis can be done over a range from -90˚ to 90˚ but the results would simply be a mirror of one another. Figure 30 shows the layout of the new manipulator. The vectors r_1, r_2 and r_3 represent the distances to the end effecter mass, mass of the base arm and the motor mass respectively.

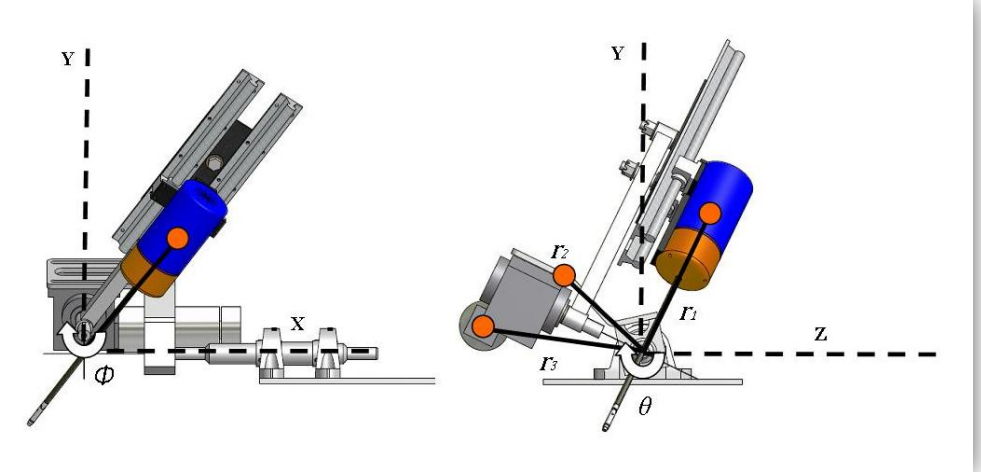

Figure 30: Single arm concept layout

Since the manipulator is no longer a four bar linkage, the accelerations of each mass can be calculated simply by the cross product of the angular acceleration and the distance vector. The moment of inertia was calculated in the same way as for the parallel arm concept.

Equations 9 to 11 describe the lengths to the centre of gravities. With the single arm concept, θ describes the angle around the X axis and Ø is the angle around the Z axis. In order to place the different weights on the right place around the X axis, β_1 describes the angle to the PSM, β_2 to the plate and β_3 to the motor. The lengths l_m and l_p are the lengths to the centres of gravity of the motor and the plate respectively.

$$\boldsymbol{r_1} = [(l_l + 0.5l_s)cos(\beta_1 - \theta) \quad (l_l + 0.5l_s)sin(\beta_1 - \theta)sin\emptyset \quad (l_l + 0.5l_s)sin\emptyset] \tag{9}$$

$$\boldsymbol{r_2} = [-l_p cos(\beta_2 - \theta) \quad l_p sin(\beta_2 - \theta)sin\emptyset \quad 0] \tag{10}$$

$$\boldsymbol{r_3} = [-l_m cos(\beta_3 - \theta) \quad l_m sin(\beta_3 - \theta)sin\emptyset \quad 0] \tag{11}$$

As with the parallel arm concepts, the dynamic torques of both motors must analysed with single and combined axis rotation. Figure 31 shows the analysis of the pitch motor. From the analysis it can be seen that the required torques are roughly the same, but that with combined axis rotation the torque requirements are not constant over the z-axis along the range of the x-axis' rotation. Since there is no significant difference in torque requirements, the simulation with z-axis rotation will be used to combine with the static torque requirements of the pitch motor.

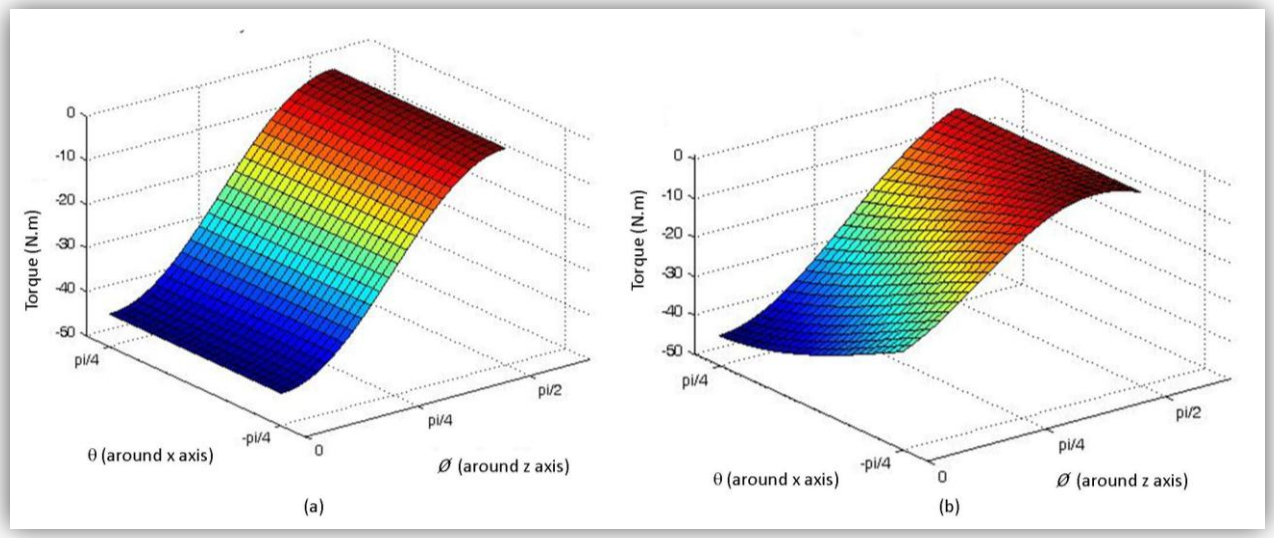

Figure 31: Pitch motor torque with (a) only z-axis rotation and (b) combined axis rotation

Figure 32 shows the results for the yaw motor. As with the pitch motor the required torques do not differ significantly, but it can be observed how the combined axis rotation torque requirements are not constant over the x-axis along the z-axis' rotation. Once again since there is no significant difference in torque requirements, the simulation with only x-axis rotation will be used to combine with the static torque requirements of the yaw motor.

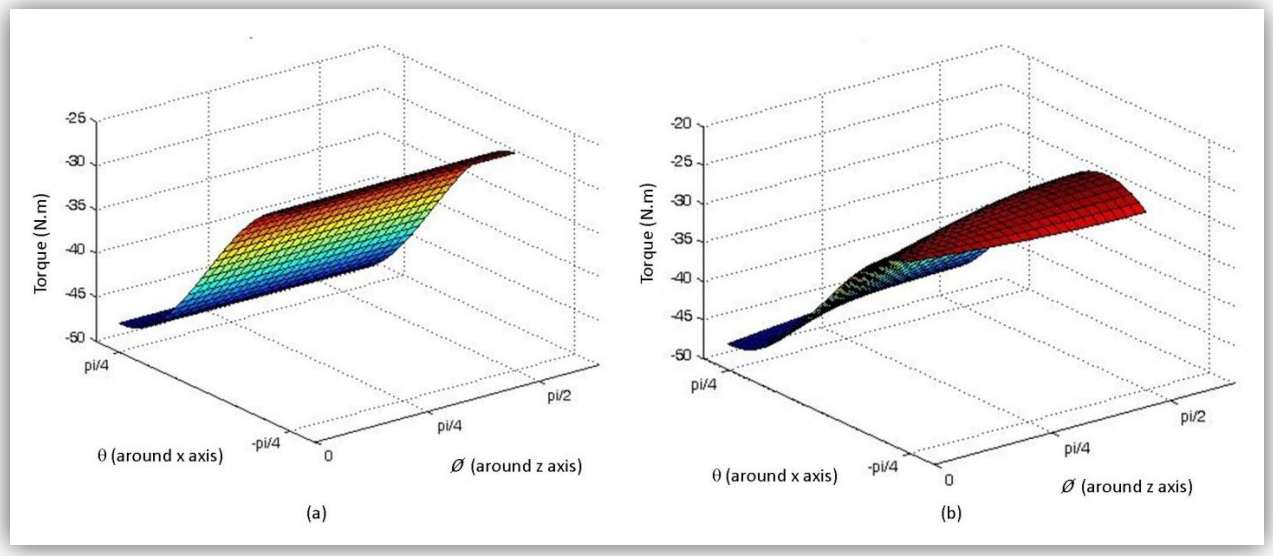

Figure 32: Yaw motor torque with (a) only x-axis rotation and (b) combined axis rotation

The results from the simulation for the pitch motor can be seen in Figure 33 and the results for the yaw motor in Figure 34.

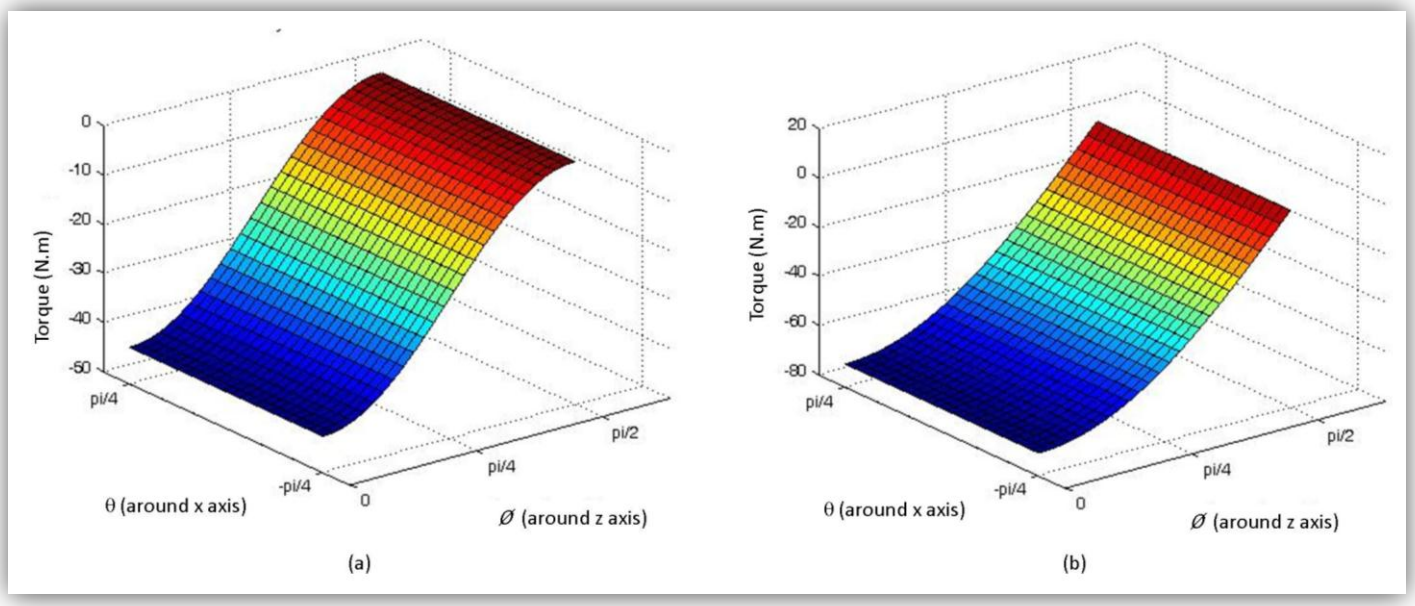

Figure 33: Dynamic torque (a) and static torque (b) requirements of the pitch motor in the single arm concept

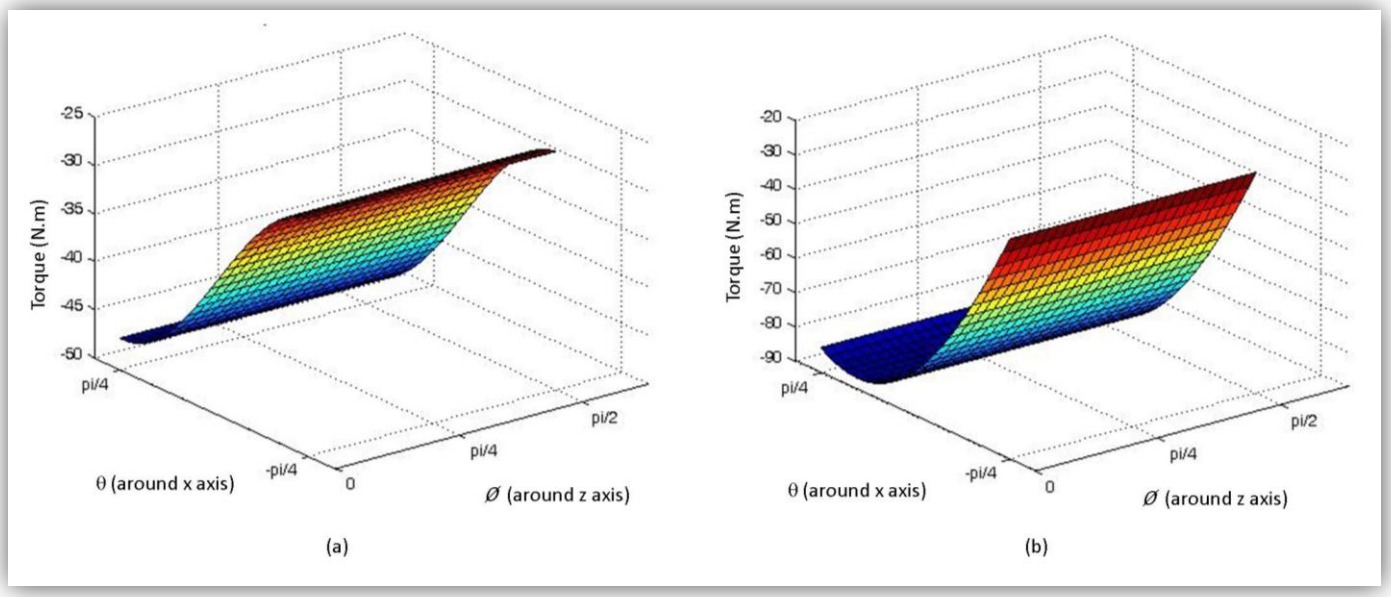

Figure 34: Dynamic torque (a) and static torque (b) requirements of the yaw motor in the single arm concept

The analysis of the spherical mechanism prototype clearly shows a significant decrease in torque requirement for the pitch motor. This now means that the spherical mechanism prototype is able to achieve the design requirements set out for angular speed along with being able to reach 90˚ in the medial/lateral direction. Also, since the spherical mechanism has to be mounted above the patient, it will have a much smaller footprint in the OR than the parallel arm manipulator. This saves space in the OR for additional machines and enables easier manoeuvrability around the operating bed.

The next step of the design process would be to manufacture the spherical mechanism. It was decided however to manufacture both of the analysed concepts, in order to practically prove that the parallel arm concept would not be able to be powered at its extremities.

3.5.2. Detail Design

This section will describe the detail mechanical design of both the parallel arm and spherical mechanism manipulators. The parallel arm manipulator was also built to prove that the torque required to move the manipulator is to great and that it is unfeasible to employ this design in the project. The design of the parallel arm manipulator will be explained first, as it has the most parts.

3.5.2.1. Motor Selection

From the calculations done in Section 3.1.5, the required torque for the rotational actuators is known. A DC motor with a worm-spur combination gearing system was purchased from Parvalux. The linear actuator would not only be required to move accurately during procedures, but also around 70 mm/s in order to remove the entire PSM arm from the abdominal cavity. This is because the PSM's design requires the tip of the robotic manipulator to be changed when the surgeon wishes to change between grasping, dissecting or electrocautery. Figure 35 below shows the PSM manipulator's gripper (left) and the elbow joint with the gripper removed (right). Thus the linear actuator's stroke should be equivalent to the length of the PSM's shaft plus the length of a trocar's head.

Figure 35: PSM gripper and elbow joint with gripper removed (Christiane, 2008)

Considering all arguments above, the following selections were made:

Rotary actuator: Parvalux PM95GWS (Brushless DC motor with worm-spur combination gearing) with 26 rpm output shaft speed, a continuous torque of 112 N.m and a maximum torque of 196 N.m (Parvalux, 2009).

Linear actuator: Linux LA30 linear electric actuator (DC motor with worm gear assembly driving screw mechanism for linear movement) with speed of 60 mm/s at a load of 50 N (Linux, 2009). To ensure the PSM can be fully removed from the abdominal cavity and trocar, a 450 mm stroke was selected for the actuator.

Both actuators were ordered with brake units. Although the Parvalux motor has a worm gearing system, which when not rotating, has self-locking characteristics, a braking unit is still required. This is due to the self-locking element of the gearbox not being reliable as a braking unit. This is caused when an external torque is applied to the rotating output of the gearing unit, which could overcome the frictional forces of the worm gear and cause continued rotation of the output. The Parvalux motor's brake sits on the back of the motor and is designed as a failsafe brake. Power to the brake disengages it, as a power failure will then result in the brake being engaged again. The linear actuator has a brake that is engaged with a wrap spring. It engages once actuation is stopped.

3.5.2.2. Mechanical Design of Parallel Arm Mechanism

Figure 36 below shows the designed SSM combined with the PSM. The section will continue to explain how the manipulator parts were designed to fit together.

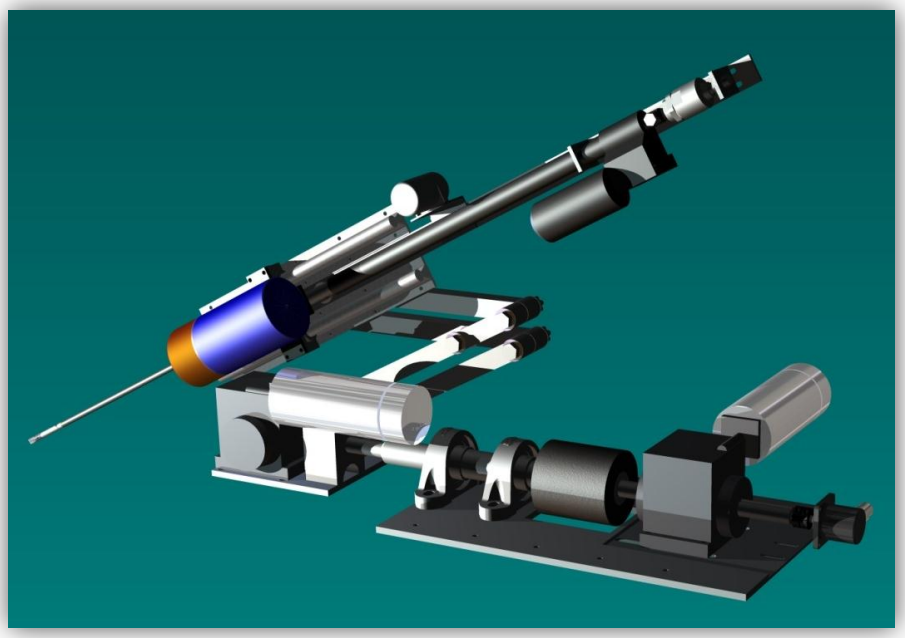

Figure 36: Parallel arm prototype

Since all the arms on the assembly will rotate relative to each other, vesconite bushes will be placed between each relative joint. Dry sliding vesconite bearings will also be machined to allow smooth rotation of the shafts that will support the actuating arms. Vesconite was used because it does not have to be greased or lubricated, gives a low wear rate on both the shaft and the bearing, is very easily machined and it is easily installed. It also does not contain any hazardous material, which is important in a medical environment. Most importantly it was used in order to keep the design simple which will aid in the low cost requirement of the design.

To allow smooth movement of the PSM, linear bearings from Bosch Rexroth were used. The bearings are an open type linear set within a cast iron housing. A hardened steel shaft mounted to a support serves as the rail for the bearing set. The bearing rail is mounted to a 250x144 mm plate with a thickness of 4.5 mm. In order to mount the PSM to the bearing, a 12 mm plate was machined to enable the PSM to fit onto the plate and then allow the plate to be bolted to the bearings. Bronze bushes were used on the bearing assembly as these bushes needed to be thinner in order to ensure the correct position of the VPR. Figure 37 shows the machined parts bolted into position.

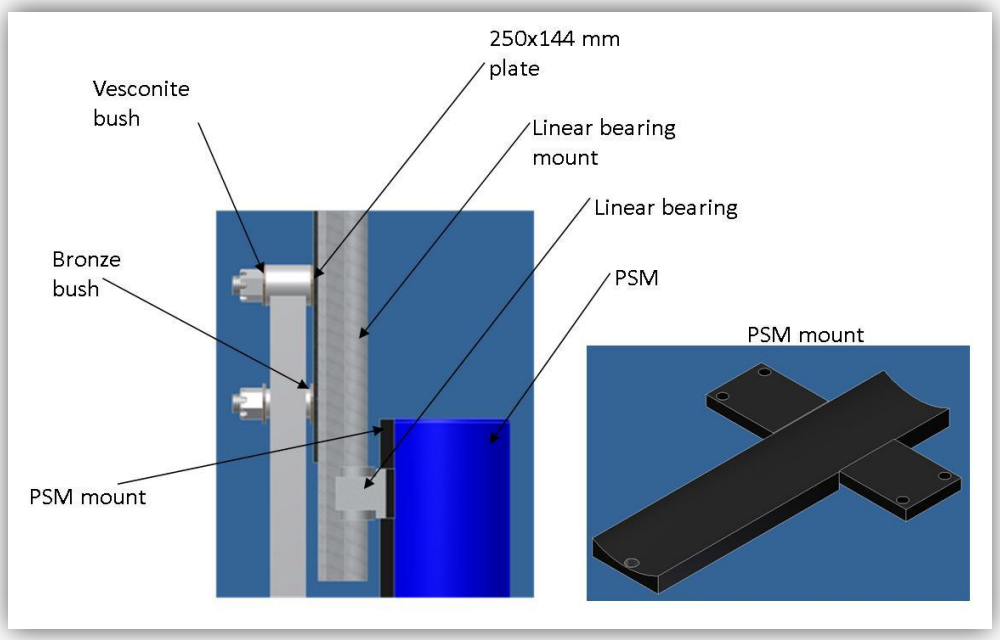

Figure 37: Attachment of PSM to bearing unit and manipulator arm

In Figure 38 the linear motor connects to a 950x40 mm arm that is 5 mm thick. It connects with the aid of two L-shaped brackets. The first attached the body of the actuator to the arm to ensure it stays in position. The second connects to a misalignment coupling (supplied by FESTO) that in turn connects to the end of the

actuator. The bottom end of the actuator is secured to the PSM mount with the linear motor mounting pin shown on the bottom right of Figure 38.

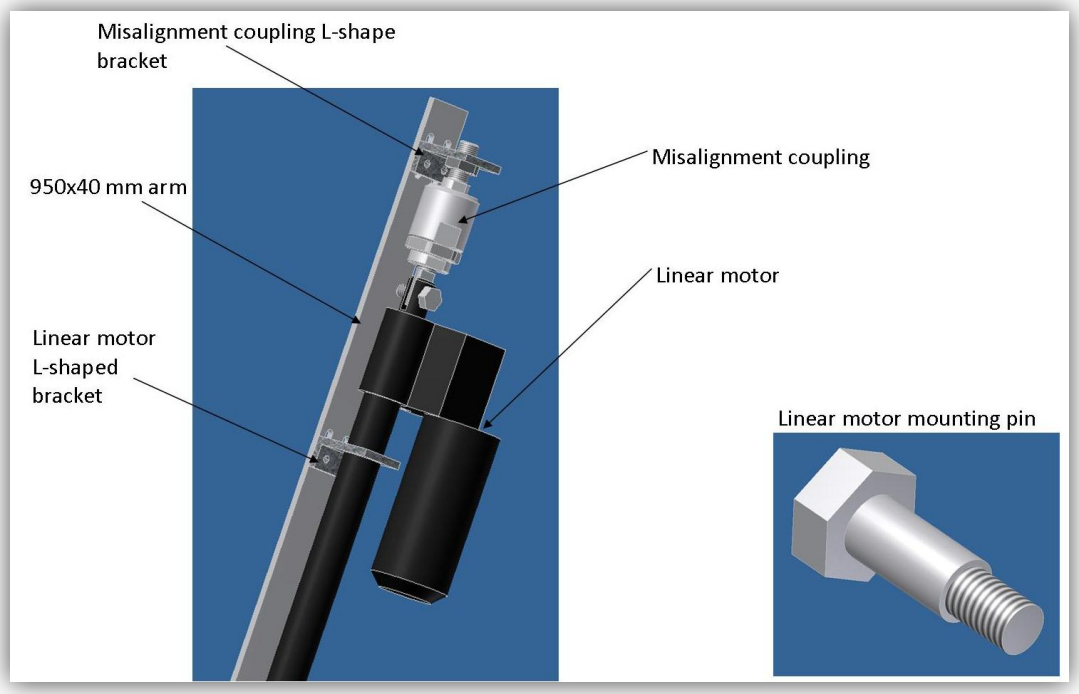

Figure 38: Connection of linear motor

The actuating arms of the manipulator need to hold the weight of the PSM, bearing assembly and linear motor. They must also allow for rotational movement between connecting arms and the bearing assembly. In order to minimise weight, the arms were manufactured from stainless steel square tubing 30x30 mm with a thickness of 3 mm. To enable rotational movement, round hubs, 38 mm long with a 35 mm diameter, were welded to the arms and machined to enable insertion of a bolt. The bolt would act as a shaft as well as a locking mechanism to keep the assembly firmly in position. In order to transfer the motor's torque to the actuating arms, the long arm that connects with the motor shaft was machined with a 25 mm diameter hole and 6 mm wide keyway. Both of the long arms had an additional 25 mm diameter hub welded on to connect to the shorter arms. The arms are shown in Figure 39. The bolts that insert into the hubs are only threaded for the remaining 20 mm at the tip. This design feature ensures that the vesconite bearings act on a smooth surface in order to maximise their lifespan.

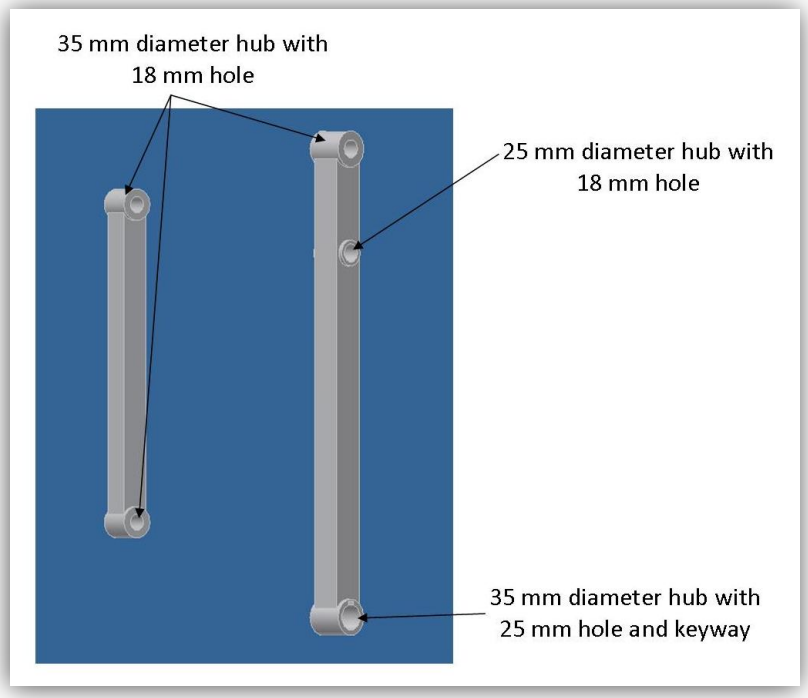

Figure 39: Manipulator long and short arms

Once the actuating arms and bearing assembly are connected, the whole assembly is mounted and connected to one of the Parvalux motors. This is achieved with a mounting plate designed to hold the motor, arms and a support to connect to the last actuating axis of the robot. Since the Parvalux motor was not part of the torque simulation done in Section **Error! Reference source not found.**, the plate was designed to mount the motor came as close as possible to the final axis of rotation. This way the motors' weight will not contribute significantly to the torque values. The plate will have a total mass of 30 kg mounted on it. The support for the final axis of rotation was given a 50 mm diameter hole in order to place a Fenlock locking element. This locking element's outer face expands while the inner face contracts when the bolts on the front are tightened in order to firmly connect the shaft to the support. The device has an inner diameter of 25 mm and can be loaded with a torque of 570 Nm. The locking element will also be used to connect the last actuation axis to the remaining Parvalux motor. Figure 40 shows the mounting plate and placement of the support structures.

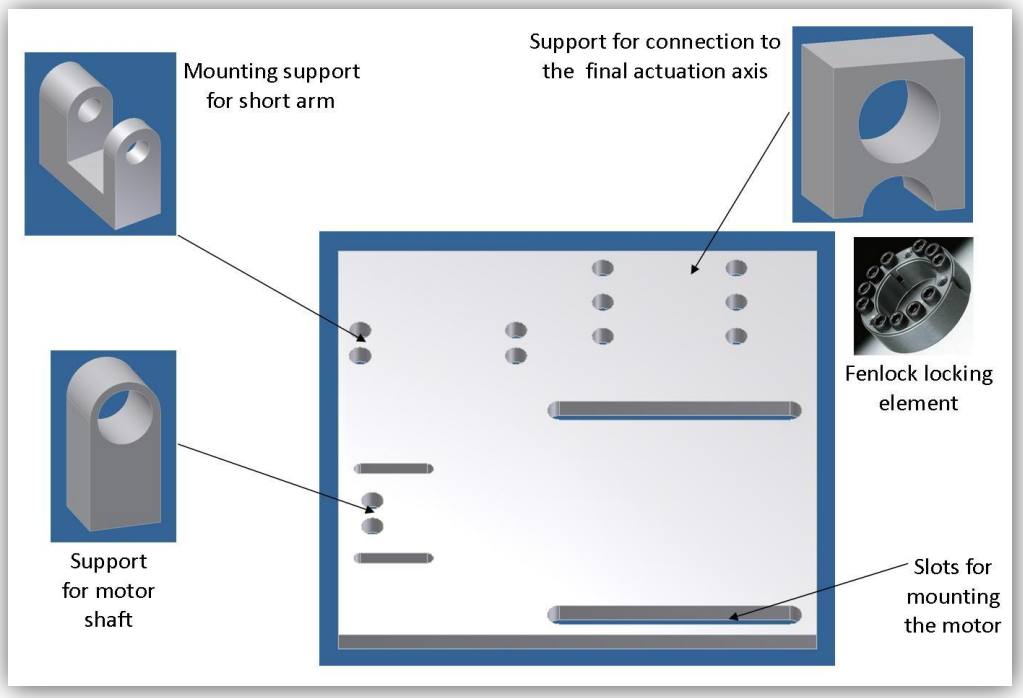

Figure 40: Mounting plate and attaching components

In order to realize the last actuation axis, a shaft had to be designed that would hold the entire mass of the preceding assembly. The shaft will be fitted with the Fenlock locking element and the combination will be inserted into the support for the final axis of rotation. The other end of the shaft will also utilize the locking element, and the combination will be inserted into the coupling which in turn connects to the motor output shaft. In order to protect the motor against misalignment, the shaft will connect to the motor with the aid of a HRC coupling. The shaft will be supported by two ball bearings secured in housings. There is no need to machine these bearing housings, which is why they were chosen rather than vesconite bearings. The shaft can be seen in Figure 41.

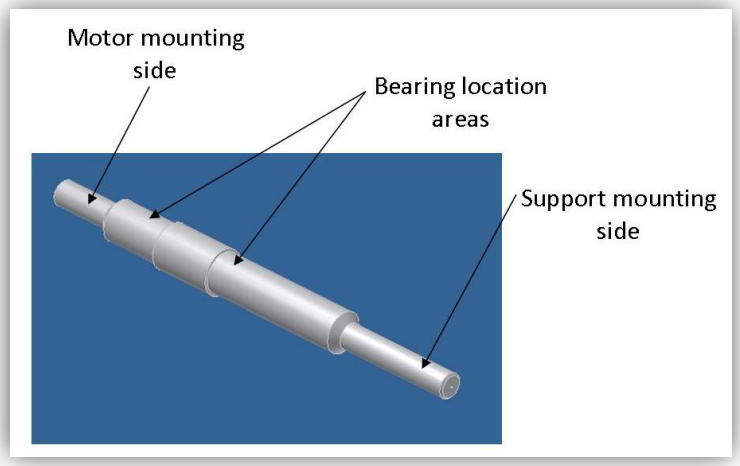

Figure 41: Manipulator shaft

Lastly the motor and bearings had to be mounted. A base mounting plate was designed that could connect easily to an additional structure using M8 bolts. The area in which the motor is mounted must be machined out in order to align the bearings' and motor's centre of rotation. The manipulator base plate is shown in Figure 42.

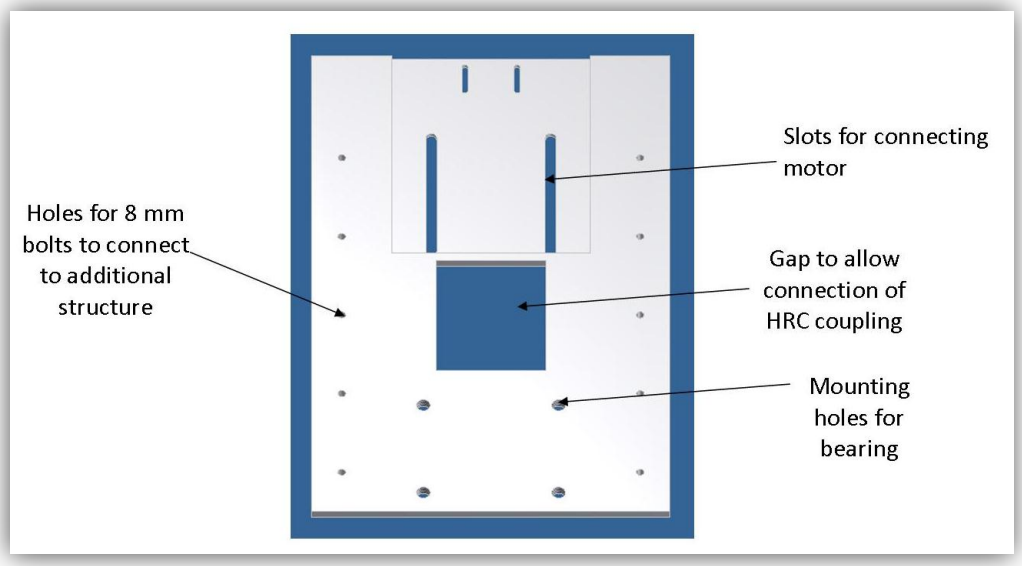

Figure 42: Manipulator base plate

The smaller slots that can be seen on both mounting plates are for the mounting of the rotary encoders (described in Section 4.3). The encoders will monitor the output shafts of each of the motors. This way the controller will have feedback on the motors' outputs. The encoders were mounted onto the plates with L-brackets and connected to the corresponding motor shaft with the aid of misalignment couplings. In order to

control the linear actuator, a UniMeasure linear encoder was used. The encoder is a rotary encoder with a cable that connects to the part being monitored. The cable is connected to the bearing, whilst the encoder is connected to the arm holding the linear actuator by means of another L-bracket. Figure 43 shows the location of the encoders as well as the HRC coupling.

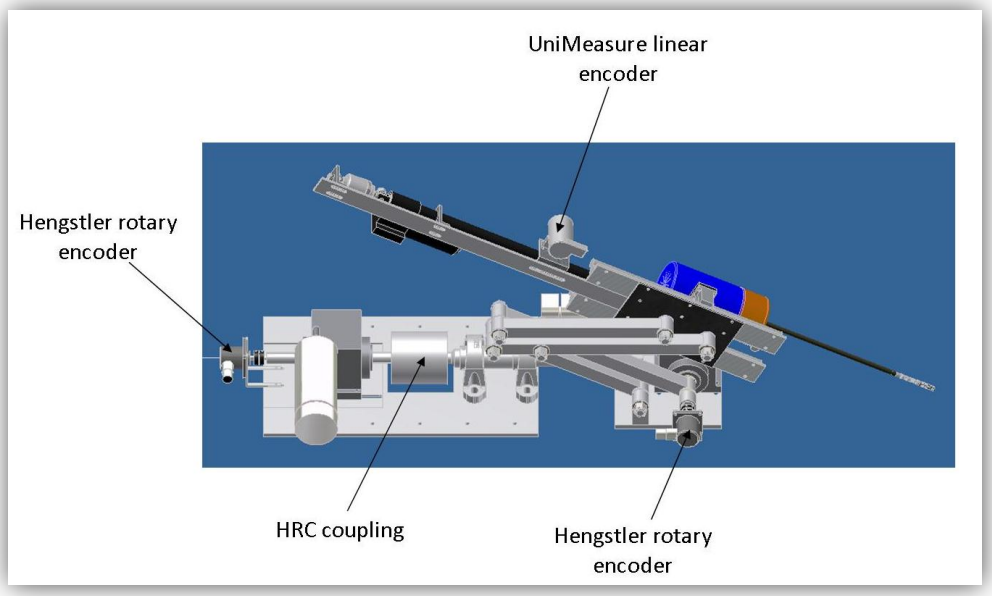

Figure 43: Fully assembled manipulator showing encoder positions

3.5.3. Mechanical Design of Spherical Mechanism

Figure 44 shows the manipulator designed in this section. The section will continue and explain how the new manipulator is assembled and how it is different from the previous manipulator.

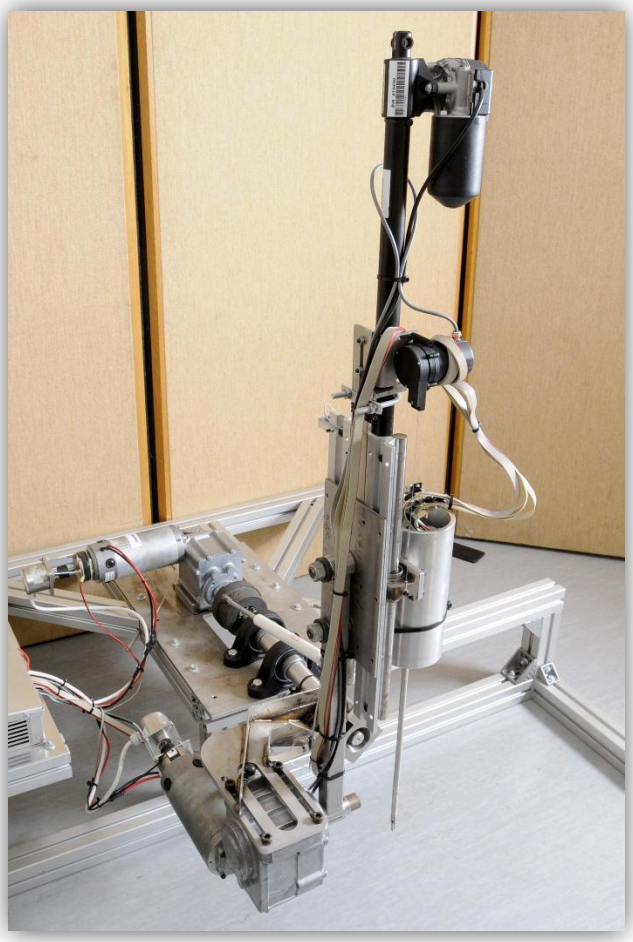

Figure 44: Spherical mechanism prototype

The design of the spherical mechanism manipulator requires the addition of a base arm, as seen in Figure 45. The base arm will mount on the existing shaft. The only difference is that the support will be rotated so that the threaded holes on the bottom face upwards and the base arm will be mounted so that the bended angles elevate the arm. The base arm design was sent to Fabrinox for manufacturing. It underwent CNC bending to create the required angles seen in, along with laser cutting for the mounting slots and holes. The angles are required so that the actuating axes of the motors can be aligned in order to maintain the pivot point required in MIRS surgery. The second Parvalux motor mounts upside down on the new base arm. The end effecter assembly can now be

mounted directly to the driven arm that is located on the output shaft of the Parvalux motor. The arm is secured with a locking ring and a 3 mm bolt.

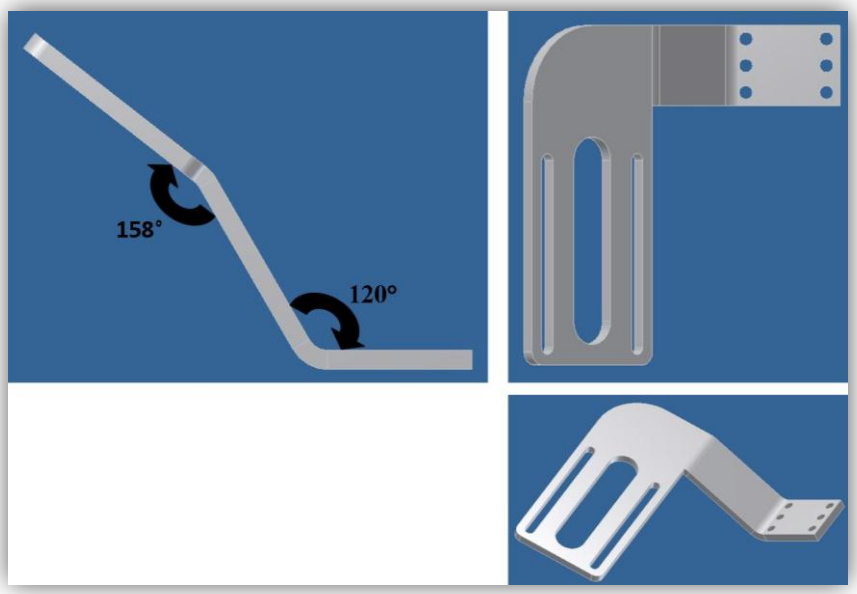

Figure 45: Base arm with bending angles to realize pivoting point

3.5.4. Manipulator Movement Analysis

In order to prove that the parallel arm concept was not feasible, it was manually positioned as shown in Figure 46. The motor was powered so that it would bring the end effecter load closer toward the point of rotation.

Figure 46: Parallel arm manipulator at extremity

The test simply required the motor driver to be enabled and to observe whether the motor was able to drive the load. As expected, it could not. The test was simple but consequently proved that the manipulator would not be feasible. No further testing was done with the parallel arm manipulator.

The spherical mechanism is capable of reaching 90° in the medial/lateral direction and 35° in the superior/inferior direction. The proposed layout of the complete robot is shown in Figure 47**Error! Reference source not found.**. Since the base of the robot is not yet designed several changes to the layout are still possible. The angle and position of the primary shafts can be changed relative to each other by changing the angle Ø as well as the positions X, Y and Z. This angle and relative positions can either be adjusted together or separately, depending on the required locations of the incisions.

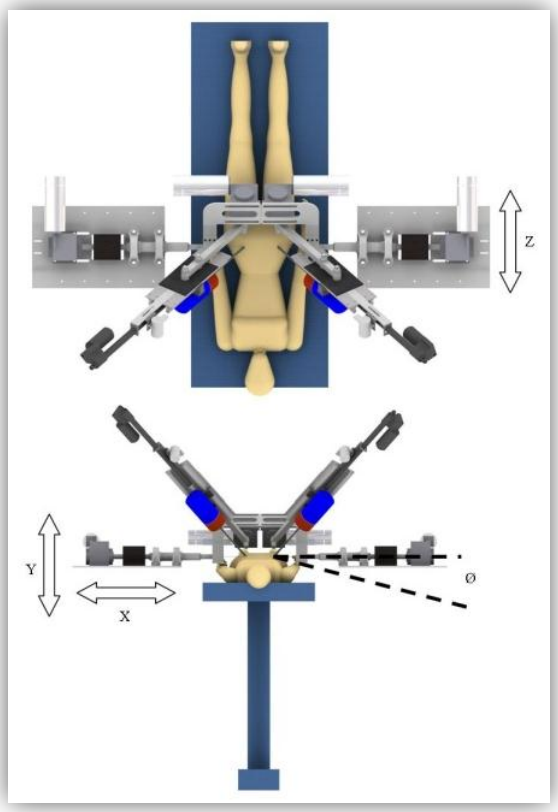

Figure 47: Full robot above patient

Unfortunately some problems were encountered with other aspects of the manipulator, the first was the backlash on the gearboxes. When actuation was ceased, the load caused movement back and forth around the shafts of the gearboxes. This is because once the mass of the manipulator is moving at a given velocity, it will have angular momentum since it is moving around a fixed point of rotation. From Meriam & Kraige (2003) the angular momentum of the mass is described by Equation 12.

$$H_o = I_o \propto \quad (12)$$

H_o is the angular momentum of a body rotating at angular velocity α and moment of inertia I_o. The angular momentum allows the mass of the manipulator to move around the axis of rotation without the need for actuation. Once the angular momentum is diminished or the range of the backlash is reached, the mass will move back to its original position because of the effect of gravity on the mass. This movement will cause severe problems in a surgical environment and must be prevented. In order to counteract this movement, spring damper combination mechanisms will be connected to the manipulator arms to stop the unwanted movement. The spring/damper system will utilise the speed of the mass (caused by the angular velocity) and the compression of the spring to create a force that opposes the angular momentum, as described by Equation 13.

$$F = c\, v_c + k\, x \quad (13)$$

The velocity v_c is the product of the angular velocity ω and the distance to the connection of the damping mechanism. The damping coefficient c is responsible for causing the force as a result of the speed of movement. The spring coefficient k utilizes the amount of compression x to generate a force. The force created by the mechanism should thus be large enough to counteract the angular momentum and stop the unwanted movement associated with the backlash of the gearboxes. The first damper connects to the pivoting arm and the coupling, while the second is connected to the frame and the bottom of the newly designed base arm. The forces created by the dampers were sufficient to stop the angular momentum from causing unwanted movements. Figure 48 shows the placement of the gas dampers on the manipulator.

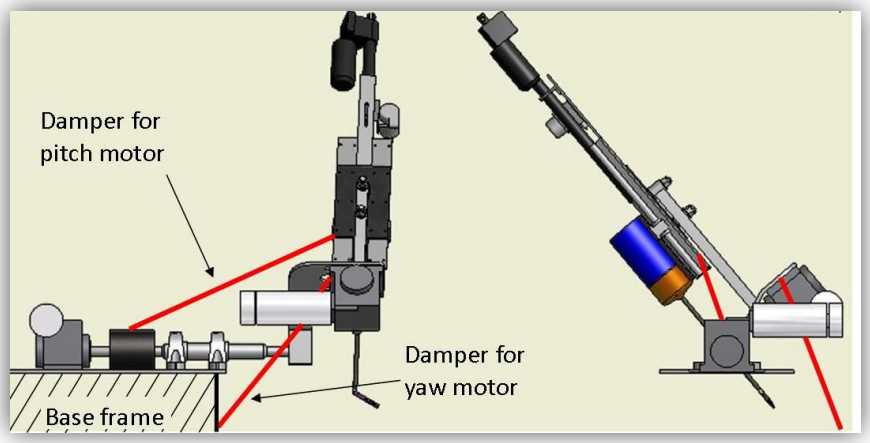

Figure 48: Location of damping pistons

The last problem encountered was that low frequency oscillation was caused on the base arm when the motors were suddenly stopped. Since the manipulator would function in a stop/start basis during procedures these oscillations will prove to be very

problematic. In order to attempt to remove the low frequency oscillation, flanges were added on the top of the plate and can be seen in Figure 49. The flanges have a height of 30 mm and a thickness of 3 mm. The addition of the flanges resulted in a 48% increase in the flexural rigidity of the arm, which was sufficient in preventing the unwanted movement caused by the sudden stopping of the motors. Appendix D shows how the flexural rigidity is calculated and how the flanges assist to increase it.

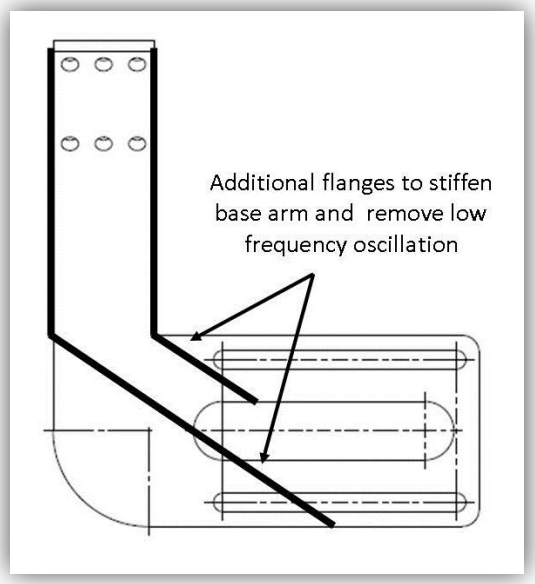

Figure 49: Base arm with additional flanges

3.6 Sterilization

The PSM manipulator designed by Christiane (2008) did not take into account how the manipulator would be sterilized. The SSM of this thesis is an external manipulator, and does not need to be sterilized. It does however need to be covered with sterile drapes. The drapes are applied before the surgery starts by the OR nurses. For the da Vinci robot, it is recommended that two people do the draping, one sterile and the other nonsterile. Draping is done by moving the robotic arms away from each other, allowing easy draping of individual arms. The draping is done by starting on one side of the robot, draping the relative arm, and moving on to the next. It is recommended that the arms are fully extended to ease the draping procedure. The sterile person will stand in front of the arms and cover them with the drapes. The nonsterile person will then pull the drapes over to cover the unsterilized parts. In this way sterility can be ensured (Bhandari *et al.*, 2005). Therefore no modifications need to be made to the manipulator with regards to sterilizability. Once the manipulator is in final assembly a draping plan can be put forward to ensure the entire manipulator is covered, protecting the patient from any possibility of infection.

3.7 Mechanical Manipulator Costs

A summary of the costs involved during the mechanical design of the manipulator is presented. The total cost of the mechanical manipulator can be seen in Table 4.

Table 4: Cost of mechanical components of manipulator

Mechanical Part	Price/unit	Units	Total
Fenlock locking element	R 88.85	3	R 266.00
HRC Coupling	R 304.67	1	R 304.00
Base arm (Fabrinox)	R 578.90	1	R 578.00
Stainless steel (Fabrinox)	R 811.18	1	R 811.00
Linear steel shaft (bearings)	R 876.90	1	R 876.00
Linear Bearing	R 883.50	1	R 883.00
Bearing housing	R 500.00	2	R 1 000.00
Stainless steel	n/a	n/a	R 2 000.00
Linux linear actuator	R 3 051.99	1	R 3 051.00
Linear encoder	R 4 974.96	1	R 4 974.00
Power supply	R 6 139.00	1	R 6 139.00
Machining	R 250.00	80	R 20 000.00
Hengstler encoder	R 6 210.00	2	R 12 420.00
Parvalux GWS motor	R 9 809.70	2	R 19 619.40
Total			**R 74 727.00**

The Parvalux motors, machining and the encoders are the most significant contributors to the total costs of the manipulator, making up R53 839.40. The costs associated with the PSM in 2008 were R63 658. If one assumes a 5% inflation rate per year, the present day costs of the PSM come to roughly R74 000. This bring the total costs of the mechanical manipulator to R 148 727.

Chapter 4: Electronics Design

This section will explain the design of the electronics for the manipulator. It will start with the functional requirements for the electronics. From there it will explain the working principle of the digital electronics and how it achieves them. The design, working principles and implementation of the power electronics will also be explained.

4.1 Functional Requirements

In order for the manipulator to function as desired, all actuators of the manipulator must be able to move bi-directionally. The movement from each actuator must also be controlled to ensure safe and accurate operation. The user must be informed of what the electronics are doing and in what position the robot assembly is. The functional requirements of the electronics are thus as follows:

- Drive motors bi-directionally
- Monitor the motors' position
- Communicate with user

In order to achieve these requirements, a digital controller must be implemented to serve as the command centre for the manipulator. In the following section, two concepts for digital control of the manipulator will be presented and evaluated.

4.2 Digital Electronics

The first concept for digital control of the complete manipulator is shown in Figure 50. This concept will use a single microcontroller for each DOF. This will ensure that if one DOF fails the other remain unaffected. Also, all DOFs can be moved simultaneously and independently.

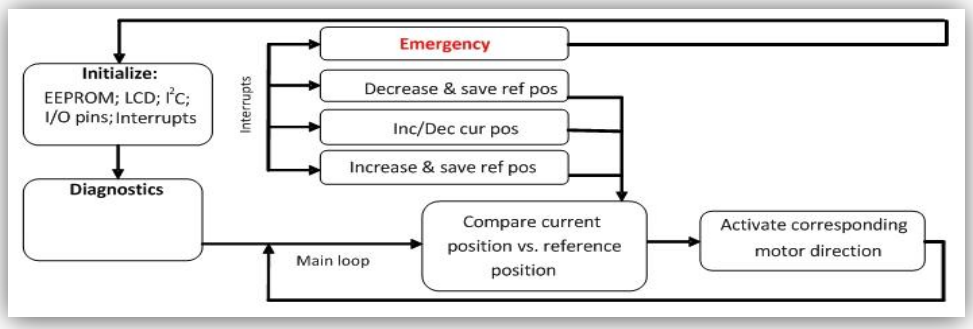

Figure 50: Concept one for digital electronics

Each microcontroller will communicate to the user via a Liquid Crystal Display (LCD) screen. All of the inputs from the user (increase/decrease reference position and emergency stop) and encoder (increase/decrease current position) will be communicated to the microcontroller in the form of interrupts. Interrupts stop what the microcontroller is busy with and execute the required commands. After the interrupt is executed the microcontroller will continue from where it stopped. A main loop continuously monitors the difference between the current position and the reference position. If a change in reference position is detected, it will activate the motor in the corresponding direction. Whilst the motor is active, signals from the encoder will interrupt and the current position will be updated. Once there is a zero difference between the two positions, the motor will be shut down. The reference position will also be saved once changed. This will ensure that at start-up (or after power loss) the position of the robot will be known.

The following hierarchy will govern the interrupts in the software (in descending order):

- Emergency stop
- Increase/decrease reference position (user)
- Increase/decrease current position (encoders)

This will allow the user to change the input to the electronics while the manipulator is in motion and the manipulator can be stopped while it is moving or when another input from the user is received. Since the electronics communicate via LCDs, the need for an external computer is removed. This way the manipulator will be a standalone unit.

The second concept shown in Figure 51 relies on a single microcontroller to control the manipulator.

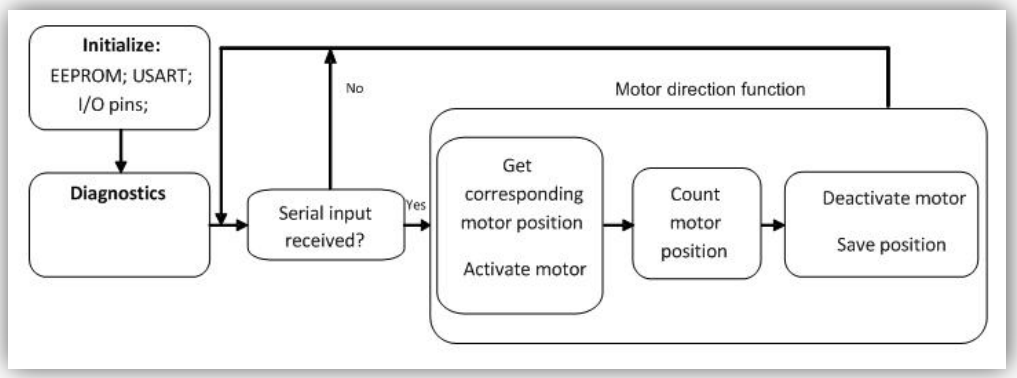

Figure 51: Concept two for digital electronics

This concept will require the use of an external computer for user-based commands and communication. A main loop will wait for a serial input from the computer. Each serial input will activate a motor direction function. The motor's current position is retrieved

from the memory and the motor is activated. Input signals from the encoder then allow the microcontroller to count the motor's position. Once the motor is in the desired position, it is deactivated and the position is saved.

Since this concept receives inputs from a computer, a simple form of tele-operated capability can be incorporated. A wireless keyboard will enable the user to transit input signals without being hardwired to the computer. Although this is a simple example of tele-operation, it will showcase the possible viability of tele-operation. There are still several aspects that would need to be addressed before the system can be fully tele-operational. Data and video transfer as well as the distance between robot and surgeon will affect the lag time experienced by the surgeon. As stated in Section 2.3, the RAVEN surgical robot has been successfully tested in several tele-operated scenarios. Even with the succesfull testing of the RAVEN, it has as of yet not performed via tele-operation on an actual patient.

It was decided to control the manipulator using only one microcontroller. A single entity in control of the manipulator makes more sense than having seven independently controlled joints. The serial communication will allow easy on-screen communication with the user. This allows more and better organized flow of information than an external LCD.

As stated before the computer-based commands also enable wireless control of the manipulator. Since funding of this project is received with the aim to create a tele-medicine application for the robot, this approach will please investors and enable easy upgrades during future work.

A single microcontroller must have enough input and output pins to ensure all of the manipulator's encoders and motor controllers can be connected. In addition it should allow for the connection of a handheld control mechanism (which is currently under development) so that the system can be easily upgraded in the future.

4.3 Detail Design of Digital Electronics

The Arduino Mega board was chosen as the controller for the manipulator. This board contains the ATmega2560 microcontroller. This controller has 54 digital pins, of which 14 can be used as pulse width modulators (PWM). The PWM signals run at a frequency of 490 Hz. Additionally it has 16 analogue inputs and four UARTs for serial communication. It has a 128 kbyte flash memory with a 4 kbyte EEPROM. The EEPROM will be used to save the motors' positions. The controller operates with a clock speed of 16 MHz which will allow smooth and seamless operation of the manipulator (with the encoders mounted on the back of the Parvalux motors, the input from the encoders would be at 24 kHz).

The Arduino board comes with a USB connection, external power input, voltage regulator and a reset button. The board is shown in Figure 52. Since signals from the board must control power electronics, an external 12 V power source will give power to the Arduino. This will ensure a common ground between the control and power electronics so signal values will be constant. The computer will communicate with the Arduino via the USB connection. The software for the Arduino has its own serial port window to allow for communication with the user. Although there are several controllers on the market capable of controlling the manipulator, the Arduino was chosen because of its number of inputs and outputs along with its ease of functionality. Once the manipulator is ready to be made into a complete robotic system, a more powerful controller can be utilized to achieve the desired control characteristics.

The encoders were introduced in Section 3.5.2.2 because they needed to be mounted on the manipulator. The encoders' electronic characteristics can now be explained in this section. The Hengstler rotary encoders are quadrature encoders with 3600 pulses/rev and require 12 V for operation. The 3600 pulses/rev was chosen since it should allow 10 pulses/degree when the encoders are mounted on the output shafts of the motors. The linear encoder is also a quadrature encoder with 10 pulses/mm and requires 5 V to operate. Each of the encoders were connected to the Arduino with only one pin. This is because the Arduino will not need to interpret the direction of movement, but simply monitor the movement of the motors. Although small oscillations on the motor shaft could be interpreted as rotational movement by the manipulator, it was established that only one signal needed to be monitored. This is simply because the controller only starts to monitor the encoder once the motor has been activated. Thus once the motor has been deactivated, small oscillations on the motor shaft would not be counted by the controller.

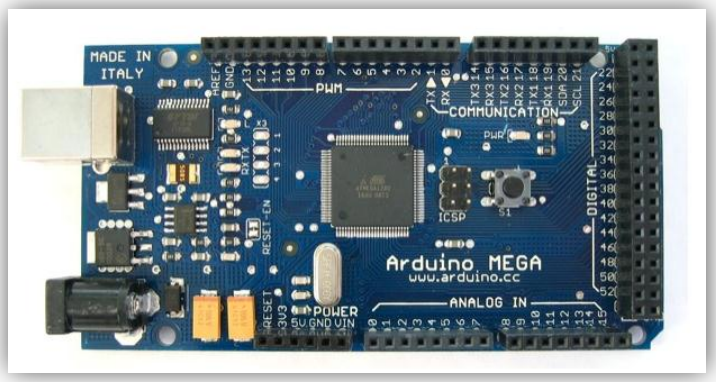

Figure 52: Arduino Mega (Arduino Mega. [S.a])

The Arduino must connect with seven encoders and motors. To ensure easy connection, a PCB (referred to as the signal connection board) was designed that will slot onto the

Arduino and allow female headers to mount onto corresponding male pins. The signal connection board has an external 12 V input to power the Hengstler encoders. The signal connection board can be seen in Figure 53. Each connection is labelled so the correct encoder/motor cable is connected where it should be. Only one pin per encoder was allocated. This is because the power electronics can only drive the motors in one direction at a time (depending on inputs received), therefore the Arduino needs only to count the number of steps, not determine the direction the motor is turning.

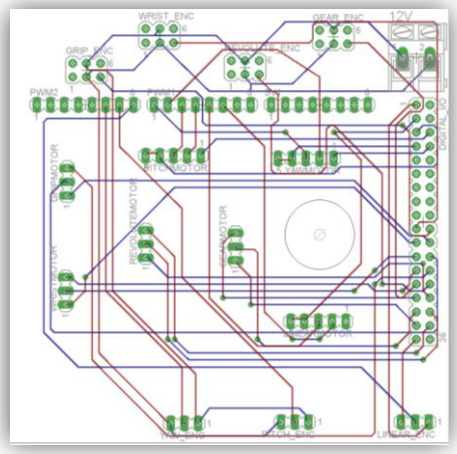

Figure 53: PCB for signal connections to Arduino

The pins for encoder and motor connections are soldered so they allow connection on the top side of the board. The pins that correspond to the Arduino pins are soldered so they extend to the bottom of the board. This allows the signal board's pins to be inserted into the Arduino to transmit the required signals. Now that the digital electronics have been designed, electronics responsible for driving the motors must be designed.

4.4 Detail Design of Power Electronics

In order to drive the motors from a signal received from the Ardiuno, circuits called motor shields must be introduced as a connection between the Arduino and the motors. The motors shields receive input signals from the Arduino and then relay signals of higher voltage and larger current capabilities to the motors.

The Parvalux motors have a start-up current of about three times their full load current. This means at start-up they will draw about 80 A (Parvalux, 2009). Since the motors will operate on a stop/start basis, the power electronics for the motors must be capable of safely handling these current values.

The IRFP1405PbF is an N-channel MOSFET from International Rectifier and is commonly used in the automotive industry. It is capable of delivering a maximum continuous current of 118 A and has a maximum supply voltage of 55 V. N-channel MOSFETs are used because when compared to P-channel MOSFETs they are cheaper and capable of handling larger currents.

In order to drive the MOSFETs with a 5 V digital controller, a MOSFET driver will be used to take the controller signals and relay them to the MOSFETs. The HIP4082 from Intersel is capable of independently driving four N-channel MOSFETs. It is commonly used in battery powered vehicles, UPS systems and DC motor control. It can deliver a peak driving current of 1.25 A (Intersel, 2006).

To enable bi-directional movement of the motors, the MOSFETs are arranged in an H-bridge configuration. The MOSFET and HIP4082 layout can be seen in Figure 54. The MOSFETs are described as the high side (Q1 and Q2) and low side (Q3 and Q4) MOSFETs. The MOSFETs will work in pairs to drive the motor. Q1 and Q4 will be switched on together to drive the motor in one direction while Q2 and Q3 will drive it in the other direction. The performance of the MOSFET depends greatly on their surface temperature. To keep them as cool as possible, a cooling fan will be used to achieve better heat dissipation.

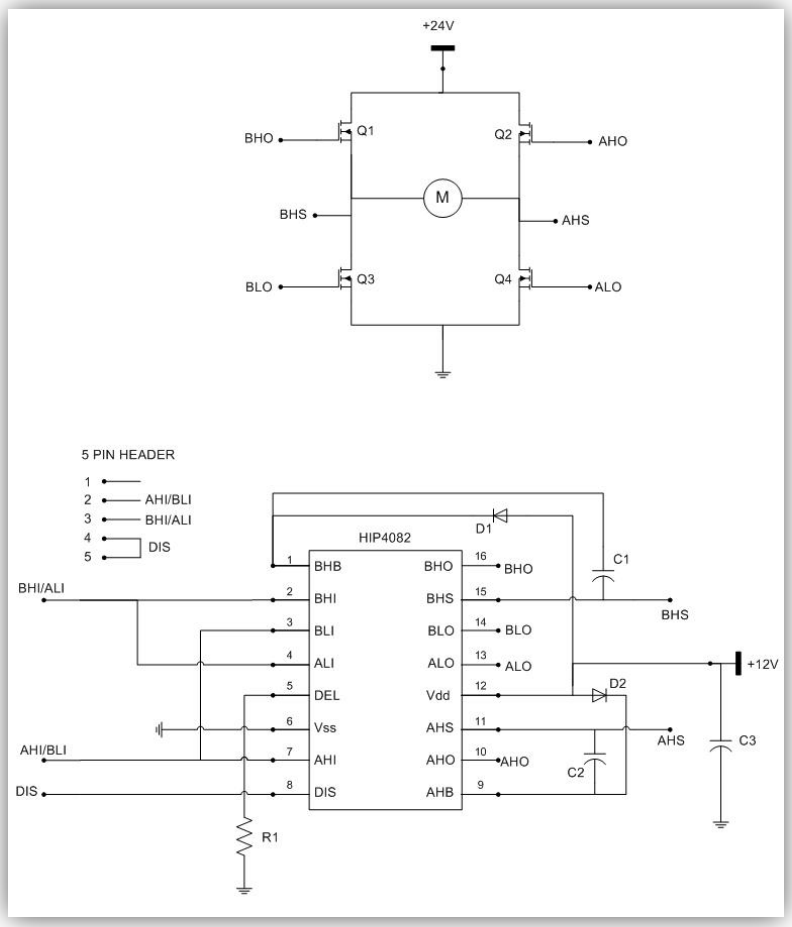

Figure 54: HIP4082 circuit diagram

The HIP4082 driver has four logic level inputs. These input pins are modified TTL pins. This means that any positive voltage within a range of 3 V to 12 V will signal the driver. The inputs are divided into A and B, with both having high and low side inputs and outputs. The high side inputs will control the high side outputs, which will drive the high side MOSFETs. The same goes for the low side inputs. Q2 and Q4 are driven by the A side while Q1 and Q3 are driven by the B side. Both A and B low side inputs would override the corresponding high side input to ensure that there is no shoot through (from Q1 to Q3 or from Q2 to Q4) that would short circuit the power supply. Table 5 shows the truth table for the HIP4082 driver. The MOSFET driver also has a delay input (DEL) that enables a time delay before the driver is capable of switching from either A or B high side to low side. Resistor R1 sets the desired delay time.

Table 5: Truth table for HIP4082 MOSFET driver (adapted from Intersel (2006)) (1 – Input/Output driven high; 0 – Input/Output driven low; x – does not matter)

Inputs			Outputs	
AHI/BHI	ALI/BLI	DIS	AHO/BHO	ALO/BLO
x	x	1	0	0
x	1	0	0	1
1	0	0	1	0
0	0	0	0	0

The signal from the microcontroller controlling direction one of the motor will switch B high side and A low side simultaneously, and vice versa for direction two. The microcontroller will also have an enable signal that can disable the driver should the motor be required to switch off. This signal will drive the disable (DIS) input on the driver. When a high level input is set to this input pin all other inputs are over ridden, when a low level input is set the outputs are driven by the corresponding inputs.

B high side bootstrap (BHB) and A high side bootstrap (AHB) are the bootstrap supplies for each side. They will provide the initial charge pump required to drive the high side MOSFETs. The charge pump is required since the high side MOSFETs gates do not have a ground reference. Therefore they require about 8 V above the supply voltage in order to switch on. The HIP4082 is capable of providing up to 80 V in order to drive the gates of the high side MOSFETs. Capacitors C1 and C2 act as bootstrap capacitors to store the required charge. Diodes D1 and D2 are the bootstrap diodes and ensure the capacitors correctly charge and discharge when required. Table 6 lists the components and their corresponding values.

Table 6: Components for HIP4082 circuit

Component	Value
R1	10 kΩ
C1 & C2	100 µF
D1 & D2	1N4007

The PCB for this circuit is shown in Figure 55. The outputs from the MOSFETs have wide tracks to tolerate the high currents experienced. The power supply's source and ground inputs also connect to these wide tracks.

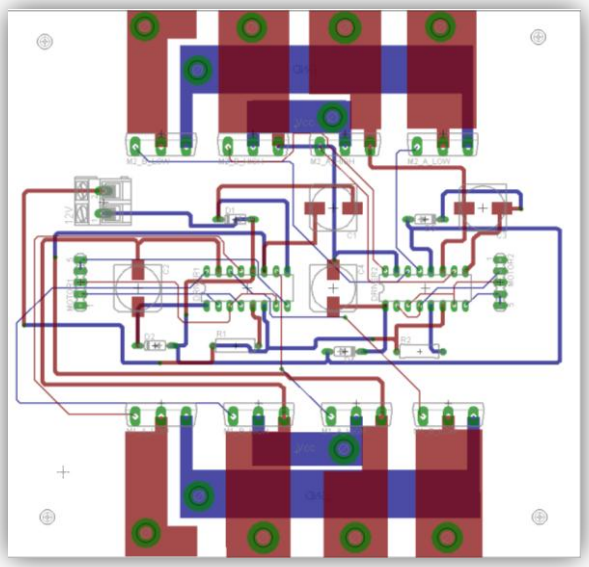

Figure 55: PCB for HIP4082 and MOSFETs

After initial testing it was found that the circuit did not fully switch on. Only about 9 V (from the desired 24V) was available at the output leads for the motor. The circuit was investigated by connecting an oscilloscope to the different output pins of the driver. The input signals' frequency was raised to a few kilohertz instead of just a few hertz. The oscilloscope showed that the drivers only switched the upper MOSFETs (AHO and BHO) fully on for a few microseconds. From this it was concluded that the bootstrap capacitors give the initial charge pump to drive the MOSFETs, but once the charge is depleted the driver is not capable of keeping the MOSFETs on. So in order to keep the high side MOSFETs on, the bootstrap capacitors must be constantly refreshed.

The B-side bootstrap capacitor is recharged when BLO is turned on. The same goes for the A-side capacitor. As said before, BLI and ALI input will override BHI and AHI in order to prevent a shoot through condition. So in order to recharge the A-side capacitor, ALO must be driven high. To achieve the charge/recharge cycle on both the A and B-sides the inputs to the driver will be changed as in Table 7.

Table 7: Updated control signals for HIP4082 (1 – Input driven high; 0 – Input driven low; PWM – Pulse Width Modulation signal; x – does not matter)

Direction	AHI	BHI	ALI	BLI	DIS
1	1	0	PWM	$\overline{PWM}$	0
2	0	1	PWM	$\overline{PWM}$	0
0	x	x	x	x	1

The inverse PWM signal will drive BLO high when ALO is driven low, and the same will happen in the opposite direction. The inverse PWM signal is achieved by sending the PWM signal through an inverter circuit and then to BLI. Figure 56 shows the new circuit.

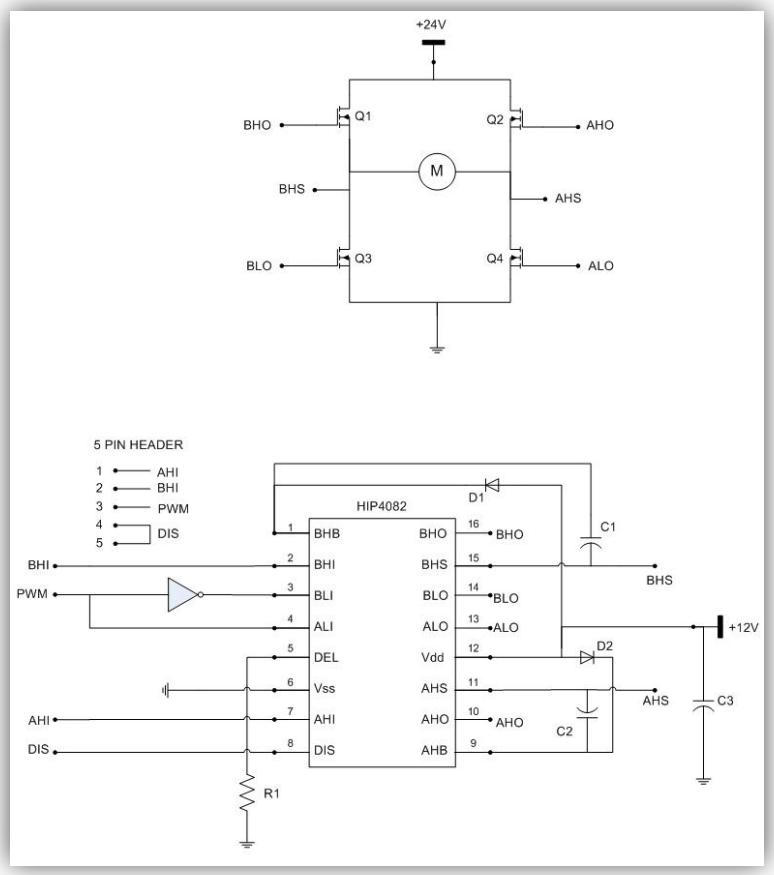

Figure 56: HIP4082 circuit with inverter

This circuit was tested on a small 24 V DC motor and it worked satisfactorily. The circuit was then connected to the Parvalux motor. During testing the circuit still suffered from MOSFET failure. The reasons why the MOSFETs failed were unclear, so the circuit had to be re-examined in order to find the solution.

After the investigation it was found that some safety features needed to be added to prevent the electronics from being destroyed. Firstly, to protect the MOSFETs from the sudden change in voltage when being turned on, a resistor on the gate is added to manage the large change in current. Unfortunately the resistor will also delay the discharge time of the MOSFET resulting in shoot through. In order to prevent this, a Schottky diode was placed parallel to the resistor. The diode is orientated so that it conducts when the MOSFET is being discharged. A Schottky diode has a smaller voltage drop over itself compared to a regular diode, thus enabling a shorter turn on time and quicker discharging of the MOSFET. Also, since the gate acts as a capacitor, it is very

sensitive to high and low voltages. The rapid charge and discharge of the gate can cause voltage spikes which in turn can damage the MOSFET. To ensure this does not happen, two Zener diodes are placed cathode to cathode across the MOSFETs gate and source. The Zeners will clip both the high and low voltages and allow for safe operation under most operating conditions.

It was also found that the discharge time of a MOSFET is larger than the charge time. Thus the MOSFET turns on much faster than it turns off. In extreme cases the discharge time is slow enough so that the delay on the HIP4082 (set by the delay resistor on the DEL pin) was not enough to prevent shoot through. Thus the delay resistor was changed to 100 kΩ to incorporate the maximum possible delay time, which is set at 4 µs.

The inductive loads caused by motors are also capable of inducing voltage spikes. Along with this the brushes on the DC motor can cause high frequency noise. In order to prevent the induced voltage spikes, Transient Voltage Suppressors (TVS) will be used to clip the voltage spikes across the lower MOSFETs as well as across the power supply terminals. Protection against the high frequency noise spikes, caused by the brushes, is provided by an RC-snubber network across the motor terminals. The snubber consists of a high frequency capacitor and a low value resistor. Filtering will also be done across the supply terminals with the aid of large electrolytic capacitors.

The bootstrap components on the HIP4082 were also changed. The diodes were swapped for ultra-fast recovery diodes. These will aid in faster charging and discharging of the MOSFETs. The bootstrap capacitor was made smaller to 1 µF which will enable a shorter charge time. The new circuit is shown in Figure 57.

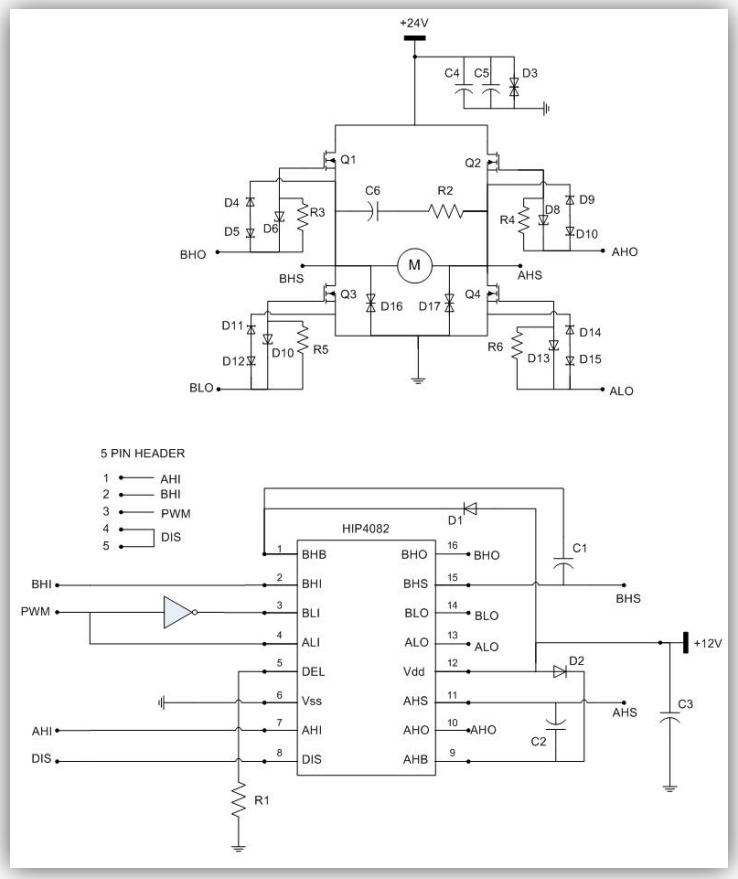

Figure 57: HIP4082 circuit with additional safety components

Table 8 below has the final component values used for the circuit.

Table 8: Components for safer HIP4082 circuit

Component	Value
C1 & C2	1 µF
C3	100 µF
C4 & C5	680 µF
C6 & C7	1 µF
Q1-Q4	IRFP1405PbF
R1	100 kΩ
R3-R6	22 Ω
D1 & D2	STTH512D
D4,D5 & D9,D10 & D11,D12 & D14,D15	1N4744A
D6,D8,D10,D13	1N5819RL
D3,D16,D17	1.5KE56CARL
HB1	HIP4081
INV1	74HC04

Further testing found that the circuit had reliability problems and was too unreliable to ensure proper future use. The reasons for failure were unclear and a large amount of time was used to investigate and repair the circuit. When the investigation became too time consuming it was decided to move on and employ a different approach to the driving circuit. It was opted to change the MOSFET driver the Intersel's HIP4081 driver.

The HIP4081 differs from the HIP4082 in the following ways: The HIP4081 has both high side and low side delay pins, so a delay can be put on both the upper and lower MOSFETs turn-on time. The PWM input signal for the driver must have a duty cycle 1-99% in order to refresh the bootstrap capacitor but the inverse PWM signal is not required. In order to ensure full recharge of the bootstrap capacitors and enable bi-directional rotation of the motors, the inputs BHI and AHI will be permanently driven high when they are required to drive the desired direction. The circuit makes use of four MOSFETs for each individual high and low side MOSFET. Figure 58 shows the schematic of the new circuit. In the figure only two MOSFETs are present in each part of the H-bridge, this is only to conserve the size of the schematic. The components in the circuit are the same as that of the HIP4082 circuit.

In order to drive the linear actuator bi-directionally, an integrated H-bridge driver will be used. The linear actuator is driving a weight of 50 N. This weight will cause the linear actuator to draw about 1 A (Linux, 2009). The L6225 from STMicroelectronics is a DMOS Dual Full Bridge designed for motor control applications. It has an operating supply voltage of 8 V to 52 V and a peak output current of 1.4 A. It is integrated with over load protection, which will disable the chip should the current drawn become too high, along with thermal shutdown which will disable the chip if its running temperature becomes too high.

Figure 59 shows the circuit that will drive the linear actuator. To reduce the power dissipation in the chip for the given current level, the outputs of the L6225 will be paralleled. This means that the motor will effectively be driven by two separate H-bridges. The H-bridges will share input signals, thus ensuring that they react the same to a given input.

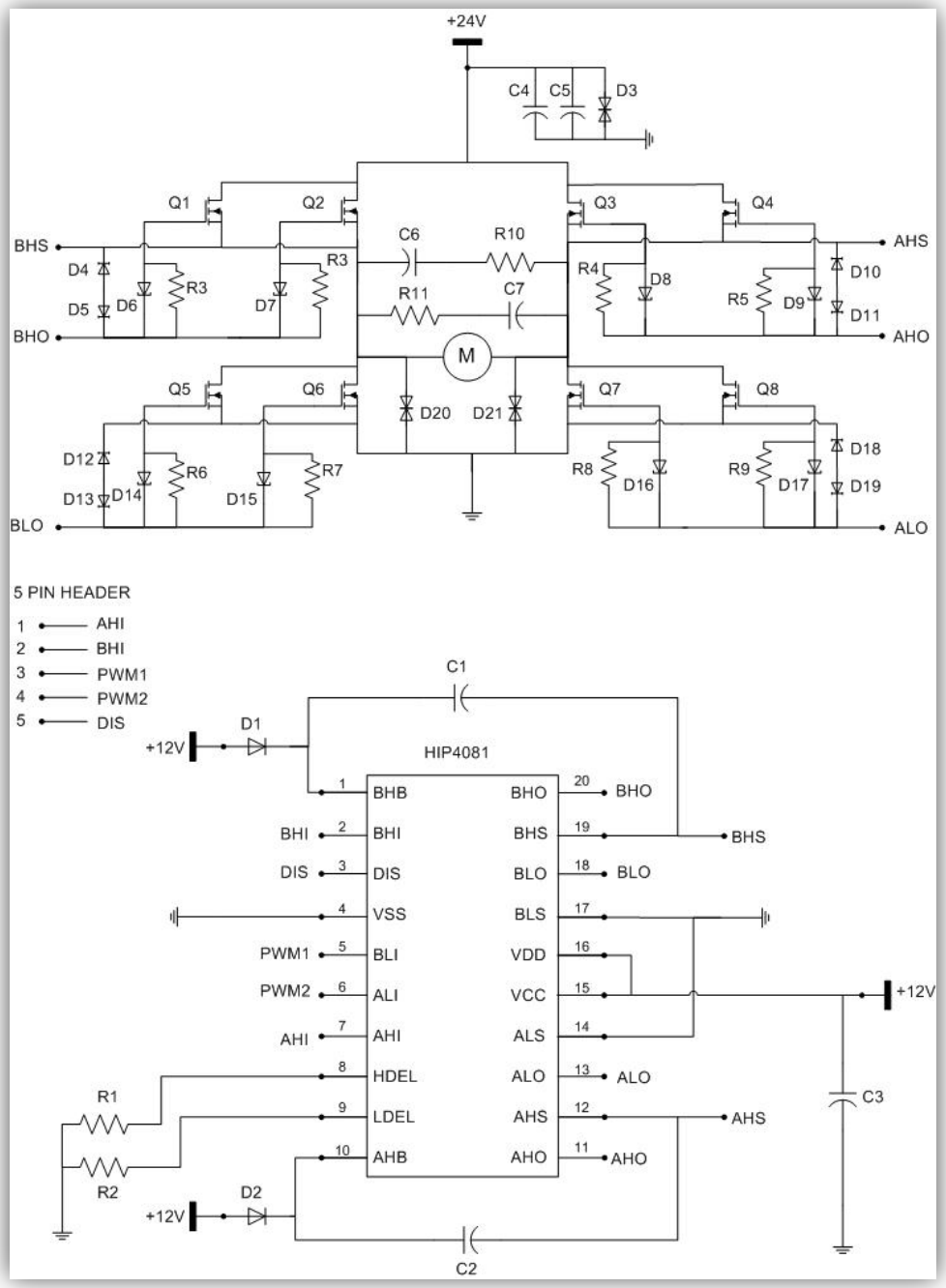

Figure 58: HIP4081 schematic

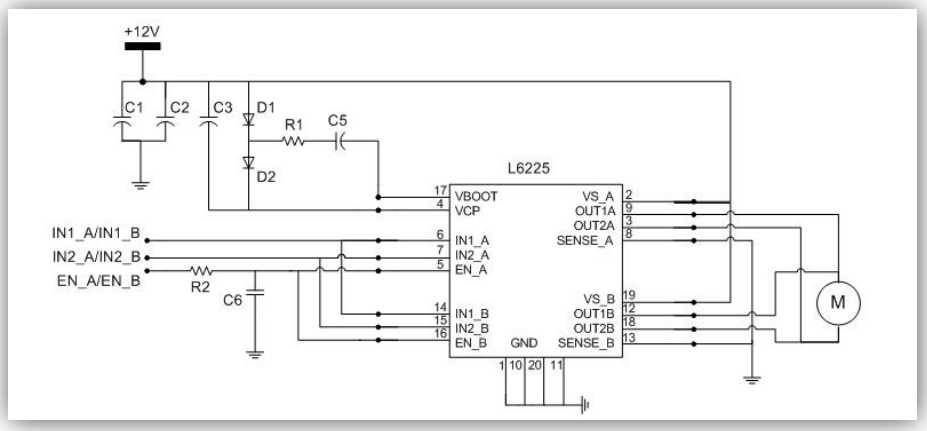

Figure 59: L6225 circuit for linear motor

The input signal for direction one will drive IN1_A and IN1_B while direction two will drive IN2_A and IN2_B. These inputs are TTL/CMOS and microcontroller compatible logic inputs. The enable signal drives EN_A and EN_B. These inputs have an identical structure except that the drains of the over current and thermal protections are also connected to these pins. Due to this R2 and C6 are required when connecting these pins.

C1 and C2 are used for high and low frequency filtering from the power supply. C3, D1, D2, R1 and C5 are the components required for the bootstrapped supply that will supply the initial charge pump for the internal N-channel MOSFETs. VS_A and VS_B are the supply pins for each of the two bridges. As with the inputs, the outputs of the bridges are paralleled to drive the linear actuator.

The circuit for control of the brakes on the Parvalux motors in shown in Figure 60. It is again the L6225 except that the inputs are driven separately and only the half bridges are utilized. The enable pins are driven with a 5 V source to ensure that the circuit is always active while there is power from the supply. The brakes (B1 & B2) will disengage once the bridges are activated by setting IN1_A and IN1_B high.

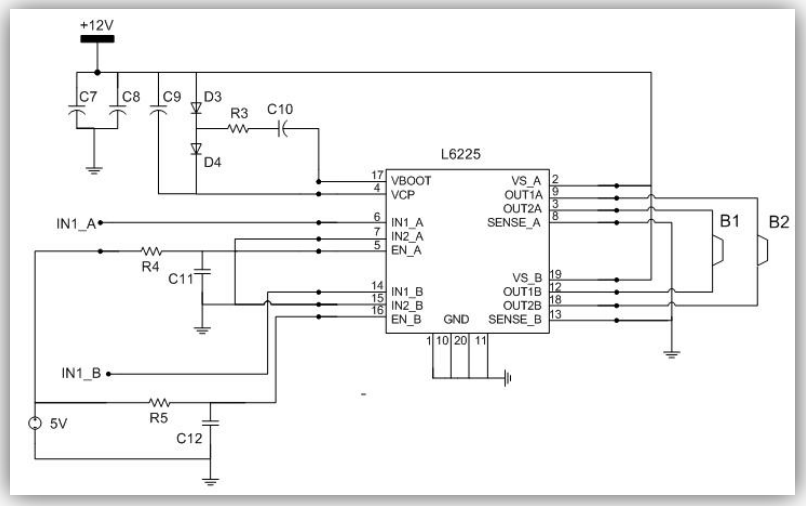

Figure 60: L6225 circuit for motor brakes

Table 9 lists the components and their corresponding values used for both the linear actuator and braking circuits.

Table 9: Components for all L6225 circuits

Component	Value
C1 & C7	100 µF
C2 & C8	100 nF
C3 & C9	220 nF
C5 & C10	10 nF
C6, C11 & C12	5. 6 nF
D1 – D4	1N4007
R1 & R3	100 Ω
R2, R4 & R5	100 kΩ

The PCB for the combined linear actuator and braking circuits is shown in Figure 61.

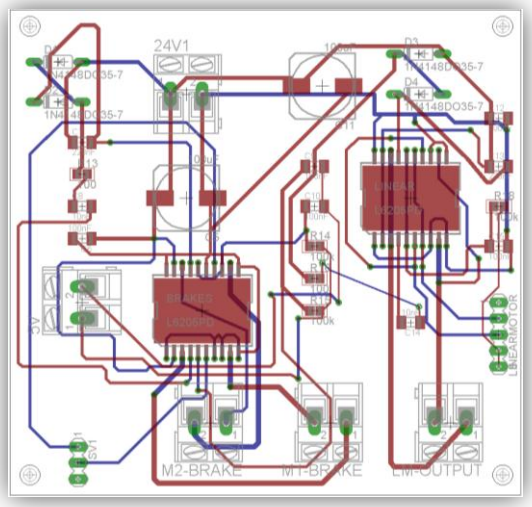

Figure 61: PCB for linear motor and braking circuit

The manipulator requires 24 V for the Parvalux and linear motors, 12 V for the PSM, Arduino and MOSFET driver and 5 V for the input on the braking circuit. A 24 V, 3 kW power supply from Current Automation will serve as the primary supply. From there a voltage regulator circuit will bring the supply down to 12 V and 5 V. The voltage regulation circuit is shown in Figure 62. The 12 V circuit drives the MOSFET driver drawing a peak of 1.25 A, the linear actuator and braking circuit with a 1.4 A peak output and the PSM motors' driver circuits which also draw a peak output of 1.4 A. The 5 V circuit only enables the braking circuit and therefore the current drawn is less than 1 A. Therefore the L78S12 and L7805 from STMicroelectronics were used to achieve voltage regulation. Diodes D1 and D2 ensure correct connection of the power supply. Capacitors C1 to C8 are used to remove ripples from both the input and output for both regulators.

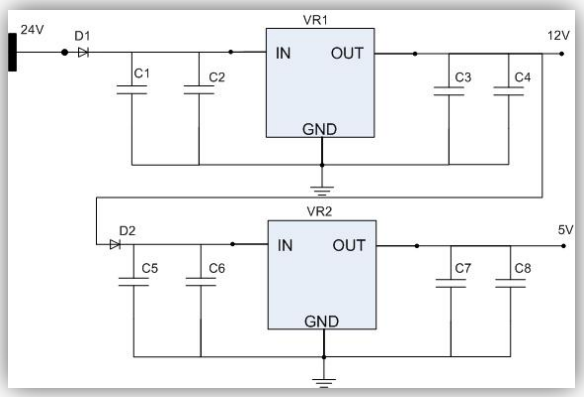

Figure 62: Regulated voltage supply circuit diagram

The PCB for the voltage regulation circuit is shown in Figure 63.

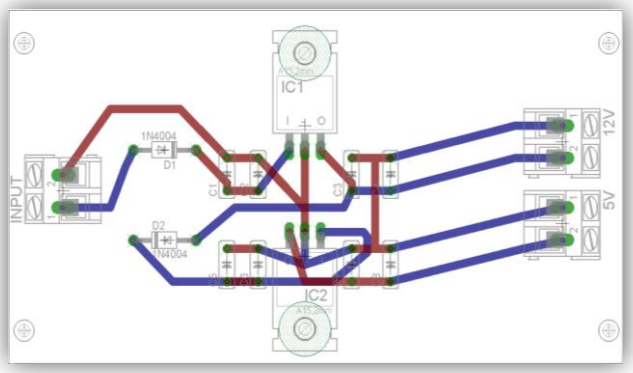

Figure 63: PCB for regulated voltage supply

Table 10 shows the components used for the voltage regulation circuit.

Table 10: Component values for voltage regulator circuit

Component	Value
VR1	L78S12
VR2	L7805
C1, C2, C5, C6	100 µF
C3, C4, C7, C8	10 nF

Since the whole manipulator must function as a single unit, the control electronics from Christiane (2008) were removed. The Arduino will be in control of the entire manipulator. The PSM has five DC motors that must be controlled. The power electronics were kept in place and only require a digital source in order to be activated. The motors require three signals, an enable, direction one and direction two signal. The H-bridges driving the motors on the PSM will be referred to as HBPSM, numbered from one to five. The revolute joint on the PSM is driven by two counter acting motors. These motors have separate power electronics, but will be driven from the same digital signals. To control the motors, only one of the two encoders will be connected. Table 11 gives the overview of the pin numbers on the Arduino, the pin description and its connection point.

Table 11: Pin numbers and description for connection to Arduino

Pin Number	Pin Description	Pin Connection
2	Linear motor direction 1	L6225 IN1_A/IN1_B
3	Linear motor direction 2	L6225 IN2_A/IN2_B
4	Pitch motor direction 1 PWM	HIP4081 (1) PWM1
5	Pitch motor direction 2 PWM	HIP4081 (1) PWM2
6	Yaw motor direction 1 PWM	HIP4081 (2) PWM1
7	Yaw motor direction 2 PWM	HIP4081 (2) PWM2
8	Linear motor encoder	Linear encoder header
9	Pitch motor encoder	Pitch encoder header
10	Yaw motor encoder	Yaw encoder header
22	Linear motor enable	L6225 EN_A/EN_B
24	Pitch motor enable	HIP4081 (1) DIS
25	Pitch motor brake	L6225 IN1_A
26	Yaw motor enable	HIP4081 (2) DIS
27	Yaw motor brake	L6225 IN1_B
28	Pitch motor direction1	HIP4081 (1) AHI
29	Pitch motor direction2	HIP4081 (1) BHI
30	Yaw motor direction1	HIP4081 (2) AHI
31	Yaw motor direction2	HIP4081 (2) BHI
38	Wrist motor encoder	Wrist encoder header
39	Gripper motor encoder	Gripper encoder header
40	Wrist motor enable	HBPSM4 enable
41	Gripper motor enable	HBPSM5 enable
42	Wrist motor direction 1	HBPSM4 direction 1
43	Gripper motor direction 1	HBPSM5 direction 1
44	Wrist motor direction 2	HBPSM4 direction 2
45	Gripper motor direction 2	HBPSM5 direction 2
46	Gear motor encoder	Gear encoder header
47	Revolute motor encoder	Revolute encoder header
48	Gear motor enable	HBPSM1 enable
49	Revolute motor enable	HBPSM(2/3) enable
50	Gear motor direction 1	HBPSM1 direction 1
51	Revolute motor direction 1	HBPSM(2/3) direction 1
52	Gear motor direction 2	HBPSM1 direction 2
53	Revolute motor direction 2	HBPSM(2/3) direction 2

4.5 Electronics Costs

This section will explain the cost of the electronic design and combine it with the mechanical design costs of the manipulator. From there it will continue and combine the costs with that of the PSM to give a sum total of the costs of the complete manipulator. Table 12 shows the cost associated with the electronics of the SSM.

Table 12: Cost of electronic components

Electronic part	Price/unit	Units	Total
Passives	n/a	n/a	R 300.00
L6225 H-bridge	R 65.26	10	R 652.00
Arduino Mega	R 450.00	1	R 450.00
Linear motor & brakes PCB	R 214.43	1	R 214.00
Signal connection PCB	R 482.46	1	R 482.00
HIP4081 PCB	R 1 400.00	2	R 2 800.00
Ribbon cables	R 200.00	2	R 400.00
Soldering	R 250.00	5	R 1 250.00
Total			**R 6 549.00**

The total costs of the electronics comes to R 6 550. The costs associated with the PSM's electronics in 2008 were R 3 911. If one assumes a 5% inflation rate per year, the modern day costs of the electronics come to roughly R4 530. Thus the costs of the PSM and SSM's electronics show a R 2 020 difference. This brings the total cost of the electronics of the complete manipulator to R 11 076. The total cost of the entire manipulator comes to R 159 800.

4.6 Cost Comparison

The costs associated with the SSM were slightly higher with both the mechanical and electronic designs. This is not surprising as a larger and more powerful manipulator would be required to move the PSM with an additional 3 DOFs. The next step would be to compare the costs of this project's manipulator to that of the da Vinci's. Since there is no credible information regarding the costs of the da Vinci at the same design stage as this project's manipulator, a comparison of the design differences will be presented to explain why this project's manipulator should be a less expensive alternative to the da Vinci.

The da Vinci requires the use of 39 motors in its design (Maxon, 2009). This is 23 more motors than the proposed design layout of the manipulator shown in **Error! Reference source not found.**. Additionally, all of the motors on the da Vinci require motor shields in order to drive them, thus also resulting in 23 additional motor shields. Another aspect

of the da Vinci's design is the use of HD quality video. In order to give the high quality video in real time to the surgeon, the da Vinci is supplied with state of the art image processing equipment. For the purpose of this manipulator, existing surgical endoscopes can be utilised. As surgeon has to use the endoscope regardless of robotic assistance, there is no increasing any expenses regarding the vision system.

Secondly, the major contributing factor toward the price of the da Vinci was its initial investment of $500 million (Haidegger & Benyó, 2010). Although the size of the investment required to gain EC certification cannot be known without a structured business plan, estimates can be made according to average investments for medical devices. According to Stein & Devaney (2007), a medical company would require an investment of around $40 to $60 million to go from start-up to an initial public offering.

Therefore it is believed that this projects manipulator will indeed be more cost effective than the da Vinci based on the arguments above. Less motors and conventional endoscopes minimise the costs on a design level, while an investment of around 20% the size of the da Vinci's investment, should see the manipulator's investors through from a start-up company to making an initial public offering.

Chapter 5: System Evaluation

The final objective of the thesis is to test the designed manipulator. This section will discuss the testing procedures as well as the results. The experiments must verify that the manipulator satisfies the design requirements and compares well to existing robotic systems. The experiments done for the manipulator were resolution and strength test.

5.1 Resolution Test

During a surgical procedure, the surgeon will want to either locate a point precisely or simply move from one point to another. Since the organs won't stay in exactly the same place whilst being handled, it will be better for a surgeon to be able to reach any point in the workspace precisely, not the same place repeatedly. Therefore a resolution test was done rather than an accuracy or repeatability test, and must prove that the manipulator can give the surgeon the ability to move more finely than when using conventional methods. Also, since the surgeon is able to view the surgical area with the aid of the endoscope, he can rely on visual feedback when trying to locate a point. Thus the ability to move finely can be combined with the visual feedback, to allow the surgeon to locate the desired point in the abdomen.

5.2 Experimental Set-up

In order to measure the resolution of the manipulator, the Polhemus Fastrak six degree-of-freedom electromagnetic tracker was used. The tracker's transmitter generates a magnetic field which is in turn picked up by the receiver. The tracker then interprets and sends the x-y-z coordinates to the GUI. The transmitter and receiver can be placed in any orientation anywhere in the test environment.

Because the Fastrak uses a magnetic field to obtain position coordinates, it must be ensured that the metal from the manipulator will not interfere with the measurements. A study done by Nixon *et al.* (1998) shows how metal at certain distances from the transmitter and receiver affect the tracker's measurements. Their study found that the tracker was influenced when the metal was placed along the transmitter receiver axis as well as when the transmitter/receiver distance becomes too large.

They found that for a fixed transmitter/metal and fixed receiver/metal distance, a 25 mm steel cube caused around a 0.2 mm error when the transmitter/receiver distance was 200 mm or less. Other tests showed that with a constant transmitter/receiver distance of 600 mm and the cube placed along the transmitter/receiver axis, the error was also around 0.2 mm when the cube was less than 200 mm from either. Therefore in

order to minimise the effects of the metal on the measurements, the transmitter and receiver must be positioned so that no metal is found along the transmitter/receiver axis. Also, the distance between the transmitter and receiver must remain smaller than 200 mm throughout the entire range of measurements. This configuration will give the tests a standard uncertainty of 0.2 mm.

The stylus pen receiver of the Fastrak was used because it allows the receiver to be mounted on the tip of the PSM which will allow the functional part of the receiver to be positioned away from any interfering metal with a distance of at least 110 mm. The orientation of the pen will be changed depending on which motor is being actuated.

The transmitter was aligned perpendicular to the frame of the manipulator by means of a 90° angle. This will allow the pitch motor's steps to be measured along the Y axis, the yaw motor along the X axis and the linear actuator along the Z axis. When testing the motors the PSM was positioned 100 mm from its lower end of range. This will allow the measurements to reflect the movement that is most likely to occur during a surgical procedure. The position if the transmitter and reciever can be seen in Figure 64.

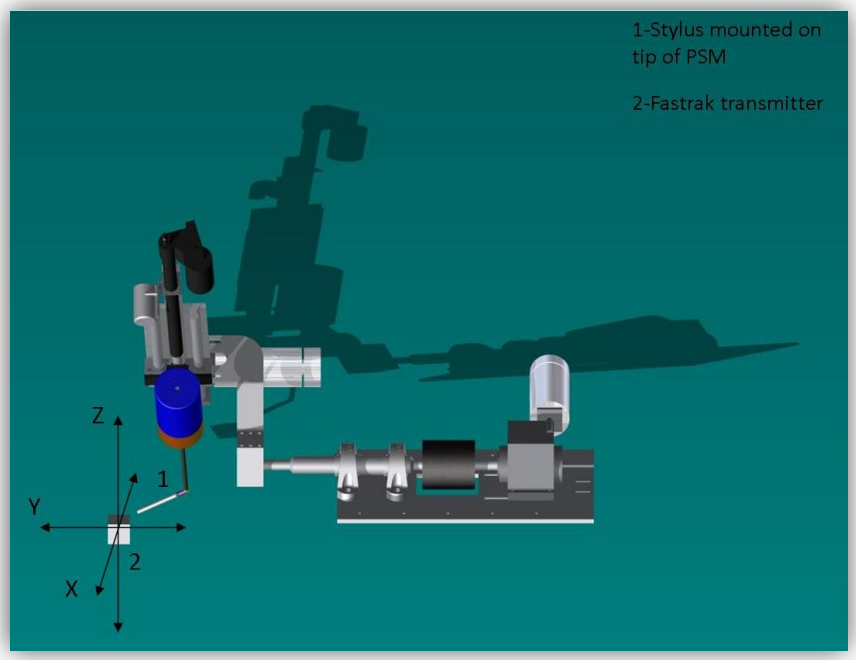

Figure 64: Placement of transmitter and receiver for resolution tests and coordinate system used

5.3 Results and Discussion

The tests were performed by moving one of the Parvalux motors from its starting position 35˚ clockwise and then back. The arm rotated by pitch motor was set to move from a vertical position and rotate in order to move the tip of the PSM toward the medial of a patient's abdomen, whilst the yaw motor moved the tip of the PSM toward the inferior direction. The Fastrak was set to measure continuously while increment commands were sent to the manipulator using the Arduino's serial communication window. The raw data was then analysed by a customised Matlab script that found each individual step and saved the step values.

With the encoders now mounted on the back of the motor, theoretically the motor shaft can be controlled to 0.1˚. This will translate through the gearbox to a rotation of 6.49 *m*˚ on the output shaft. Practically however, it was found that the motor shaft required at least around 15˚ rotation, otherwise the shaft would rotate back to its starting position before the brake could be engaged. Due to this effect a minimum rotation of 0.1˚ could be expected during testing. With the stylus located 220 mm from the point of rotation, the expected minimum resolution of the motors was around 0.4 mm. The resolution will likely be affected by the latency of the brake along with the required torque of the motor. If the motor is able to turn more easily its shaft will rotate a few degrees more before the brake is engaged. The results are show the step size (in mm) for each individual step the motor made. Therefore the number of steps do not represent the step count of the encoder, it represents each time the manipulator was moved by one command from the serial input.

The results of the yaw motor are shown in Figure 65 and Figure 66. Direction one indicates clockwise movement of the manipulator, moving the load downward. Direction two indicates anti-clockwise movement, moving the load upward. The tests show that the motor uses about 25 steps less to move the load downwards compared to when it moves upwards. This is due to increased torque requirements from the motor, causing it to rotate slightly more than desired before the brake is engaged. The step size would also increase slightly as the torque required from the motor becomes less when moving upward against the load.

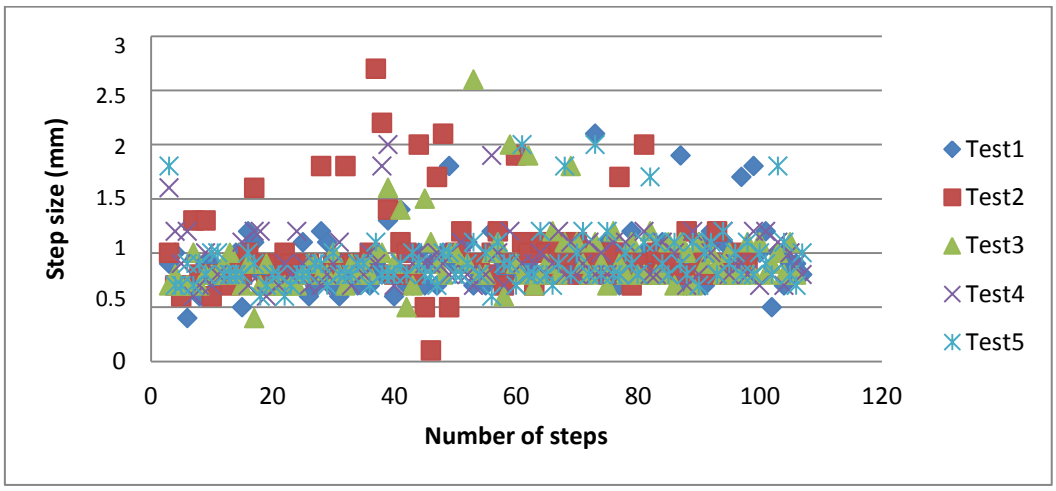

Figure 65: Resolution of yaw motor in direction one

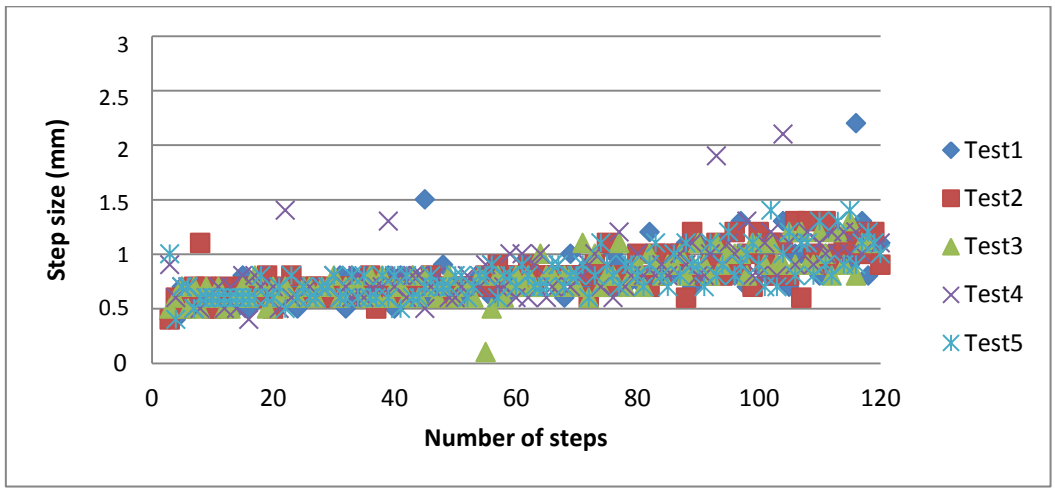

Figure 66: Resolution of yaw motor in direction two

Before the next results are discussed, the damping behaviour must be addressed. Since the damper is able to extend under its own weight, it can also be compressed when the force acting on it becomes greater than its internal spring force. The same happens when the spring expands, and the damper is capable of pushing the load back. These actions did occur when the motor was moving the load. Once the force acting on the damper was sufficient, it was able to compress/expand until the backlash on the gearbox was accounted for. The effect of this spring force accounts for the outliers found in Figure 68 and Figure 70. This did not adversely affect the results, it only contributed to a small area of larger resolution. A discussion on how this could be prevented will follow in Section 0.

The results from the pitch motor can be seen in Figure 67 to Figure 70. The results show that whilst moving the load downward, the step size would increase slightly as the required torque becomes larger.

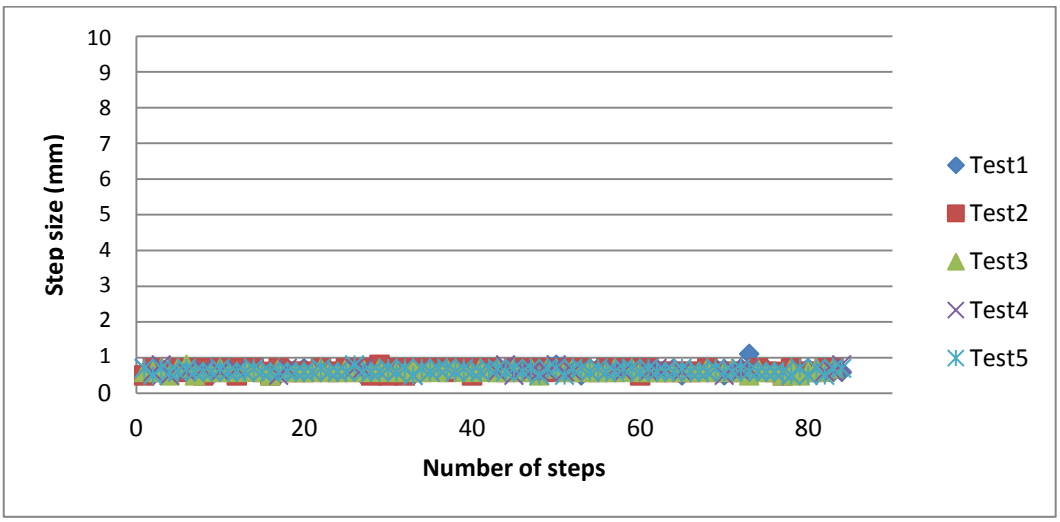

Figure 67: Resolution of pitch motor in direction one (downward) - before damper contribution

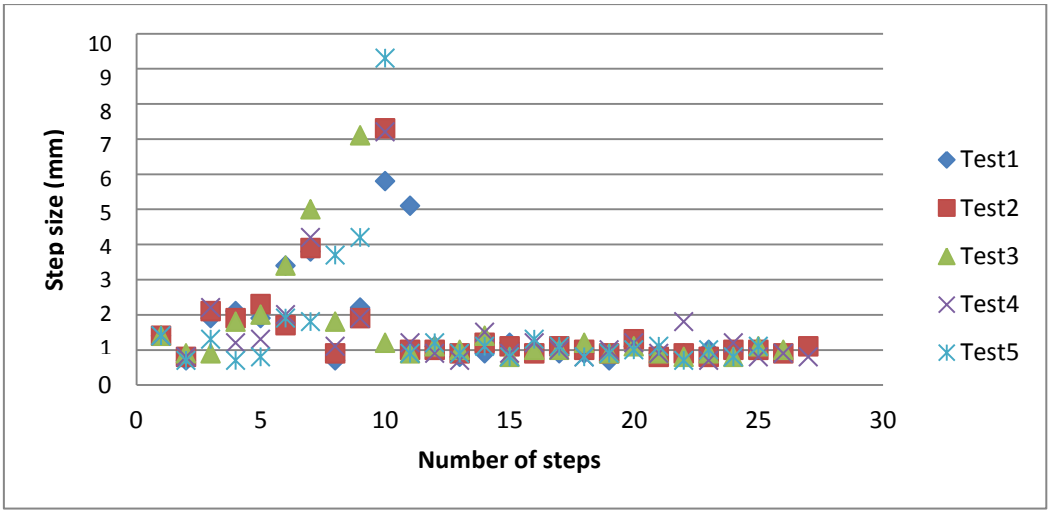

Figure 68: Resolution of pitch motor in direction one (downward) - after damper contribution

The same results can be seen in Figure 69 and Figure 70 when moving the motor in the opposite direction. At the start of the test the steps are small while the motor is has a large torque requirement. As the torque required becomes smaller, the step size would start to increase slightly.

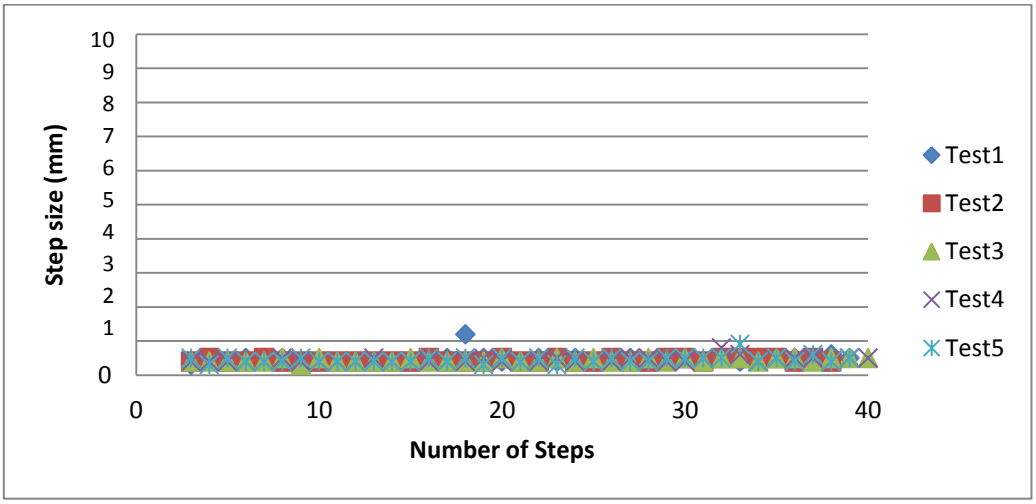

Figure 69: Resolution of pitch motor in direction two (upward) - before damper contribution

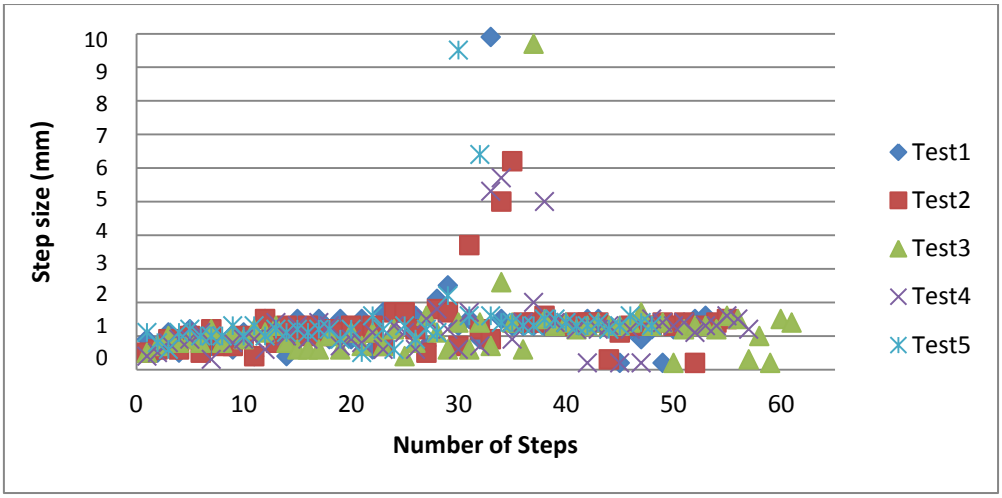

Figure 70: Resolution of pitch motor in direction two (upward) - after damper contribution

In order to summarize the results, the average step sizes across all tests were taken. The results are shown as:

Mean ± standard deviation.

A confidence rating is made by looking at how many points are located outside the area of the mean step band (mean ± standard deviation) and comparing that with the number of steps inside the step band as seen in Equation 14:

$$Confidence = 1 - \frac{steps\ outside\ average\ step\ size\ \pm uncertainty}{steps\ inside\ average\ step\ size\ \pm uncertainty} \times 100\% \qquad (14)$$

Table 13 summarises the yaw motor's performance.

Table 13: Summary of yaw motor resolution

	Step Size	Confidence
Yaw motor direction one (0 – 35 steps)	0.9 ± 0.3 mm	98%
Yaw motor direction one (35 - ~105 steps)	1 ± 0.3 mm	98%
Yaw motor direction two (0 – 70 steps)	0.7 ± 0.2 mm	97%
Yaw motor direction two (70 – ~120 steps)	1 ± 0.3 mm	98%

Table 14 summarises the movement of the pitch motor. The step confidence is found in the same way as with the yaw motor. The low step confidence of direction one (steps 81 - ~110) and direction two (steps 41 ~100) are contributed to the damper moving the load.

Table 14: Summary of pitch motor resolution

	Step size	Confidence
Pitch motor direction one (0 – 80 steps)	0.6 ± 0.2 mm	98%
Pitch motor direction one (81 – ~110 steps)	1 ± 0.4 mm	85%
Pitch motor direction two (0 – 40 steps)	0.5 ± 0.2 mm	98%
Pitch motor direction two (41 – ~100 steps)	1 ± 0.4 mm	89%

The resolution of the motors can now be linked back to radians with Equation 15:

$$\#degrees = sin^{-1}\left(\frac{(\#steps\ in\ resolution\ range) \cdot resolution}{220}\right) \quad (15)$$

The results from the linear motor tests can be seen in Figure 71 and Figure 72. Since the motor's range is known and the load does not change with range, it was tested over a small region. The motor was moved up approximately 15 steps, and then down to the same start location. After this the motor was moved to the same start and end locations. As with the Parvalux motors the linear motor showed load dependent behaviour. It took the motor around five steps less (over a distance of 2 mm) to reach the same position when moving downward. During the upward movement of the linear motor, it can be seen that most steps fall under the minimum resolution value of 0.2 mm. It will be concluded that the minimum step is therefore 0.2 mm plus the uncertainty of 0.2 mm.

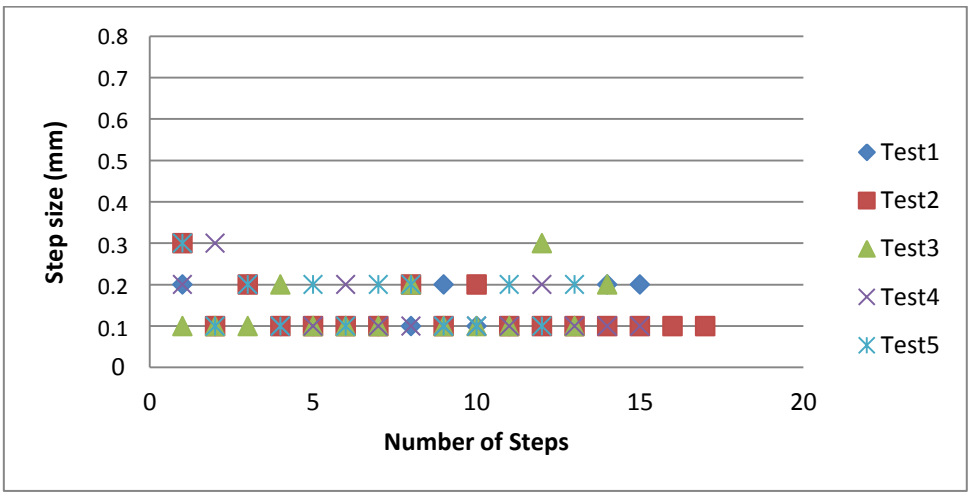

Figure 71: Linear motor resolution with upward movement

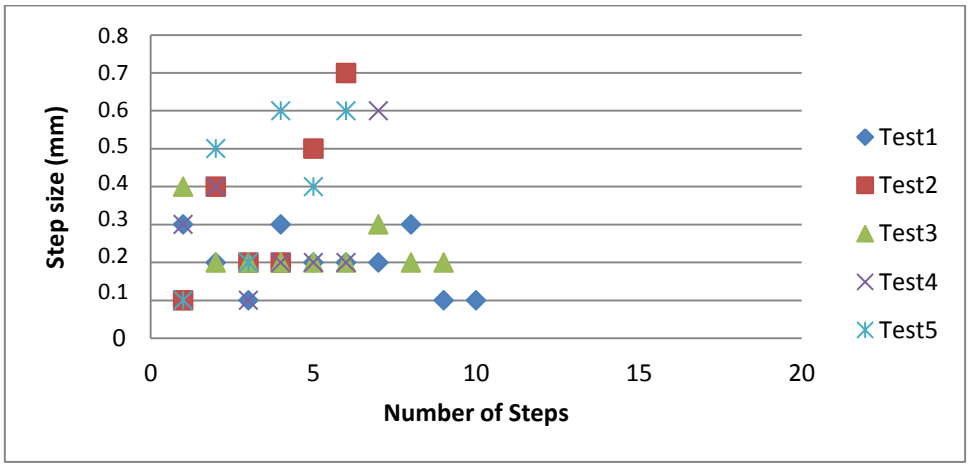

Figure 72: Linear motor resolution with downward movement.

Table 15 summarises the resolution of the linear motor.

Table 15: Linear motor resolution

	Resolution	Confidence
Linear Motor Upward	0.2 + 0.2 mm	100%
Linear Motor Downward	0.3 ± 0.2 mm	98%

5.4 Strength Test

One of the design requirements faced by Christiane (2008) was that the manipulator must be capable of withstanding an opposing tip force of 10 N. The strength test was aimed at proving that the manipulator could withstand as well as apply the required force, not to measure the maximum force that the manipulator can apply or withstand.

5.4.1. Experimental Set-up

The tests will be done in two ways. Firstly the manipulator was kept still while a 10 N force is applied externally. The force was applied by means of a pull scale. This test will determine whether the manipulator deflects in the presence of a 10 N force. Additionally the pull scale was fixed whilst the manipulator was actuated until the required force is reached. This test will prove that the manipulator is capable of generating the required torque to realize the 10 N force. The manipulator will be positioned at various positions along its range and actuated in both directions to verify the force capability. The tip of the PSM will be positioned so that the pull scale can be connected over it and allow actuation to pull the scale. Figure 73 shows the directions in which the external forces were applied to the manipulator.

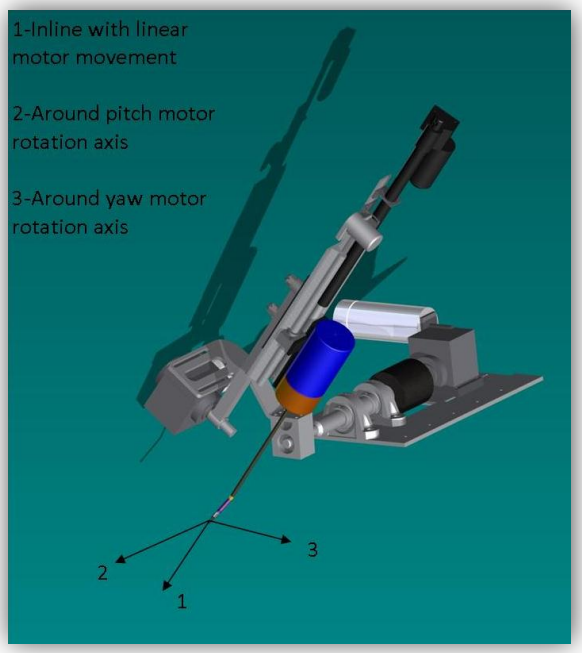

Figure 73: External forces applied to manipulator.

5.4.2. Results and Discussion

Since the motors used for actuation are capable of moving very large loads, there was never any doubt that they will encounter problems whilst attempting to generate a 10 N force. All of the manipulator's motors were capable of producing the 10 N force anywhere within their working range.

Whilst applying the external 10 N forces, it was found that the force was able to deflect the PSM's shaft by a few millimetres. Since it was not the scope of this thesis to ensure that the PSM does not deflect, the stylus pen was connected to the top of the linear actuator, and the transmitter was placed 100 mm away. With the stylus placed there the deflection of the SSM can be monitored whilst applying the external forces. Due to the

robust construction of the SSM, the 10 N forces had no effect on the manipulator. This was measured by applying the force and continuously measuring the position of the stylus, which remained unchanged.

5.5 Manipulator Evaluation Discussion

The resolution tests showed that the manipulator is dependent on the load requirements. The tests showed that the manipulator's pitch motor has step size of 0.6 ± 0.2 mm when moving downward with a small torque requirement, while the step size increases to 1 ± 0.4 mm as the torque requirements increase. When moving upward against the load, the step size is 0.5 ± 0.2 mm and increases to 1 ± 0.4 mm as the required torque decreases. The yaw motor showed a slight change in step size when moving with the load, with a step size of 0.9 ± 0.3 mm with low torque requirements and a step size of 1 ± 0.3 mm with larger torque requirements. When moving back up against the load, the step size is 0.7 ± 0.2 mm with large torque requirements, and 1 ± 0.3 mm with smaller requirements. The reason the step size increases with higher torque requirements when moving downward with the load is because the motor is able to rotate more easily. The same effect is seen when the motor is moving the load upward and the torque demand is decreased. The linear motor also showed load dependant behaviour. When moving downward with the load the step size was 0.3 ± 0.2 mm and 0.2 ± 0.2 mm when moving upward. During testing with the da Vinci robot, it was found that it is capable of locating a point with an accuracy of 0.22 mm and a standard deviation of ± 0.15 mm (Lobontiu, 2007).

The change in step value experienced by the manipulator can be controlled by implementing a control algorithm that varies the applied torque or encoder increment depending on where the manipulator is located. The results obtained are thought to be acceptable since the required resolution from the manipulator was set at 1 mm. The speeds required from the manipulator were also satisfied. Depending on the PWM input to the motors, the Parvalux motors can be moved from 5 rpm to 26 rpm whilst the linear actuator can be moved from 5 mm/sec to 60 mm/sec. The range of motion of the manipulator is 90˚ in the medial/lateral direction and 35˚ in the superior/inferior direction. The range of movement in all three directions is consistent with the requirements set out in Section 3.3.

Since the pitch motor tests showed that the damper contributed to the movement of the manipulator, the set-up must be changed in order to eliminate the undesired movement. The damper requires a compression force to be moved along its length. If the damper is switched for one that requires an extension force, the problem will be solved. Alternatively, the damper can be moved to connect to the other side of the pivoting arm. At the time of testing there was not adequate time to design a mounting mechanism, therefore tests were done with the damper as it was.

The manipulator proved it is capable of generating a 10 N force as required. Also, no deflection was picked up when the external force was applied. These tests confirmed that the manipulator can be relied on to perform the necessary tasks in a MIRS procedure.

In conclusion, it was found through the resolution and strength test that the manipulator could possibly perform the required task in a basic MIRS procedure. Once the necessary corrections are made on the manipulator, the movement can be constant and precise, allowing the surgeon to operate with complete confidence.

Chapter 6: Conclusion and Recommendations

MIS is done by making small incisions in the abdomen of the patient and manipulating organs with thin rod-shaped instruments. These procedures benefit patients since the wounds due to surgery are much smaller in comparison with conventional surgery. This implies that the patient has less pain and consequently spends less time in hospital. Unfortunately, the instruments currently being used for MIS restrict the movement the surgeon can make inside the abdomen. The lack of a wrist on the instrument means the surgeon has to occasionally move into unconvertible positions to reach a required area or organ. Along with this are the difficulties associated with the loss of dexterity with the instruments. Since the movement of the tools pivoted around the entry point in the abdomen, it is also mirrored. Surgical robots attempt to alleviate these drawbacks by providing the surgeon with a more natural and comfortable operating position. A robotic system is capable of removing the Fulcrum effect, restoring the wrist movement and enabling more accuracy when compared to conventional methods.

Unfortunately the only existing commercial system, the da Vinci surgical robot, is extremely expensive. The cost is usually the prohibiting factor for medical centres when considering purchasing a robotic system. This thesis is a continued effort to design a low cost seven DOF minimally invasive robotic surgical manipulator at the Biomedical Engineering Research Group at Stellenbosch University. The scope of the thesis included:

- Designing the three DOF external manipulator. This manipulator must combine with the four DOF internal manipulator designed by Christiane (2008).
- Designing the control electronics. The electronics are mainly used to showcase the functionality of the manipulator by controlling it during the resolution and strength tests.

The successfully designed manipulator is actuated through two DC motors with a worm-spur gearing combination along with a linear actuator. All motors have braking units to ensure movement is ceased when required as well as in the case of a power failure or emergency. The geared DC motors are driven with the aid of high current H-bridges while the linear motor is driven by an integrated H-bridge driving chip. The control signals for the driving circuits are given by the Arduino Mega interface PCB. This PCB contains the ATmega2560 microcontroller and allows it to be interfaced with 54 external inputs/outputs. The Arduino receives input from a serial based host and sends the relative output signals to the motors and brakes whilst monitoring the encoders.

In order to verify the functioning of the manipulator, two tests were done. The first test was a resolution test. The resolution tests showed that the manipulator is slightly depended on the load requirements. The tests showed that the manipulator's pitch motor has a step size of 0.6 ± 0.2 mm when moving downward with a small torque requirement, while the step size increases to 1 ± 0.4 mm as the torque requirements increase. When moving upward against the load, the step size is 0.5 ± 0.2 mm and increases to 1 ± 0.4 mm as the required torque decreases. The yaw motor showed a slight change in step size when moving with the load, with a step size of 0.9 ± 0.3 mm with low torque requirements and a step size of 1 ± 0.3 mm with larger torque requirements. When moving back up against the load, the step size is 0.7 ± 0.2 mm with large torque requirements, and 1 ± 0.3 mm with smaller requirements. The linear motor also displayed load dependant behaviour. When moving downward with the load the step size was 0.3 ± 0.2 mm and 0.2 ± 0.2 mm when moving upward. The second test done was a strength verification test. This test was done to ensure the manipulator is capable of applying a 10 N force stated as a requirement by Christiane (2008). All motors were capable of applying this force without difficulty.

Before this manipulator is ready to be tested in a surgical environment, some improvements need to be made. Firstly, the damping system used to prevent movement on the pitch motor because of the backlash must be changed. The damper was capable of moving the manipulator load when the force acting on them was smaller than the internal spring force. This gave rise to larger movement than desired for the manipulator. The damper can either be switched for an extension damper, or moved to connect on the other side of the pivoting arm. Secondly, a control system must be implemented that can manipulate the torque and/or increment values to obtain constant step sizes.

The designed manipulator is characterised by the following strengths:

- With the addition of the three DOF SSM, the entire robotic manipulator has seven DOF which can resemble the surgeon's hand movement more closely than conventional MIS tools.
- The SSM is made of relatively few parts. This eases the assembly procedure and allows for short maintenance visits.
- Drawbacks such as the fulcrum effect and scaled movement can be eliminated by the manipulator's software.
- The manipulator is strong enough to produce the required forces of MIRS procedures.
- The cost of the manipulator is thought to be low when compared to that of existing commercial systems.

Weaknesses and limitations that were identified:

- The resolution of the motors is dependent on torque requirements.

The cost of the manipulator was R91 081. This is divided between R74 727 for the mechanical assembly and R6 549 for the electronic components. When these costs are combined with the costs of the PSM (adjusted with an inflation rate of 5%/year), R78 526, the total comes to R159 800. The cost can be reduced once high production of the manipulator is in effect. Since a structured business plan is not available yet, the costs of the complete robotic manipulator were compared to the da Vinci on a design and initial investment level. From the arguments made it is believed that the robotic manipulator presented in this thesis will indeed be a low cost system, when compared to the da Vinci.

References

1. Advincula A. 2006. Surgical techniques: Robot-assisted laparoscopic hysterectomy with the da Vinci surgical system. *The international journal of medical robotics and computor assisted surgery*, Vol: 2, 305–311.

2. *Arduino Mega*. [S.a.]. [Online]. Available: http://www.arduino.cc/en/Main/ArduinoBoardMega [2010 October 12].

3. American Society for Reproductive Medicine. 2008. *PATIENT FACT SHEET - Minimally Invasive Surgery.* Alabama: The American Society for Reproductive Medicine.

4. Bhandari A., Hemal A. & Menon M. 2005. Instrumentation, sterilization, and preparation of robot. *Indian journal of Urology*, Vol: 21 (2), 283--88.

5. Bogue R. 2011. Robots in healthcare. *Industrial Robot: An International Journal*, Vol: 27, 218–223.

6. Brown J., Rosen J., Chang L., Barreca M., Sinanan M. & Hannaford B. 2002. The Blue Dragon - A System for Measuring the Kinematics and the Dynamics of Minimally Invasive Surgical Tools In–Vivo. *Proceedings of the 2002 IEEE International Conference on Robotics & Automation*, 11-15. Washington DC.

7. Christiane P.J. 2008. Development of a Minimally Invasive Robotic Surgical Manipulator. Unpublished Master's disertation. Stellenbosch: Stellenbosch University.

8. Craig R.R. Jr. 2000. *Mechanics of Materials, New Jersey*: John Wiley & Sons.

9. Das L.C. & Du lger M.T. 2005. Mathematical Modelling, Simulation and Experimental Verification of a SCARA Robot. *Simulation Modelling Practice and Theory*, Vol: 13, 257–271.

10. Davies B.L., Hibberd R.D., Timoney A.G. & Wickham J.E.A. 1991. A Surgeon Robot for Prostatectomies. *Fifth International Conference on Advanced Robotics*, 871–875.

11. Davies B. 2008. *Robot and Computer Assisted Surgery*. [Online]. Available: http://www.raeng.org.uk/events/pdf/Engineering_Better_Health/Brian_Davies.pdf. [3 April 2010].

12. Eto M. & Naito S. [S.a.]. *Robotic Surgery Assisted by the ZEUS System.* [Online] Available: http://ad-teaching.informatik.uni-

freiburg.de/zbmed/Springer%20Verlag%20E-Books/Pruefung/4-431-27173-2_Chapter_4.pdf. [2010 April 8].

13. Fichter E.F. 1986. A Stewart Platform Based Manipulator: General Theory and Practical Construction. *International Journal of Robotics*, 157–182.

14. Gomes P. 2011. Surgical Robotics: Reviewing the Past, Analysing the Present, Imagining the Future. *Robotics and Computers - Integrated Manufacturing*, Vol: 27, 261–266.

15. Haidegger T. & Benyó Z. 2010. Extreme Telesurgery. *Robot Surgery,* 26-44.

16. Hockstein N.G., Gourin C.G.,Faust R.A. & Terris D.J. 2007. A History of Robots: from Science Fiction to Surgical Robotics. *Journal of Robotic Surgery*, Vol: 1, 113–118.

17. Holloway R. W., Patel S. D. & Ahmad S. 2009. Robotic Surgery in Gynecology. *Scandinavian Journal of Surgery*, Vol: 98, 96–109.

18. Hubens G., Balliu L., Ruppert M., Gypen B., Van Tu T. & Vaneerdeweg W.2008. Roux-en-Y Gastric Bypass Procedure Performed with the da Vinci Robot System: Is It Worth It? *Surgical Endoscopy*, 1690–1696.

19. Intersel. 2006. *HIP 4082 Datasheet.* Intersel.

20. Intuitive Surgicals Inc. 2011. The da Vinci Surgical System. [Online]. Available: http://www.intuitivesurgical.com/products/ [8 March 2010].

21. Intuitive Surgical. 2009. *Robotic Surgical System "da Vinci™S HD".* Intuitive Surgical.

22. Jakopec M., Baena F.R., Harris S.J., Gomes P., Cobb J. & Davies B.L. 2003. The Hands-on Orthopaedic Robot "Acrobot": Early Clinical Trials of Total Knee Replacement Surgery. *IEEE Transactions on Robotics and Automation*, Vol: 19, 902-911.

23. Jaspers J.E.N. 2006. *Design and Evaluation of Mechanical Alternatives for "Robotic" Instruments for Minimally Invasive Surgery.* Delft: Technische Universiteit Delft.

24. Kazanzides P. [S.a.]. Development of the ROBODOC® System for Image-Directed Surgery [Online]. Available: http://www.cisst.org/~cista/445/Lectures/Robodoc903.pdf. [2010 April 7].

25. Kwoh Y.S., Hou J., Jonckheere E.A. & Hayati S. 1988. A Robot with Improved Absolute Positioning Accuracy for CT Guided Stereotactic Brain Surgery. *IEEE Transactions on Biomedical Engineering*, Vol: 35(2), 153–60.

26. Lanfranco A.R., Castellanos A.E., Desa J.P. & Meyers W.C. 2004. Robotic Surgery: A Current Perspective. *Annals of Surgery*, Vol: 239, 14-21.

27. Lazarevic Z. n.d. *Feasibility of a Stewart Platform with Fixed Actuators as a Platform for CABG Surgery Device.* Columbia: Columbia University.

28. Lee Y.J., Kim J., Ko S.K., Lee W.J. & Kwon D.S. 2003. Design of a Compact Laparoscopic Assistant Robot: KaLAR. *ICCAS2003*.

29. Linux. 2009. *LA30 product data sheet.* Linux.

30. Lobontiu A. & Loisance D. 2007. Robotic Surgery and Tele-surgery: Basic Principles and Description of a Novel Concept. *Jurnalul de Chirurgie*, Vol: 3 (3), 1584 – 9341.

31. Mabie H. & Reinholtz C.F. 1987. *Mechanisms and Dynamics of Machinery.* Canada: Wiley.

32. Marescaux J. & Rubino F. 2003. The ZEUS Robotic System: Experimental and Clinical Applications. *Surgical Clinics North America*, 1305–1315.

33. Markine V.L [S.a.]. *Optimization of a manipulator for a flight simulator* [Online] Available: http://www.brad.ac.uk/staff/vtoropov/burgeon/b_flsim.htm [2010 March 19].

34. McAfee P.C *et al*. 2010. Minimally Invasive Spine Surgery. *SPINE*: Vol: 35 (26), 271-273.

35. Meriam J.L., Kraige L.G. 2003. *Engineering Mechanics: Dynamics. Fifth Edition. New Jersey: John Wiley & Sons.*

36. Milutinov D. & Potkonjak V.1990. A New Concept of the SCARA Robot. *Robotics & Computer-Inteorated Manufacturing*, Vol: 7 (4), 337-343.

37. Mitchell J. & Lum H. 2004. *Kinematic Optimization of a 2-DOF Spherical Mechanism for a Minimally Invasive Surgical Robot.* Washington: University of Washington.

38. Mitchell J., Lum H., Rosen J., Sinanan M.N. & Hannaford B. 2006. Optimization of a Spherical Mechanism for a Minimally Invasive Surgical Robot: Theoretical and Experimental Approaches. *IEEE transactions on biomedical engineering*, Vol: 53 (7), 1440-1445.

39. Mitchell J., Lum H., Diana C., Friedman W., Sankaranarayanan G., King H., Fodero K., Leuschke R., Hannaford B., Rosen J. & Sinanan M.N. 2009. The RAVEN: Design and Validation of a Telesurgery System. *The International Journal of Robotics Research*, Vol 28, 1183-1197.

40. Motoman. 2011. *Industrial robot - HP3XF/HP3L/HP5 product information sheet*. Motoman.

41. Nixon M.A., McCallum B.C., Fright W.R. & Price N.B. 1998. The Effects of Metals and Interfering Fields on Electromagnetic Trackers. *Presence*, Vol 7 (2), 204–218.

42. Oehler M.K. 2009. Robot-assisted Surgery in Gynaecology. *Australian and New Zealand Journal of Obstetrics and Gynaecology*, Vol: 49, 124–129.

43. Parvalux. 2009. *Permanent Magnet Catalogue.* Parvalux.

44. Quaid A.E. & Hollis R.L. 1996. Cooperative 2-DOF Robots for Precision Assembly. *Proceedings of the 1996 IEEE International Conference on Robotics and Automation*, 2188-2193. Minneapolis, Minnesota.

45. *Raven IV - Colaborative Surgery*. [S.a.]. [Online]. Available: University of California - Santa Cruz Bionics lab: https://bionics.soe.ucsc.edu/research/surgery_device_5.html[2010 March 2].

46. *Raven - Mini Robot Design for Military Telesurgery in the Battlefield - Breaking the Size Barrier for Surgical Manipulators.* [S.a.]. [Online]. Available: University of California - Santa Cruz Bionics lab: https://bionics.soe.ucsc.edu/research/surgery_device_4.html. [2010 March 2].

47. Reynolds W. 2001. The First Laparoscopic Cholocystectomy. *Journal of the Society of Laparoendoscopic Surgeons*, Vol: 5, 89-94.

48. Ruurda J.P., van Vroonhoven T.J.M.V. & Broeders I.A.M.J 2002. Robot-assisted Surgical Systems: A New Era in Laparoscopic Surgery. *Royal Colegel of Surgeons of England*, Vol: 84, 223-226.

49. Satava R.M. 2006. The Early Chronicles: A Personal Historical Perspective [Online]. Available: http://www.websurg.com/ref/doi-ed01en0021.htm. [2010 April 12].

50. Satava R.M., Bowersox J.C. & Mack M.2001. Robotic Surgery: State of the Art and Future Trends. *Contemp Surgery*, Vol: 57, 489–499.

51. Schur M.O., Buess G.F. & Neisius B. 2000. Robotic and Telemanipulation Technologies for Endoscopic Surgery: a Review of the ARTEMIS Project. *Surgical Endoscopy*, 375-381.

52. Sim H.G., Yip S.K.H. & Kwon D.S. 2006. Equipment and Technology in Surgical Robotics. *World Journal of Urology*, Vol: 24, 128-135.

53. Stewart D. 1965. A Platform with Six Degrees of Freedom. *Proceedings of the Institution of Mechanical Engineers*, Vol: 180 (15), 372-386.

54. Stein T. & Devaney T. 2007. Just What the Doctor Ordered. *Venture Capital Journal.*

55. Sung G.T. & Gill I.S. 2001. Robotic Laparoscopic Surgery:A Comparison of the da Vinci and ZEUS Systems. *Adult urology*, Vol: 58 (6), 893-898.

56. Svensson L.G. *et al*. 2010. Minimally Invasive Versus Conventional Mitral Valve Surgery: A Propensity-matched Comparison. *The Journal of Thoracic and Cardiovascular Surger,* 926-932.

57. Taylor R., Paul H.A., Mittelstadt B., Glassman E., Musits B.L. & Bargar W.L. 1989. A Robotic System for Cementless Total Hip Replacement Surgery in Dogs. *Second workshop on medical and healthcare robotics*, 79–89.

58. Taylor R., Paul H.A.,Mittelstadt B.,Glassman E.,Musits B.L. & Bargar W.L. 2009. Design of a Minimally Invasive Surgical Teleoperated Master-Slave System with Haptic Feedback. *IEEE International Conference on Mechatronics and Automation*, 60-65. Changchun.

59. *The Puma 200* [S.a.]. [Online]. Available: http://www.prsrobots.com/puma200.html. [2010 March 5].

60. Tria A.J. 2003. Advancements in Minimally Invasive Total Knee Arthroplasty. *Orthopaedics*, Vol: 26 (8), 859-863.

61. *Vesconite Material Datasheet*. [S.a.]. [Online]. Available: http://www.hydro-watt.com/vesconite/VesconiteChemicalResistance.pdf. [2010 July 5].

62. Waldman B.J. 2003. Advancements in Minimally Invasive Total Hip Arthroplasty. *Orthopaedics*, Vol: 26 (8), 833-836.

63. Wildi T. 2006. *Electrical Machines, Drives and Power Systems Sixth Edition.* New Jersey. Pearson.

64. Wilson E.B. 2009. The Evolution of Robotic General Surgery. *Scandinavian Journal of Surgery*, Vol: 98, 125–129.

Appendix A – Technical Drawings

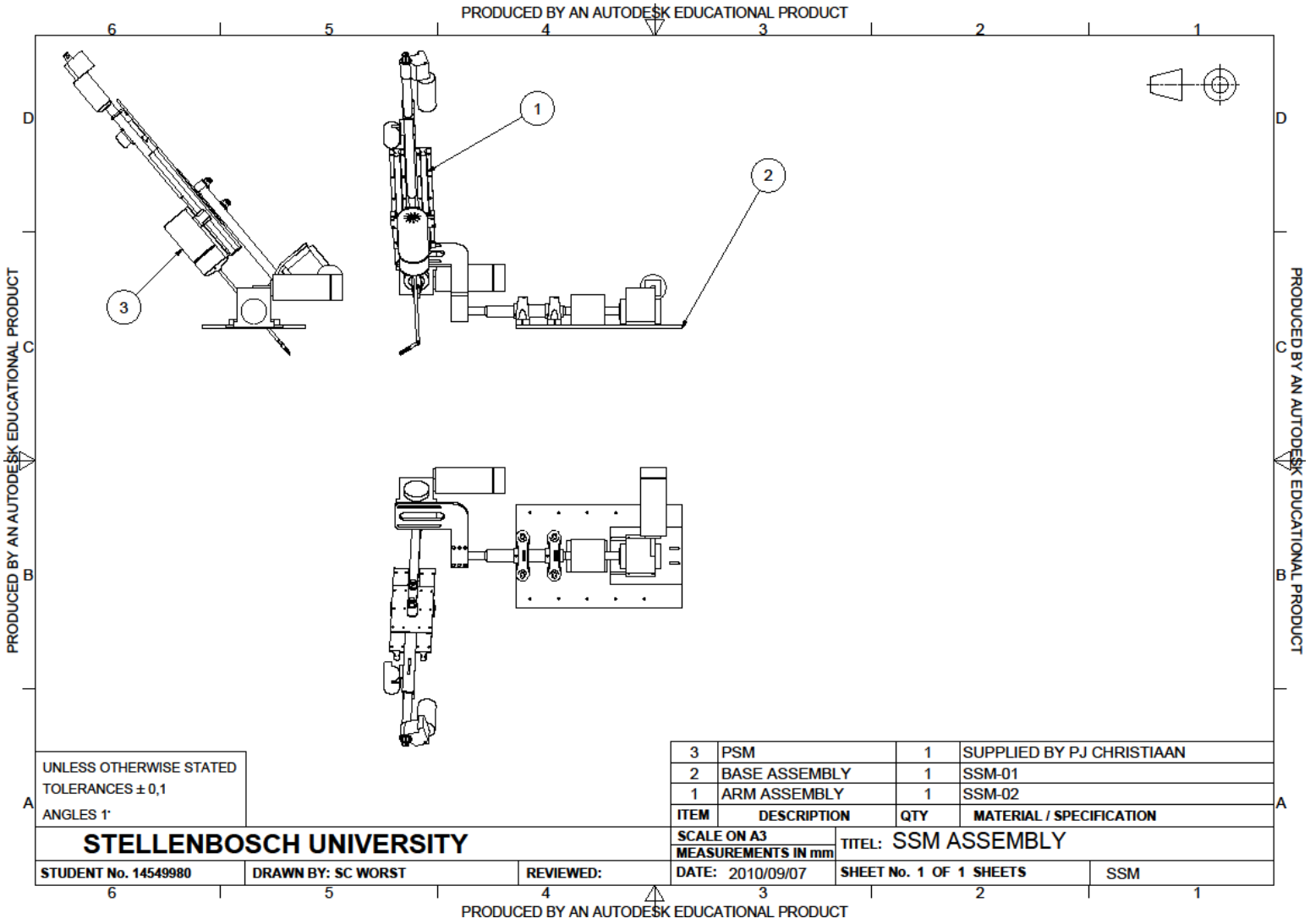
PRODUCED BY AN AUTODESK EDUCATIONAL PRODUCT
1
2
3
UNLESS OTHERWISE STATED
TOLERANCES ± 0,1
ANGLES 1°
3 PSM 1 SUPPLIED BY PJ CHRISTIAAN
2 BASE ASSEMBLY 1 SSM-01
1 ARM ASSEMBLY 1 SSM-02
ITEM DESCRIPTION QTY MATERIAL / SPECIFICATION
STELLENBOSCH UNIVERSITY
SCALE ON A3
MEASUREMENTS IN mm
TITEL: SSM ASSEMBLY
STUDENT No. 14549980
DRAWN BY: SC WORST
REVIEWED:
DATE: 2010/09/07
SHEET No. 1 OF 1 SHEETS
SSM

A2

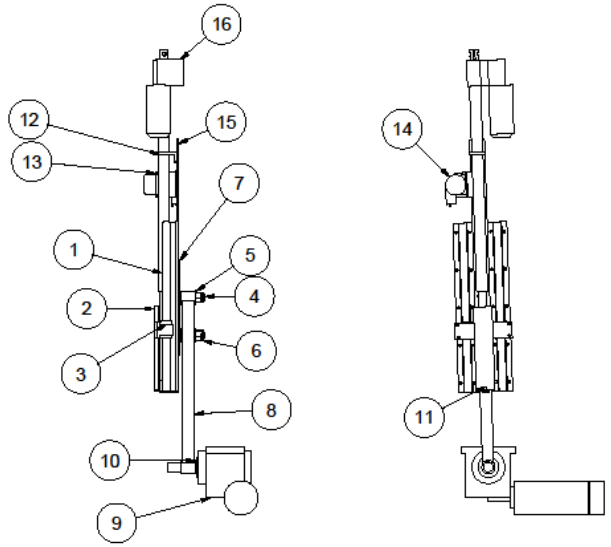

ITEM	DESCRIPTION	QTY	MATERIAL / SPECIFICATION
16	LINEAR MOTOR	1	SUPPLIED BY LINUKS
15	LINEAR MOTOR SUPPORT ARM	1	SSM-02-06
14	LINEAR ENCODER	1	
13	LINEAR ENCODER MOUNTING BRACKET	1	SSM-02-04
12	LINEAR MOTOR ALIGNMENT BRACKET	1	SSM-02-05
11	LINEAR MOTOR MOUNTING PIN	1	SSM-02-07
10	THRUST BEARING FOR MOTOR SHAFT	1	SSM-02-01
9	PARVALUX MOTOR	1	SUPPLIED BY PARVALUX
8	ACTUATING ARM	1	SSM-02-02
7	LINEAR BEARING RAIL MOUNTING PLATE	1	SSM-02-03
6	M16 NUT	2	SUPPLIED BY BOLTFAST
5	VESCONITE THRUST BEARING	4	SSM-02-09
4	M16 BOLT WITH VESCONITE BUSH	2	SUPPLIED BY BOLTFAST & MAIZY PLASTICS
3	LINEAR BEARING	2	SUPPLIED BY BOSCH REXROTH
2	PSM MOUNT	1	SSM-02-08
1	LINEAR BEARING RAILS	2	SUPPLIED BY BOSCH REXROTH

UNLESS OTHERWISE STATED
TOLERANCES ± 0,1
ANGLES 1°

STELLENBOSCH UNIVERSITY

SCALE ON A3
MEASUREMENTS IN mm

TITEL: ARM ASSEMBLY

STUDENT No. 14549980 | DRAWN BY: SC WORST | REVIEWED: | DATE: 2010/09/07 | SHEET No. 1 OF 1 SHEETS | SSM-02

PRODUCED BY AN AUTODESK EDUCATIONAL PRODUCT

A3

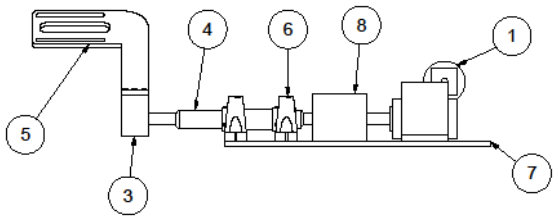

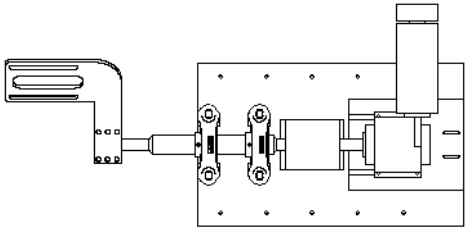

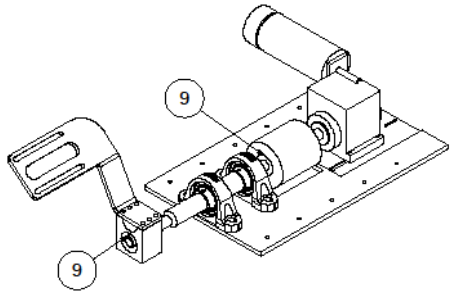

ITEM	DESCRIPTION	QTY	MATERIAL / SPECIFICATION
9	FENLOCK POWER COUPLING	3	SUPPLIED BY BMG
8	COUPLING	1	SUPPLIED BY BMG
7	BASE PLATE	1	SSM-01-01
6	SKF BEARING	2	SUPPLIED BY SKF
5	BASE ARM	1	SSM-01-04
4	SHAFT	1	SSM-01-03
3	FINAL ACTUATION AXIS CONNECTION	1	SSM-01-02
1	PARVALUX MOTOR	1	SUPPLIED BY PARVALUX

UNLESS OTHERWISE STATED
TOLERANCES ± 0,1
ANGLES 1°

STELLENBOSCH UNIVERSITY

SCALE ON A3
MEASUREMENTS IN mm

TITEL: BASE ASSEMBLY

STUDENT No. 14549980	DRAWN BY: SC WORST	REVIEWED:	DATE: 2010/09/07	SHEET No. 1 OF 1 SHEETS	SSM-01

PRODUCED BY AN AUTODESK EDUCATIONAL PRODUCT

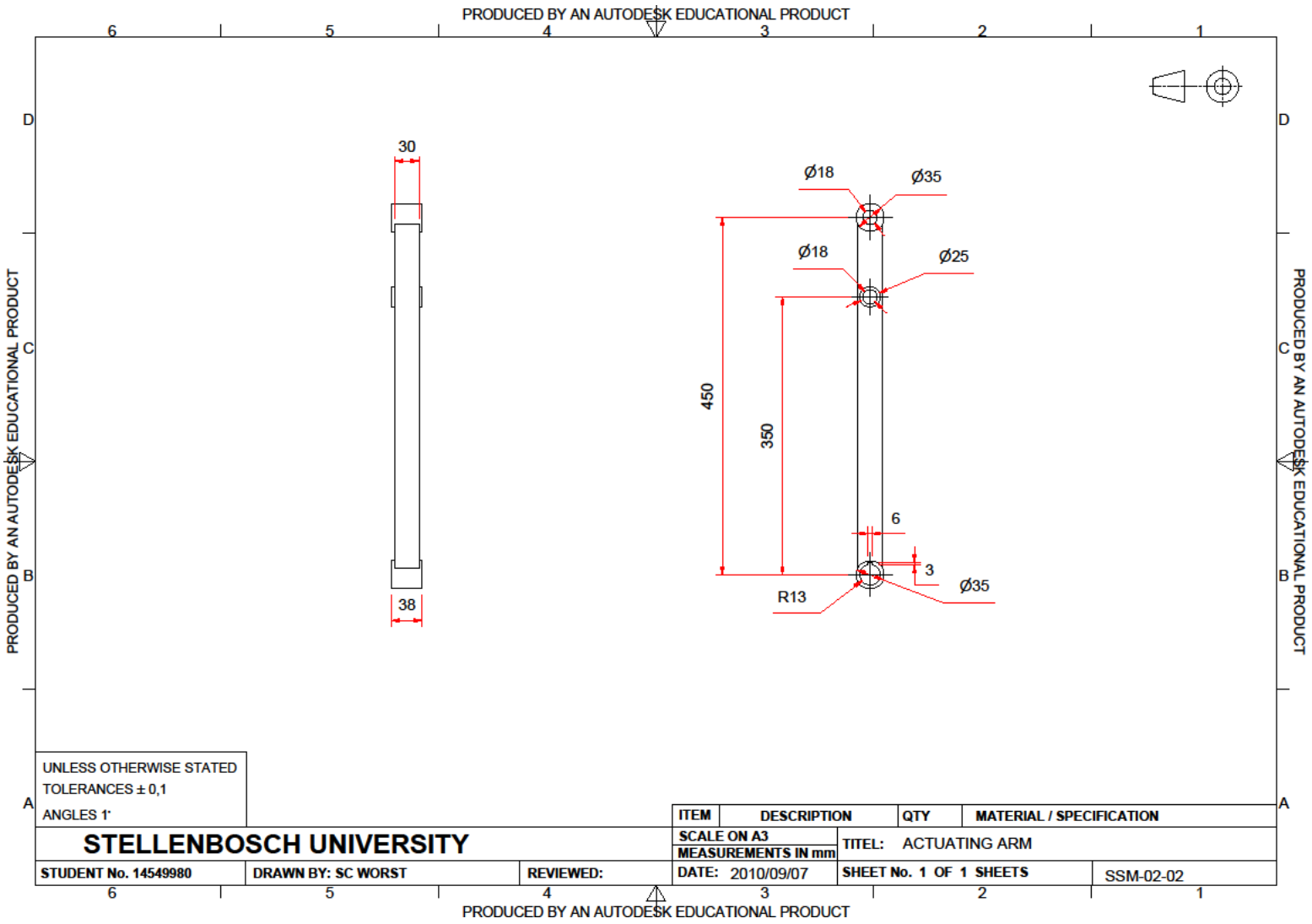
PRODUCED BY AN AUTODESK EDUCATIONAL PRODUCT
30
38
Ø18
Ø35
Ø18
Ø25
450
350
6
3
R13
Ø35
UNLESS OTHERWISE STATED
TOLERANCES ± 0,1
ANGLES 1°
ITEM
DESCRIPTION
QTY
MATERIAL / SPECIFICATION
STELLENBOSCH UNIVERSITY
SCALE ON A3
MEASUREMENTS IN mm
TITEL: ACTUATING ARM
STUDENT No. 14549980
DRAWN BY: SC WORST
REVIEWED:
DATE: 2010/09/07
SHEET No. 1 OF 1 SHEETS
SSM-02-02

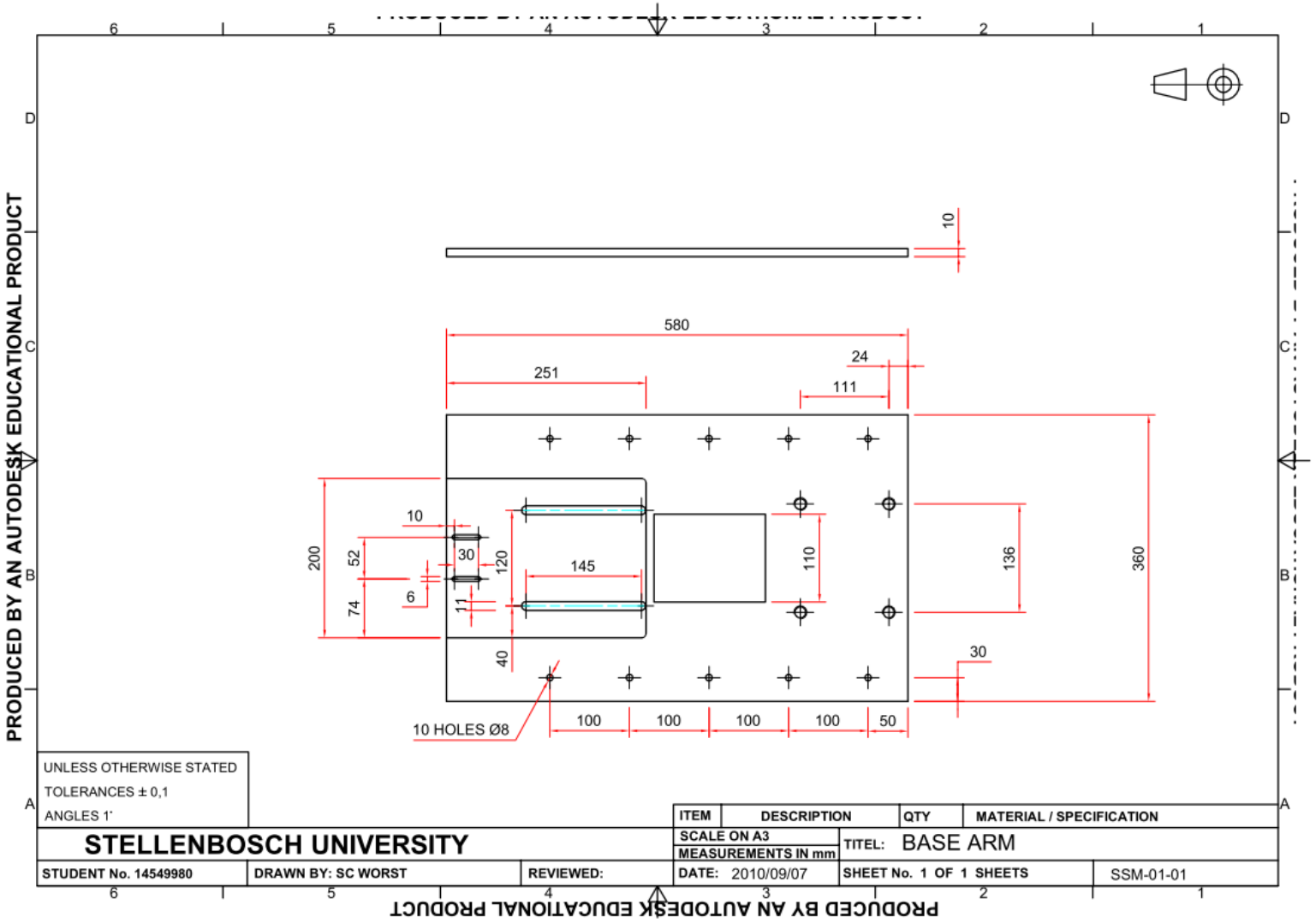
PRODUCED BY AN AUTODESK EDUCATIONAL PRODUCT
10
580
24
251
111
10
30
120
145
110
136
360
200
52
74
6
11
40
30
10 HOLES Ø8
100
100
100
100
50
UNLESS OTHERWISE STATED
TOLERANCES ± 0,1
ANGLES 1°
ITEM
DESCRIPTION
QTY
MATERIAL / SPECIFICATION
STELLENBOSCH UNIVERSITY
SCALE ON A3
MEASUREMENTS IN mm
TITEL: BASE ARM
STUDENT No. 14549980
DRAWN BY: SC WORST
REVIEWED:
DATE: 2010/09/07
SHEET No. 1 OF 1 SHEETS
SSM-01-01
PRODUCED BY AN AUTODESK EDUCATIONAL PRODUCT

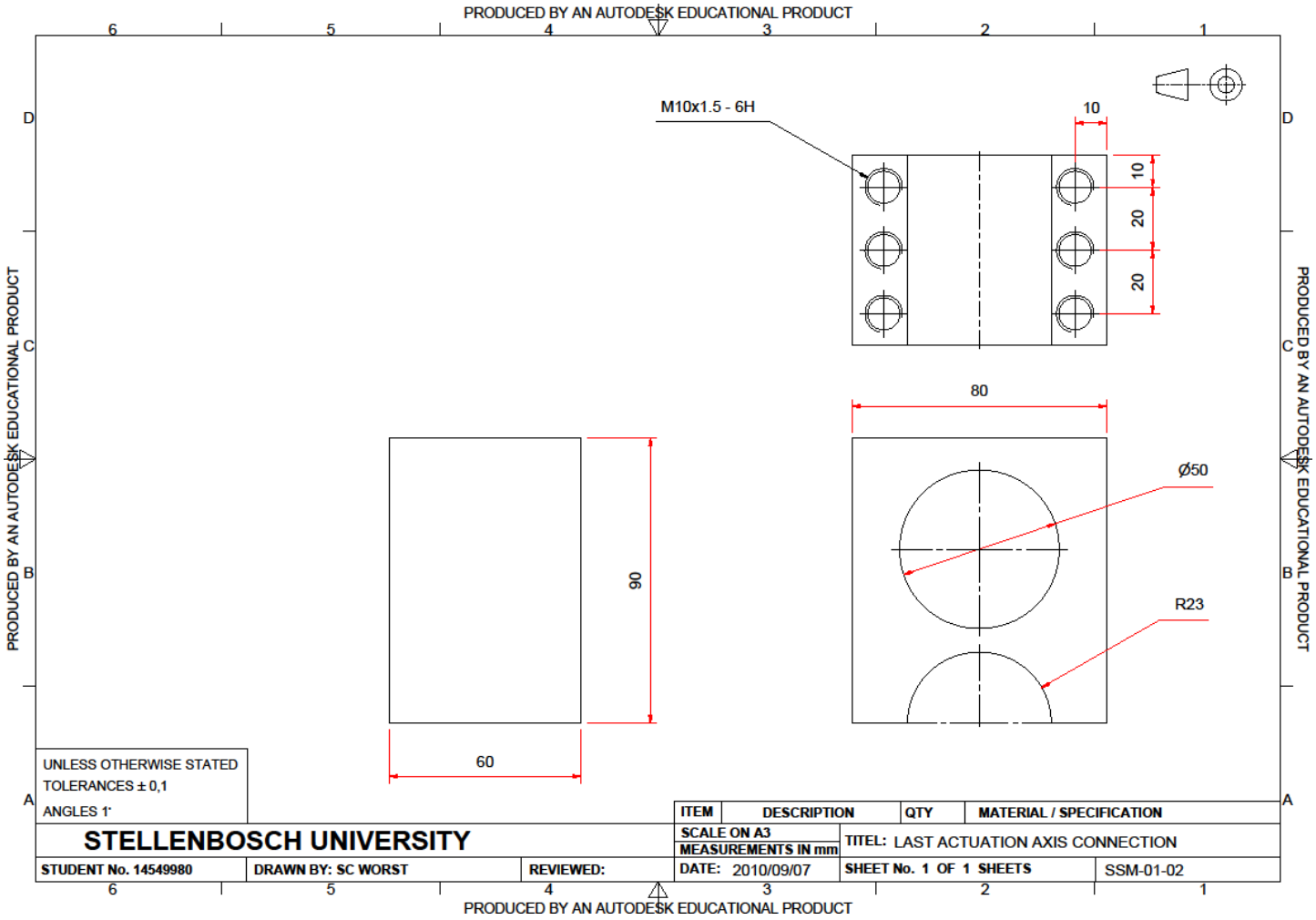
PRODUCED BY AN AUTODESK EDUCATIONAL PRODUCT
M10x1.5 - 6H
10
10
20
20
80
Ø50
R23
90
60
UNLESS OTHERWISE STATED
TOLERANCES ± 0,1
ANGLES 1°
ITEM
DESCRIPTION
QTY
MATERIAL / SPECIFICATION
STELLENBOSCH UNIVERSITY
SCALE ON A3
MEASUREMENTS IN mm
TITEL: LAST ACTUATION AXIS CONNECTION
STUDENT No. 14549980
DRAWN BY: SC WORST
REVIEWED:
DATE: 2010/09/07
SHEET No. 1 OF 1 SHEETS
SSM-01-02

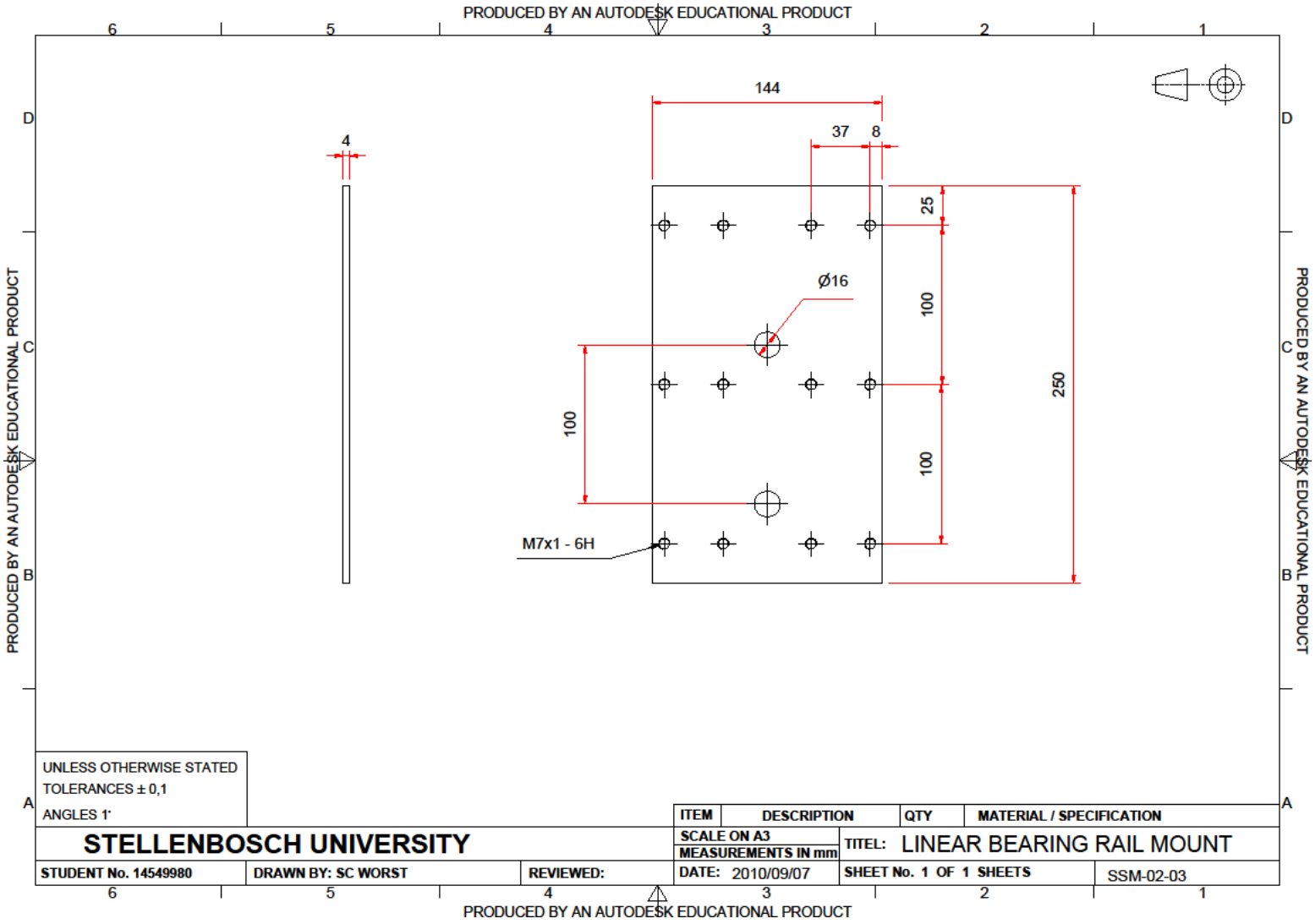
PRODUCED BY AN AUTODESK EDUCATIONAL PRODUCT
144
37
8
4
25
100
100
100
250
Ø16
M7x1 - 6H
UNLESS OTHERWISE STATED
TOLERANCES ± 0,1
ANGLES 1°
ITEM
DESCRIPTION
QTY
MATERIAL / SPECIFICATION
STELLENBOSCH UNIVERSITY
SCALE ON A3
MEASUREMENTS IN mm
TITEL: LINEAR BEARING RAIL MOUNT
STUDENT No. 14549980
DRAWN BY: SC WORST
REVIEWED:
DATE: 2010/09/07
SHEET No. 1 OF 1 SHEETS
SSM-02-03

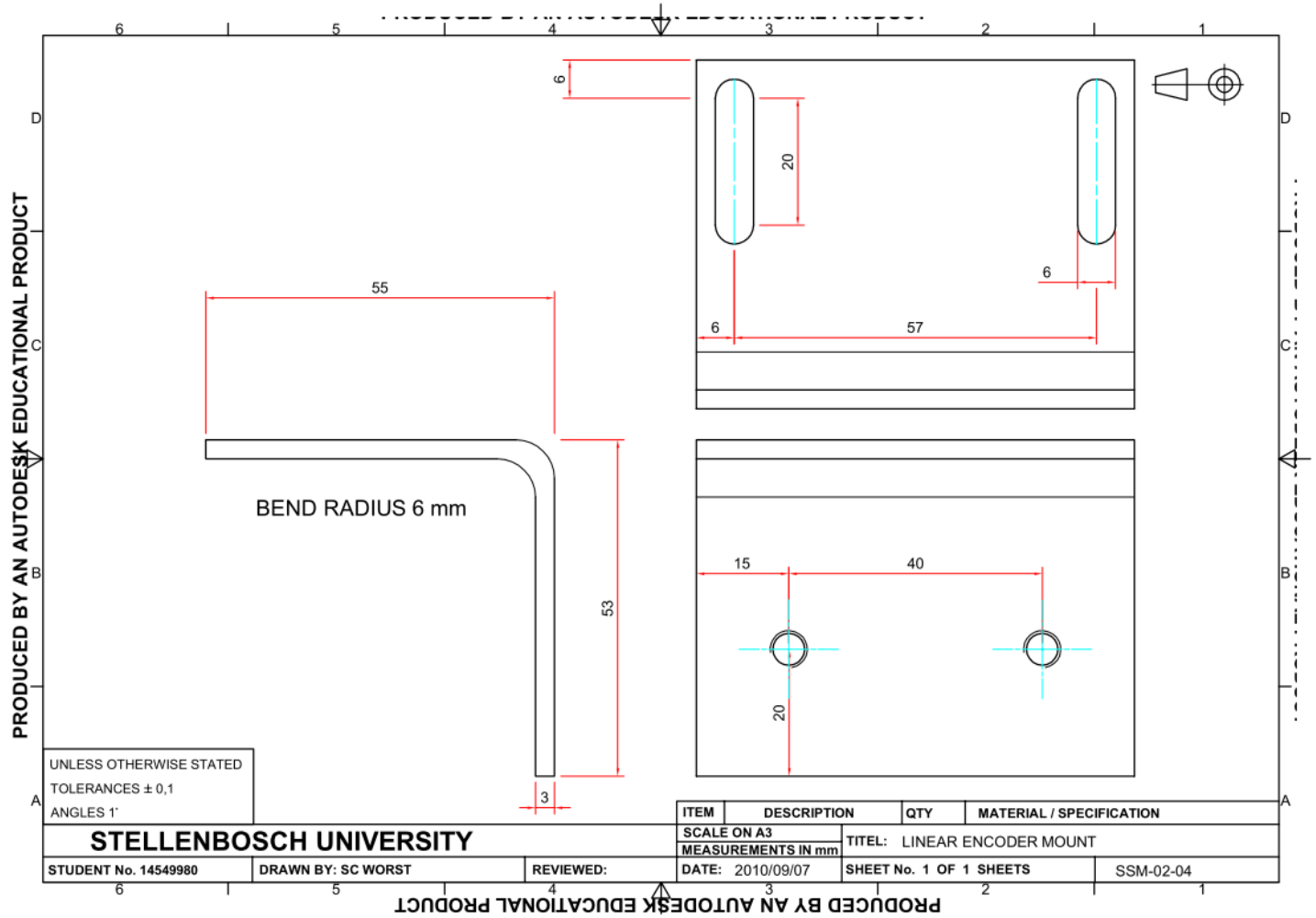
PRODUCED BY AN AUTODESK EDUCATIONAL PRODUCT
6
20
55
6
6
57
BEND RADIUS 6 mm
53
15
40
20
3
UNLESS OTHERWISE STATED
TOLERANCES ± 0,1
ANGLES 1°
ITEM
DESCRIPTION
QTY
MATERIAL / SPECIFICATION
STELLENBOSCH UNIVERSITY
SCALE ON A3
MEASUREMENTS IN mm
TITEL: LINEAR ENCODER MOUNT
STUDENT No. 14549980
DRAWN BY: SC WORST
REVIEWED:
DATE: 2010/09/07
SHEET No. 1 OF 1 SHEETS
SSM-02-04
PRODUCED BY AN AUTODESK EDUCATIONAL PRODUCT

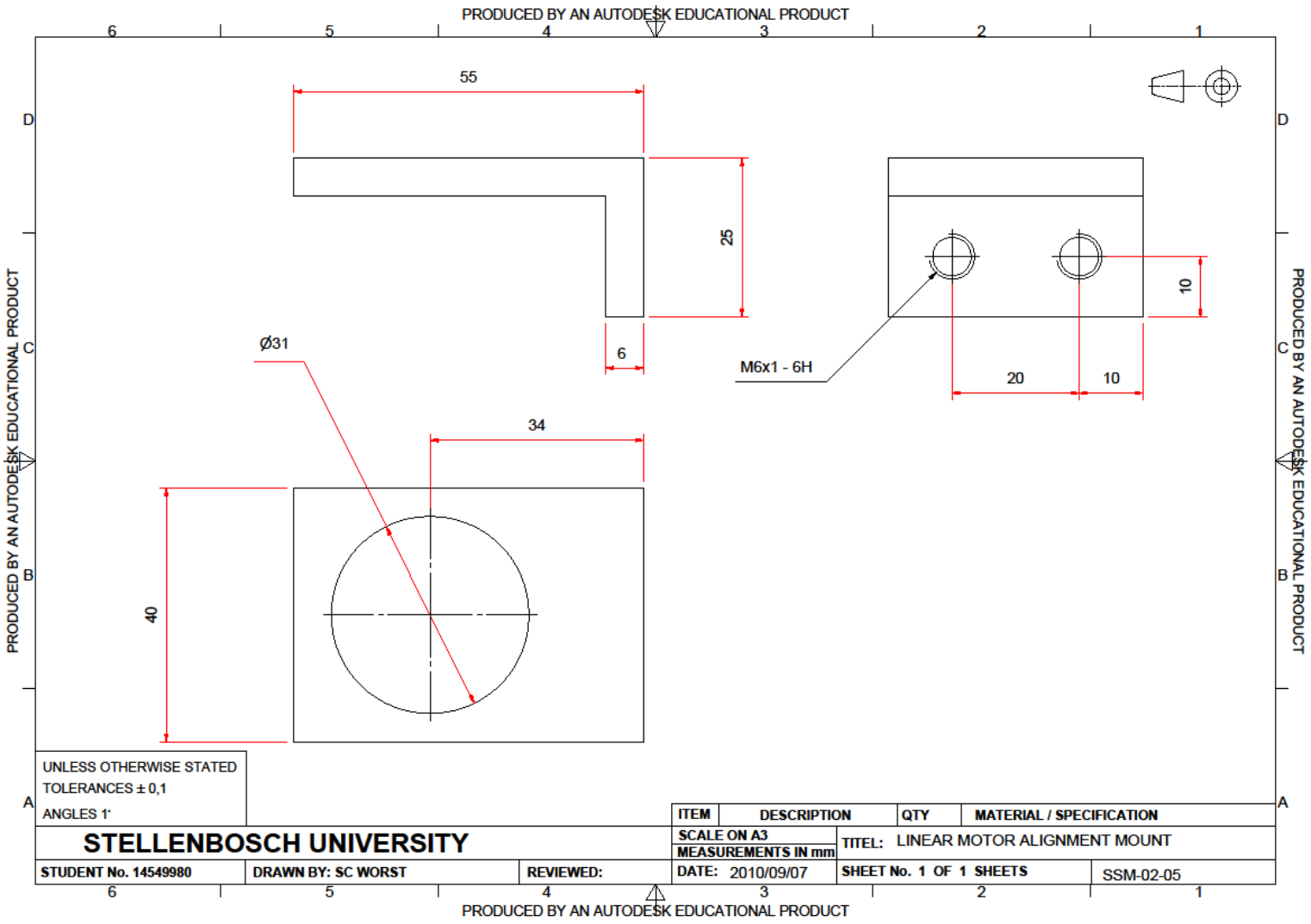
PRODUCED BY AN AUTODESK EDUCATIONAL PRODUCT
55
25
6
Ø31
34
40
M6x1 - 6H
20
10
10
UNLESS OTHERWISE STATED
TOLERANCES ± 0,1
ANGLES 1°
ITEM
DESCRIPTION
QTY
MATERIAL / SPECIFICATION
STELLENBOSCH UNIVERSITY
SCALE ON A3
MEASUREMENTS IN mm
TITEL: LINEAR MOTOR ALIGNMENT MOUNT
STUDENT No. 14549980
DRAWN BY: SC WORST
REVIEWED:
DATE: 2010/09/07
SHEET No. 1 OF 1 SHEETS
SSM-02-05

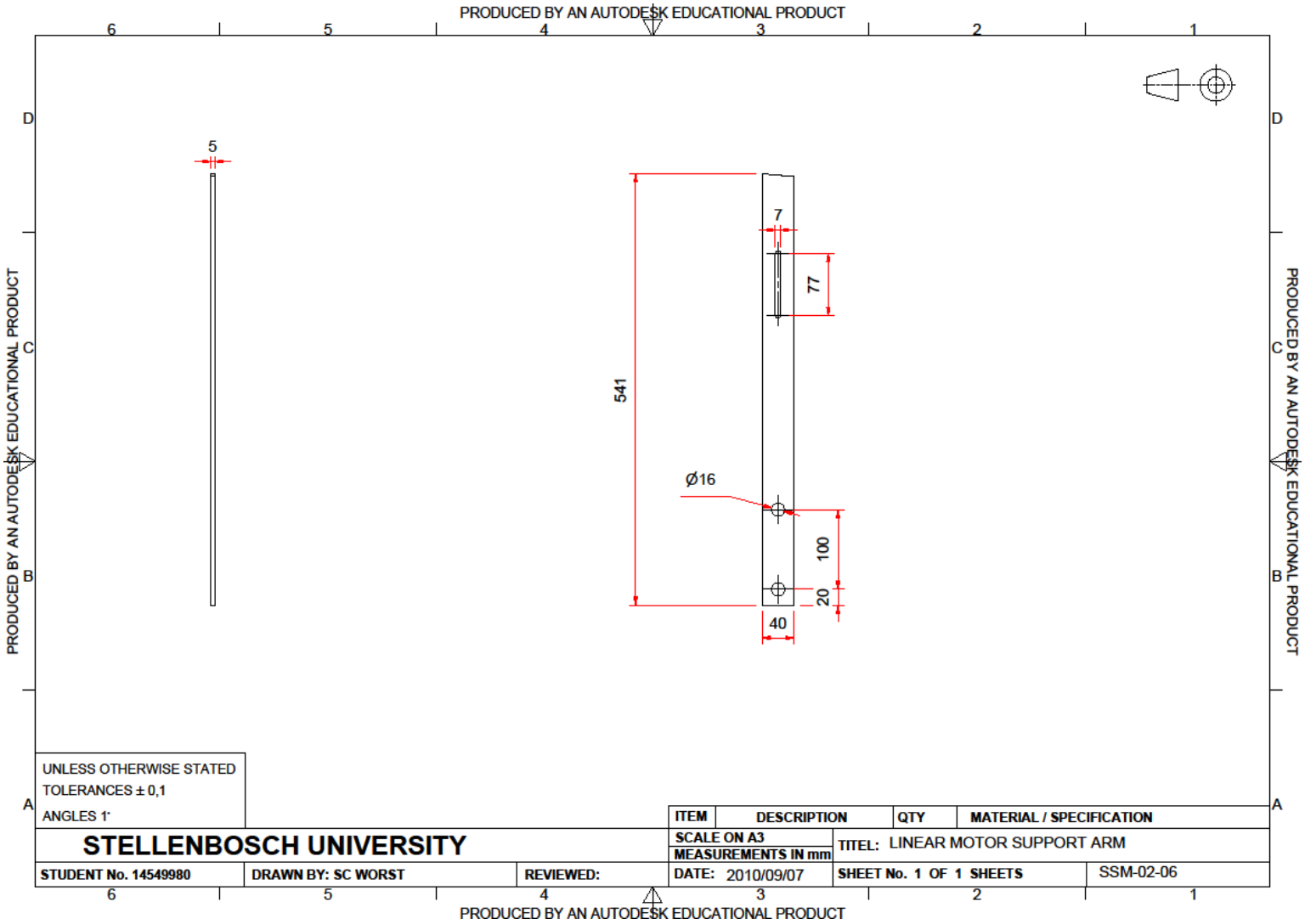
PRODUCED BY AN AUTODESK EDUCATIONAL PRODUCT
5
7
77
541
Ø16
100
20
40
UNLESS OTHERWISE STATED
TOLERANCES ± 0,1
ANGLES 1°
ITEM
DESCRIPTION
QTY
MATERIAL / SPECIFICATION
STELLENBOSCH UNIVERSITY
SCALE ON A3
MEASUREMENTS IN mm
TITEL: LINEAR MOTOR SUPPORT ARM
STUDENT No. 14549980
DRAWN BY: SC WORST
REVIEWED:
DATE: 2010/09/07
SHEET No. 1 OF 1 SHEETS
SSM-02-06

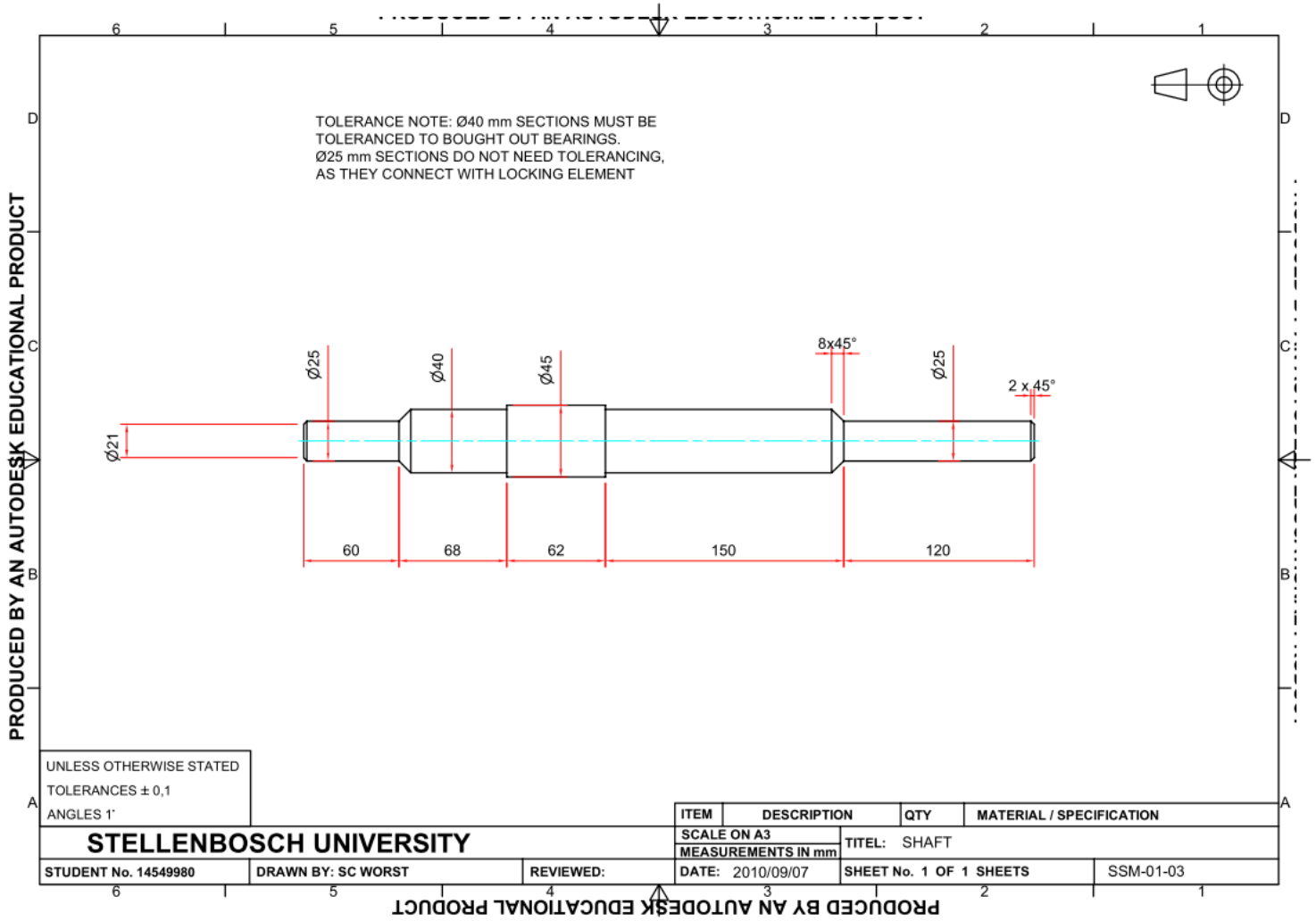
TOLERANCE NOTE: Ø40 mm SECTIONS MUST BE
TOLERANCED TO BOUGHT OUT BEARINGS.
Ø25 mm SECTIONS DO NOT NEED TOLERANCING,
AS THEY CONNECT WITH LOCKING ELEMENT
Ø25
Ø40
Ø45
8x45°
Ø25
2 x 45°
Ø21
60
68
62
150
120
PRODUCED BY AN AUTODESK EDUCATIONAL PRODUCT
UNLESS OTHERWISE STATED
TOLERANCES ± 0,1
ANGLES 1°
ITEM
DESCRIPTION
QTY
MATERIAL / SPECIFICATION
STELLENBOSCH UNIVERSITY
SCALE ON A3
MEASUREMENTS IN mm
TITEL: SHAFT
STUDENT No. 14549980
DRAWN BY: SC WORST
REVIEWED:
DATE: 2010/09/07
SHEET No. 1 OF 1 SHEETS
SSM-01-03

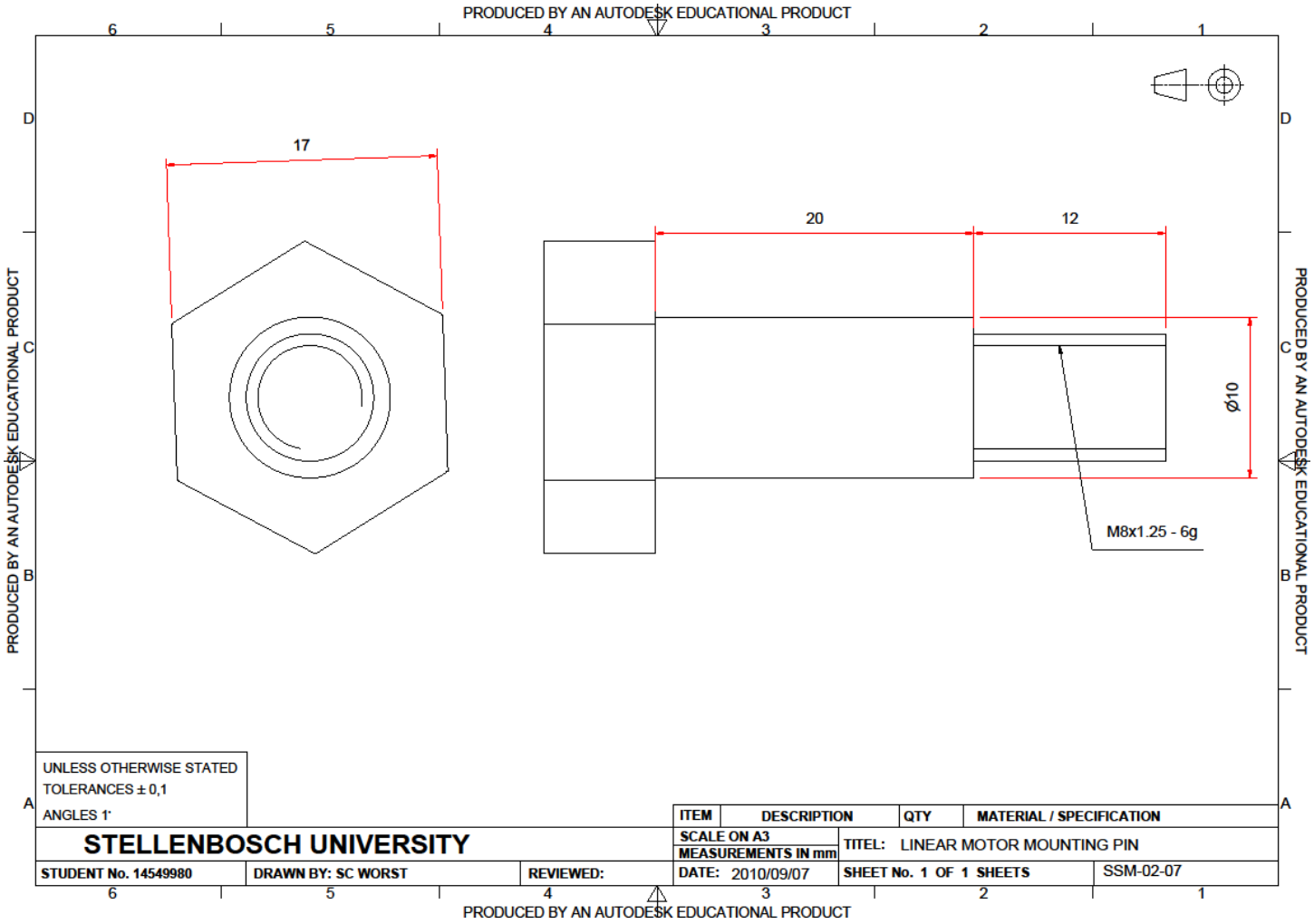
PRODUCED BY AN AUTODESK EDUCATIONAL PRODUCT
17
20
12
Ø10
M8x1.25 - 6g
UNLESS OTHERWISE STATED
TOLERANCES ± 0,1
ANGLES 1°
ITEM
DESCRIPTION
QTY
MATERIAL / SPECIFICATION
STELLENBOSCH UNIVERSITY
SCALE ON A3
MEASUREMENTS IN mm
TITEL: LINEAR MOTOR MOUNTING PIN
STUDENT No. 14549980
DRAWN BY: SC WORST
REVIEWED:
DATE: 2010/09/07
SHEET No. 1 OF 1 SHEETS
SSM-02-07

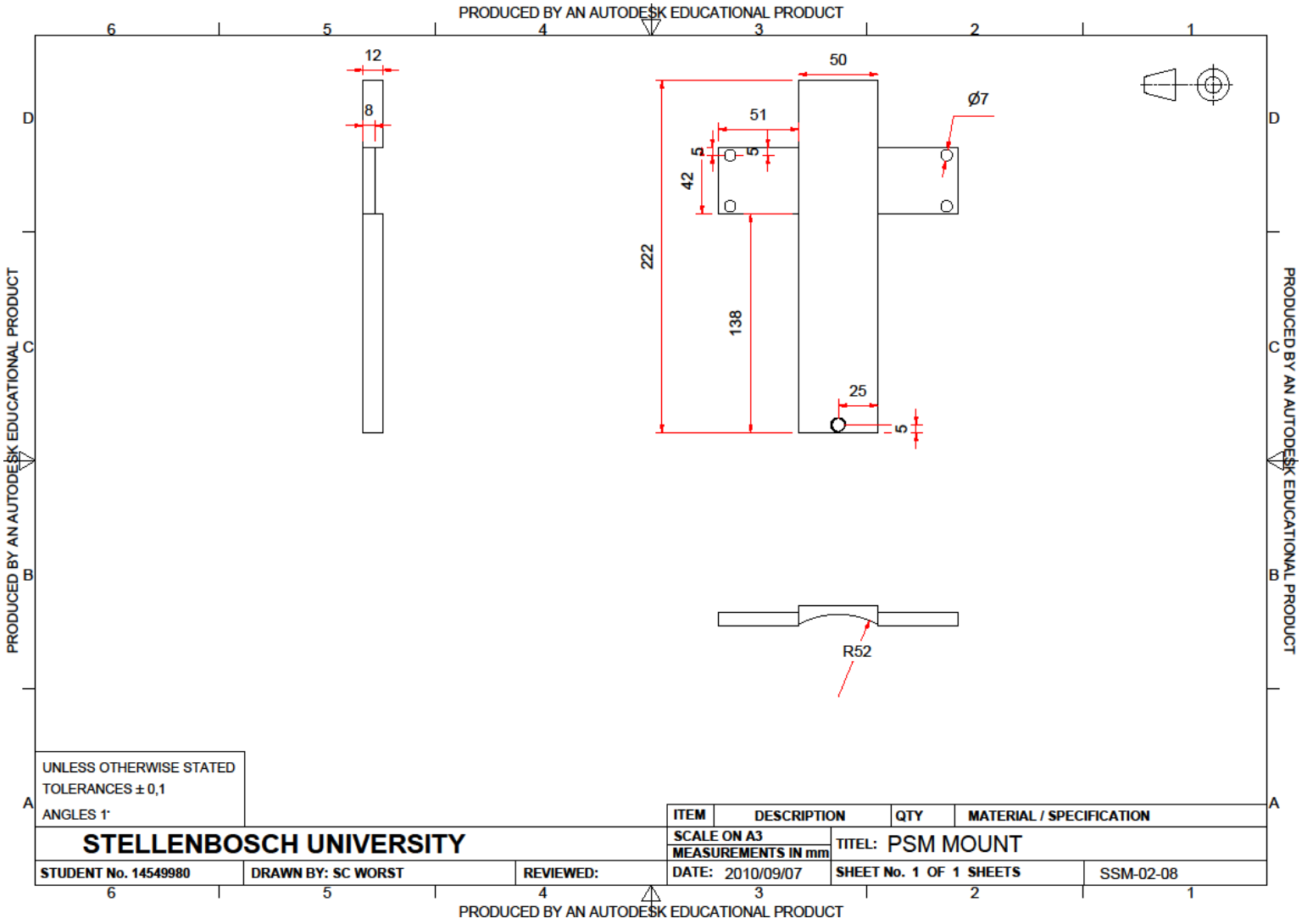
PRODUCED BY AN AUTODESK EDUCATIONAL PRODUCT
12
8
50
51
Ø7
5
5
42
222
138
25
5
R52
UNLESS OTHERWISE STATED
TOLERANCES ± 0,1
ANGLES 1°
ITEM
DESCRIPTION
QTY
MATERIAL / SPECIFICATION
STELLENBOSCH UNIVERSITY
SCALE ON A3
MEASUREMENTS IN mm
TITEL: PSM MOUNT
STUDENT No. 14549980
DRAWN BY: SC WORST
REVIEWED:
DATE: 2010/09/07
SHEET No. 1 OF 1 SHEETS
SSM-02-08

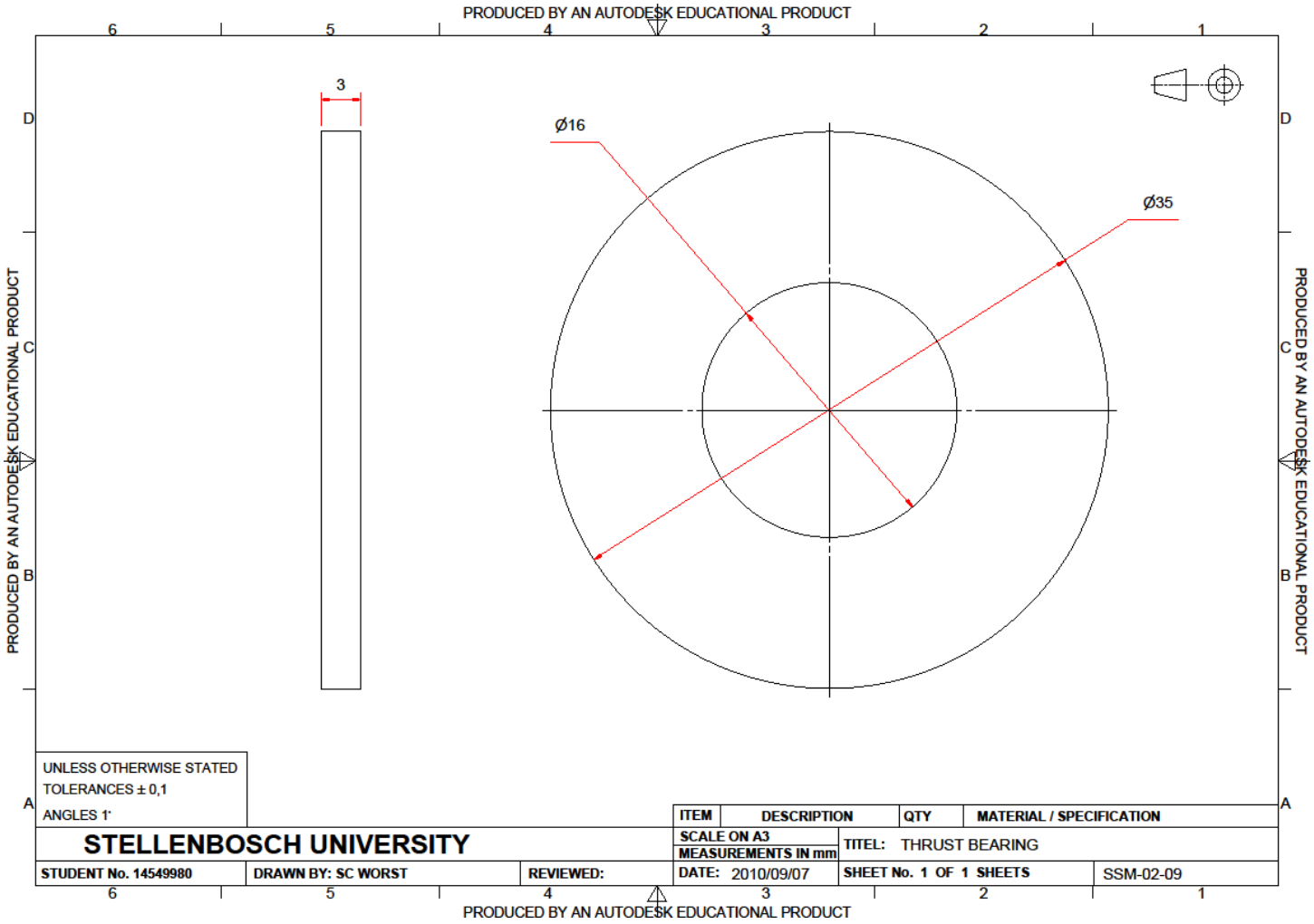
PRODUCED BY AN AUTODESK EDUCATIONAL PRODUCT
3
Ø16
Ø35
UNLESS OTHERWISE STATED
TOLERANCES ± 0,1
ANGLES 1°
STELLENBOSCH UNIVERSITY
ITEM
DESCRIPTION
QTY
MATERIAL / SPECIFICATION
SCALE ON A3
MEASUREMENTS IN mm
TITEL: THRUST BEARING
STUDENT No. 14549980
DRAWN BY: SC WORST
REVIEWED:
DATE: 2010/09/07
SHEET No. 1 OF 1 SHEETS
SSM-02-09

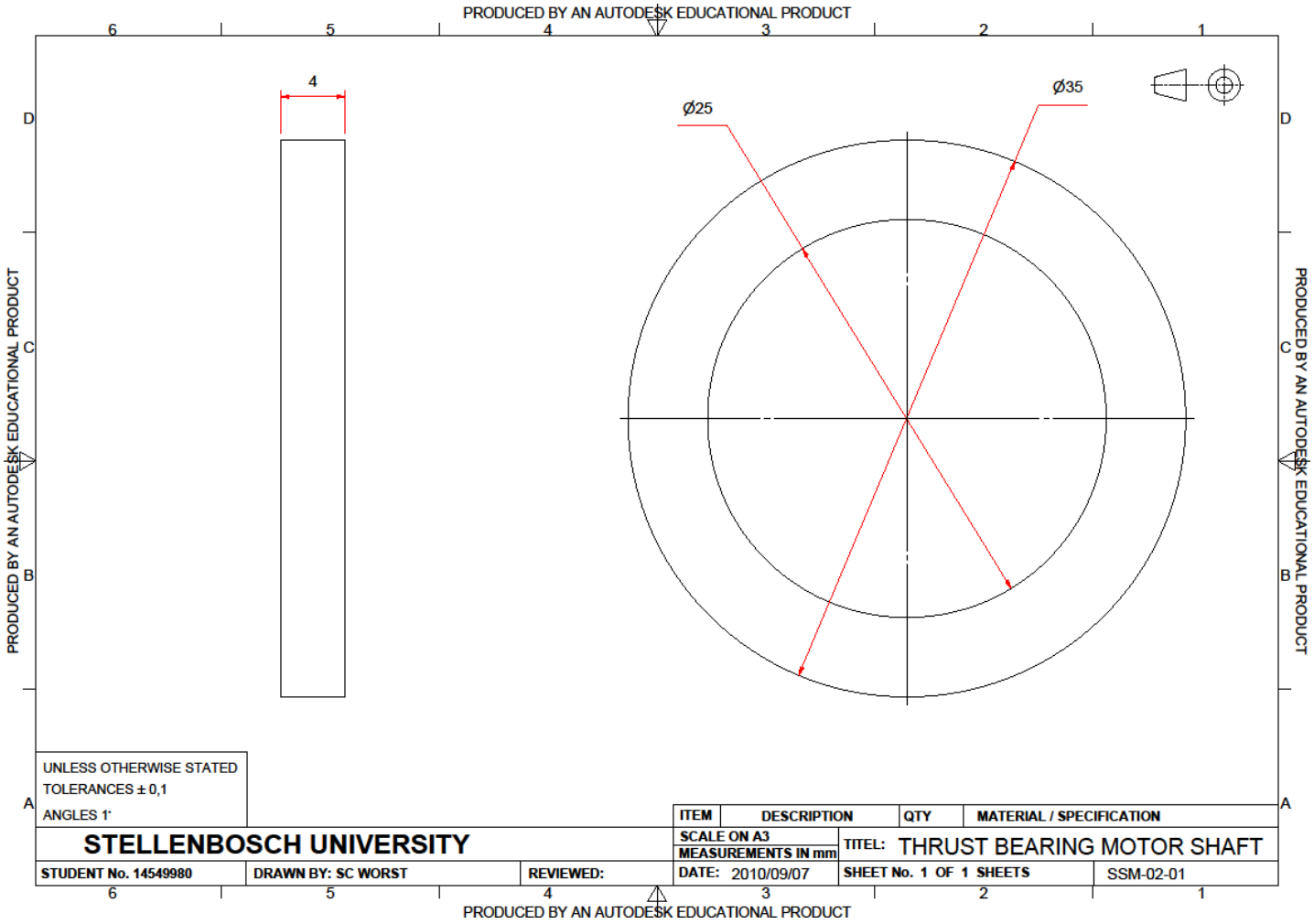
PRODUCED BY AN AUTODESK EDUCATIONAL PRODUCT
4
Ø25
Ø35
UNLESS OTHERWISE STATED
TOLERANCES ± 0,1
ANGLES 1°
ITEM
DESCRIPTION
QTY
MATERIAL / SPECIFICATION
STELLENBOSCH UNIVERSITY
SCALE ON A3
MEASUREMENTS IN mm
TITEL: THRUST BEARING MOTOR SHAFT
STUDENT No. 14549980
DRAWN BY: SC WORST
REVIEWED:
DATE: 2010/09/07
SHEET No. 1 OF 1 SHEETS
SSM-02-01

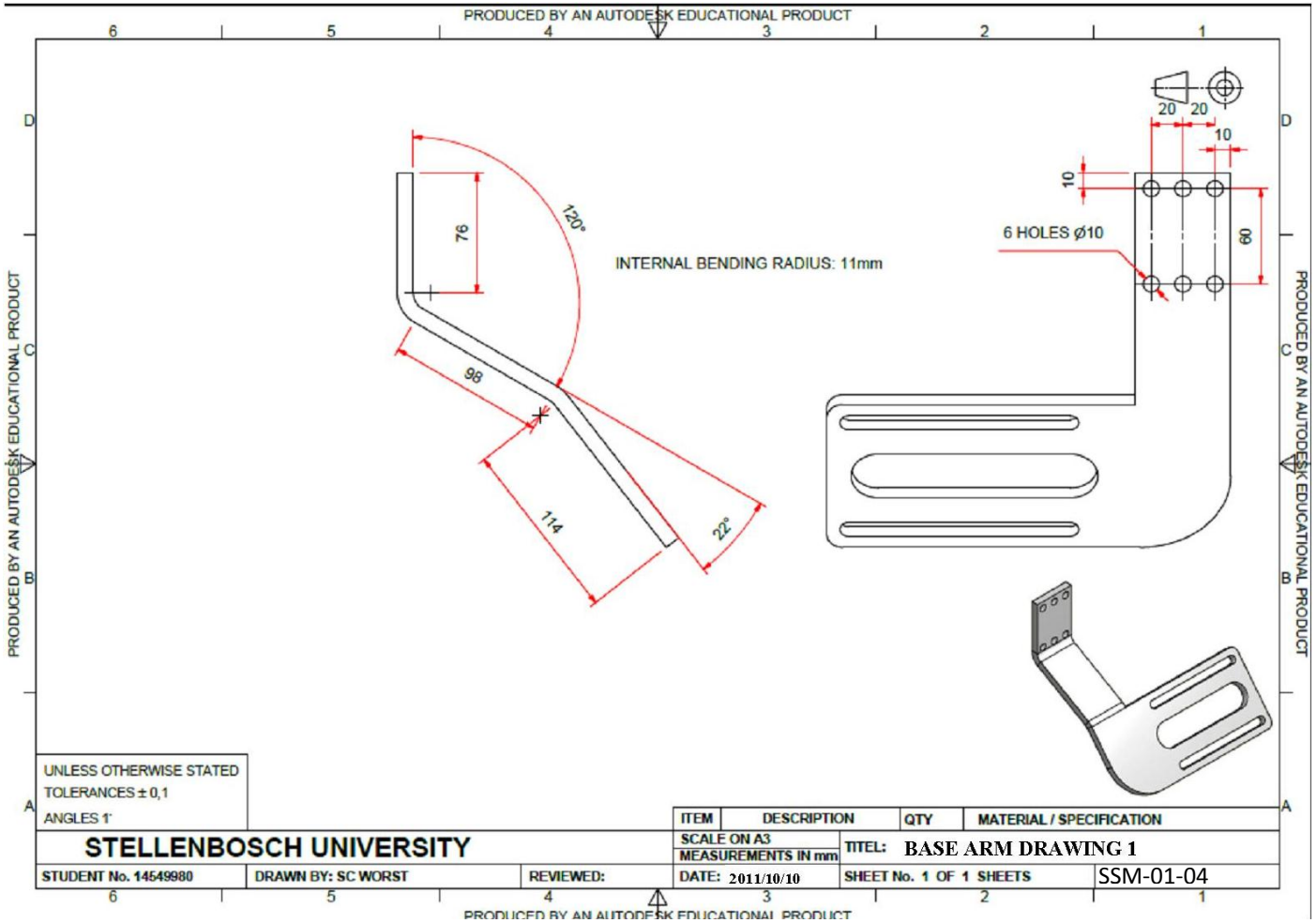
PRODUCED BY AN AUTODESK EDUCATIONAL PRODUCT
INTERNAL BENDING RADIUS: 11mm
6 HOLES Ø10
76
120°
98
114
22°
20
20
10
10
60
UNLESS OTHERWISE STATED
TOLERANCES ± 0,1
ANGLES 1°
ITEM
DESCRIPTION
QTY
MATERIAL / SPECIFICATION
STELLENBOSCH UNIVERSITY
SCALE ON A3
MEASUREMENTS IN mm
TITEL: BASE ARM DRAWING 1
STUDENT No. 14549980
DRAWN BY: SC WORST
REVIEWED:
DATE: 2011/10/10
SHEET No. 1 OF 1 SHEETS
SSM-01-04

Appendix B - Manipulator Assembly Procedure

The base mounting plate for the bearing housings and Parvalux motor can easily be mounted to a frame or base assembly. Once this plate is mounted, the Parvalux motor can be mounted (do not fully tighten any bolts as the parts may be required to be moved slightly). Slide the locking elements into the HRC coupling, and mount one side on the motor's shaft. The locking element and coupling must be mounted so that it is still possible to tighten the bolts on the locking element with an Allen key. Slide the bearing housings over the shaft and insert the short end into the locking element on the other side of the HRC coupling. Ensure the HRC coupling is mounted over the square hole on the base plate to ensure it does not rub against it. Once all parts are in their correct positions, all bolts can be securely tightened.

Insert the last locking element into the support for the shaft and slide the combination over the shaft. The shaft's face must line up with the opposite face of the support housing. Tighten the locking element to secure the shaft to the support. Bolt the base arm onto the shaft support so that the bends of the arm elevates it.

Mount the remaining Parvalux motor upside down on the base arm so that the output shaft faces towards the mounting shaft. Insert a 4 mm thick Vesconite bush on the shaft of the motor. Insert the key into the keyway and mount the actuating arm. Secure the arm into place with the 25 mm diameter ring and 3 mm bolt.

The end effecter assembly must be mounted next. Figure 74 shows the positions of all parts on the assembly (except for the linear actuator's mounting bolt). The bearing supports must be mounted on the 4.5mm plate so that it is centred in its length. Place the linear motor's mounting arm so that the mounting holes line up. Slide the Vesconite bushes over the bolts and insert them through the mounting holes. The bronze bearings come already pressed into the plate. Insert the bolts through the actuating arms, insert the Vesconite bushes and secure the bolts with the nuts. The PSM mount connects to the PSM's outer shell with two 3 mm bolts. Now the PSM mount can be attached to the bearings. The outer bolts connect from the front of the bearings whilst the inner bolts connect from the back.

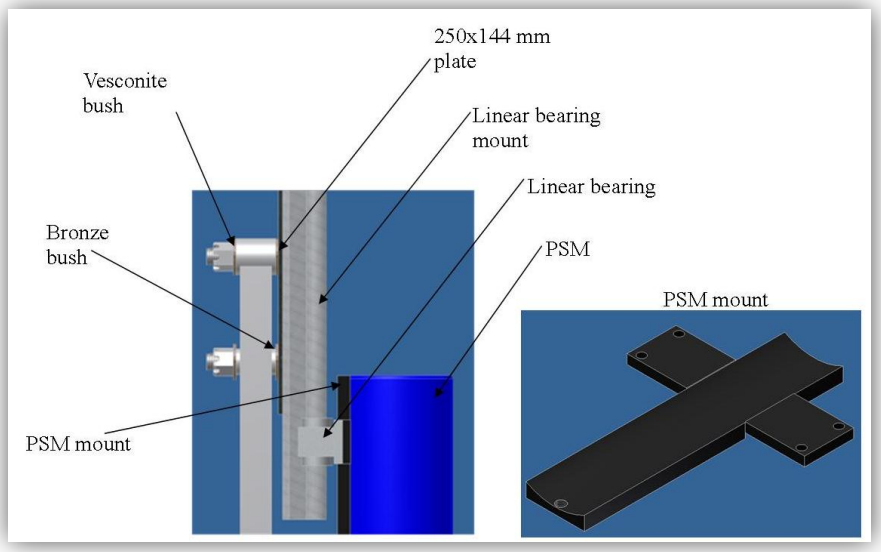

Figure 74: Assembly of end effecter parts

Slide the linear actuator's L-bracket over the body and bolt it onto the support. Insert the bearings with the PSM shell over the bearing supports. Connect the bottom of the actuator to the PSM mount with the remaining mounting pin. Since the arm holding the linear actuator has been shortened, it is held in place with the aid of a U-bolt. The combination of the U-bolt and the linear actuator's L-bracket will cause a holding force on the actuator that will keep in firmly in place.

The linear encoder can be mounted onto its L-bracket. It has a non-threaded plastic housing, so it must be secured with two 5 mm screws. Mount the bracket on the arm on the single slot that remains unused. Connect the cable of the encoder with the linear bearing with a M3 bolt.

Appendix C – Concept Evaluation

In order to evaluate the concepts against each other, the manipulators must be measured against each other on how well they fulfil certain criteria. In order to make this project successful, the designed manipulator must be cost effective and achieve all required movement that a MIRS procedure would require. Thus, the manipulator must adhere to the following criteria:

- Manipulator must not exert a force on the abdomen wall.
- Two DOFs must pivot perpendicular to each other around the point of incision. The perpendicular movement will allow the manipulator to reach the largest possible area allowed by its design.
- As far possible, the manipulator must not have singular positions inside the working space of the abdomen.
- As stated, the manipulator must be cost effective.

Each of the manipulators will be rated out of three on how well they fulfil the given criteria. Table 16 to Table 19 show how the manipulators will be rated.

Table 16: Concept evaluation, force exerted on abdomen

Score out of 3	Exerting force on abdomen wall
1	Forcefully pushes against wall
2	Uses wall as passive joint
3	Doesn't exert any force

Table 17: Concept evaluation, perpendicular pivoting movement

Score out of 3	Perpendicular pivoting movement
1	Creates one DOF with more than one actuator (each DOF requires more than one actuator)
2	Creates one DOF with two actuators (both DOFs require the same actuators)
3	Creates one DOF with one actuator

Table 18: Concept evaluation, existence of singular positions

Score out of 3	Existence of singular positions
1	Several singular positions inside required working area
2	Some singular positions inside required working area
3	Singular positions only at end of range of movement

Table 19: Concept evaluation, cost effectiveness

Score out of 3	Cost effectiveness
1	Expensive bought out manipulator
2	Requires more than three actuators
3	Minimum amount of actuators (three) can be used

Appendix D – Flexural Rigidity of Base Arm

From Craig (2000), Flexural rigidity is defined by Equation 16:

$$Flexural\ rigidity = EI \tag{16}$$

E is the Modulus of Elasticity of a material and *I* is the area Moment of Inertia of a profile. The Moment of inertia for the base arm as it is given by Equation 17:

$$I_o = \frac{1}{12} b\, h^3 \tag{17}$$

where *b* is the width of the arm and h the material thickness. The original Moment of Inertia for the plate is:

$$50 \times 10^{-9} m^4$$

The addition of the flanges on the plate will cause the centre of gravity of the profile to shift slightly. In order to find the new centre of gravity, an arbitrary origin at the bottom of the arm is chosen and the coordinate in the y direction be called η. Then, by summing the area contributions to the first moment as in Equation 18:

$$\eta A = \eta_1 A_1 + 2(\eta_2 A_2) \tag{18}$$

The subscript one refers the area of the original arm, and subscript two refers to the flanges. From this it is found that the new centre of gravity is located at 9.6 mm from the bottom of the plate. In Equation 19 the new Moment of Inertia can be calculated using the parallel axis theorem:

$$I_n = (I_1 + A_1 d^2{}_1) + 2(I_2 + A_2 d^2{}_2) \tag{19}$$

This expands to Equation 20:

$$I_n = \left(\frac{1}{12} b\, h^3 + A_1 d^2{}_1\right) + 2\left(\frac{1}{12} h\, b^3 + A_2 d^2{}_2\right) \tag{20}$$

The new Moment of Inertia is found to be:

$$I_n = 74 \times 10^{-9} m^4$$

Thus with a constant Modulus of Elasticity, the increase in Flexural Rigidity is found by Equation 21:

$$\Delta Flexural\ regidity = \left(1 - \frac{74 \times 10^{-9}}{50 \times 10^{-9}}\right) \times 100\% \tag{21}$$

This gives an increase of 48% in Flexural rigidity.